University of Sheffield

Epithelial-mesodermal interactions in digit patterning and evolution

Sarah Wiggins

A thesis submitted in partial fulfilment of the requirements for the degree of Doctor of Philosophy

The University of Sheffield

Faculty of Science

School of Biosciences

July 2024

ACKNOWLEDGEMENTS

I would like to express my deepest appreciation to my supervisors, Dr Matthew Towers and Professor Marysia Placzek for their invaluable advice, support and patience throughout this PhD. Their combined knowledge and experience has inspired and guided me into becoming a better scientist. I would also like to extend my thanks to my advisors, Dr Freek van Eeden and Dr Elena Rainero, for their insightful suggestions and comments. I am also thankful for the past and present members of the Towers and Placzek lab who have given me priceless support, advice and companionship over the last few years.

Finally, I would be remiss in not mentioning my parents Simon and Louise, my sister Katie, my partner Ben, his family and our friends. I am so grateful for their unwavering love, support and encouragement during my PhD. I am also grateful to my cats, Moon and Geddy, who have provided great emotional support and entertainment. This thesis would not have been possible without the tremendous support of all the people mentioned here, to whom I will be forever appreciative.

INDEX

CHAPTER 6

Expression of cell cycle regulators in the mouse limb

CHAPTER 7

Discussion

ABBREVIATIONS

AER - Apical ectodermal ridge

AP - Anterior-posterior

Bmp - Bone morphogenic protein

Cyb26b1 - Cytochrome P450 26B1

DMEM - Dulbecco's Modified Eagle Medium

DOI - Days of incubation

DPC - Days post conception

DV - Dorsal-ventral

EdU - Ethynyl-2'-deoxyuridine

En1 - Engrailed 1

FBS - Fetal bovine serum

Fgf - Fibroblast growth factor

GFP - Green fluorescent protein

Gli - Glioma-associated oncogene

Grem1 - Gremlin 1

HBC - 2-hydropropyl-β-cyclodextrin

HCR-FISH- Hybridisation chain reaction fluorescent *in situ* hybridisation

HH - Hamburger-Hamilton stage

Lmx1b - LIM homeobox transcription factor 1-beta

PBS - Phosphate-buffered saline

PD - Proximal-distal

PFA - Paraformaldehyde

PR - Polarising region

Ptch1 - Patched 1

ozd - oligozeudactyly

RA - Retinoic acid

Shh - Sonic hedgehog

Smo - Smoothened

Tbx - T-box transcription factor

Wnt - Wingless-related integration site

ZPA - Zone of polarising activity (also known as PR)

ZRS - ZPA regulatory sequence

ABSTRACT

Pattern formation in the limb requires communication between two principal signalling centres: the apical ectodermal ridge (AER) in the epithelium and the polarising region (PR) in the mesoderm. However, understanding the individual contributions of these signalling centres in development is very difficult *in vivo*, as the AER is vital for the outgrowth of the limb. Studies in the chick wing have suggested that Sonic hedgehog (Shh) signalling intrinsically regulates the rate of proliferation in PR cells via an autoregulatory cell cycle mechanism which prevents it from forming posterior digits, a characteristic seen in the mouse/mammalian limb.

In my thesis, I have dissected and cultured PR tissue without the AER or anterior mesenchyme to develop a PR explant model to understand the relative roles of these organisers. By examining the duration of Shh signalling and proliferation parameters, I determine that the PR maintains *in vivo* parameters in the absence of the AER. Attenuating Shh signalling in the PR explants reveals that it inhibits proliferation through a Bmp2-$p27^{kip1}$ pathway to prevent the formation of an additional

digit. Interestingly, in this process, my results reveal that the PR explants display an unexpected ability to self-organise and re-establish a population of AER-like cells.

Finally, analysis of cell cycle regulators in the mouse PR indicate that the avian wing PR has evolved the Bmp2-$p27^{kip1}$ pathway to prevent the formation of PR-derived digits. I present a potential evolutionary mechanism to explain how posterior digits were lost in the evolution of the bird wing.

CHAPTER 1

Introduction

1. Introduction

Understanding how complex organs form from undifferentiated cells has long been a fundamental question for developmental biologists. Pattern formation - a process in which cells acquire positional information depending on their relative spatial position in the tissue - is essential to organogenesis. Organogenesis also involves growth which, for the most part, is achieved by cells increasing their size or, more commonly, their number through proliferation.

Animal models have been used widely to understand the biological mechanisms underlying organogenesis. Two commonly used species are mouse (Mus musculus) and chicken (Gallus gallus). Mouse embryos are powerful for understanding mammalian development, as they breed rapidly and can be easily genetically manipulated. Chick embryos are excellent models because they are

accessible and easy to manipulate through classic embryological and pharmacological approaches in ovo.

The limb is an ideal organ to study the process of organogenesis, particularly in the chick embryo. The chick limb is an accessible organ which is not required for survival, meaning experimental manipulation does not compromise the survival of the embryo. For these reasons, decades have been spent examining mechanisms behind the growth and patterning of the limb in both chick and mouse embryos.

1.1. Limb development

Forelimbs and hindlimbs develop as small buds of cells at reproducible anteroposterior positions on either side of the embryos flank. Limb buds consist of cells derived from the somatopleural layer of the lateral plate mesoderm (Hamburger, 1938, Altabef et al., 1997) and myogenic cells from the somatic plate mesoderm (Christ et al., 1977) which are encased in an epithelial layer. Limb buds are first visible in chick embryos after 3 days of incubation (DOI), at approximately Hamburger-Hamilton stage 16/17 (HH16/17; Hamburger and Hamilton, 1951), or at 9.5 days post conception (DPC) in mice (Wanek et al., 1989).

Pattern formation in the limb takes place along three principal axes (Figure 1.1. A): the proximal-distal (PD; shoulder to fingertips), the anterior-posterior (AP; thumb to little finger) and the dorsal-ventral (DV; knuckle to palm). DV polarity dictates the position of the apical ectodermal ridge (AER) - a thickening of the ectoderm at the distal edge of the limb bud (Figure 1.1. B) - which is required for PD outgrowth and patterning. The AER forms along the boundary of the dorsal and ventral compartments of the limb. The AP polarity of the embryo dictates the position of the polarising region (PR; also known as the zone of polarising activity (ZPA)) - an area of mesenchyme on the posterior margin of the limb bud (Figure 1.1. B) - that subsequently patterns the AP axis. The axial patterning of the limb is associated with

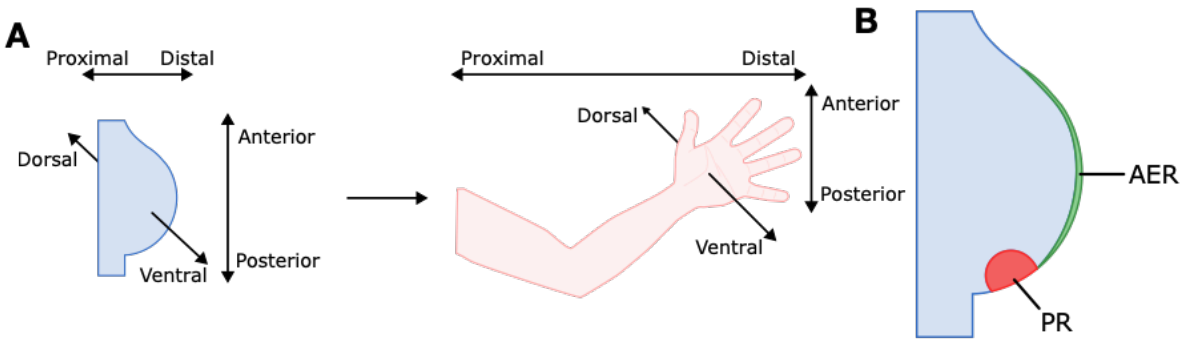

Figure 1.1. Pattern formation takes place across three axes.
A) Schematic showing the three axes of the limb. The proximal-distal axis runs from shoulder to fingertips, the anterior-posterior axis runs from thumb to little finger and the dorsal-ventral axis runs from knuckles to palm. B) Schematic showing the position of the AER (green) and PR (red) in the limb bud.

signalling proteins. The AER produces Fibroblast growth factors (AER-Fgfs; Crossley et al., 1996, Vogel et al., 1996), the PR produces Sonic Hedgehog (Shh; Riddle et al., 1993) and the dorsal and ventral ectoderm produce Wingless-related integration site 7a (Wnt7a; Parr and McMahon, 1995) and Bone morphogenic proteins (Bmps) respectively to fully pattern the developing limb (Pizette et al., 2001). I will discuss the roles of Fgfs and Shh in more detail in Sections 1.4. and 1.5.

1.2. Establishment of limb polarity

For the axes of the limbs to be specified, the limb bud must first become polarised. As already mentioned, DV polarity dictates the positioning of the AER, whilst AP polarity ensures the PR forms along the posterior margin of the limb bud. In this section, I will discuss how the limb bud becomes polarised across the DV, PD and AP axes.

1.2.1. Establishing DV polarity in the limb

DV polarity of the wing bud was determined to arise before the limb bud first becomes visible. It was demonstrated that rotating the limb mesoderm 180º dorsoventrally under the ectoderm at HH17 results in a limb with reversed DV axis, thus indicating the polarity of the limb was established before this time point (Akita, 1996). It was shown that DV polarity is conferred in the ectoderm by signals from the somites and lateral somatopleure between HH13 and HH15 (Figure 1.2. A; Michaud et al., 1997); grafting somites in place of the neural tube so that the presumptive limb ectoderm was flanked by somites resulted in bidorsal limbs (i.e. the ventral limb became dorsalised), whilst blocking signalling from the of the lateral somatopleure also gave rise to bidorsal limbs (Michaud et al., 1997). Thus, polarity is imposed on the overlying ectoderm, with the somites conferring dorsal identity whilst the lateral somatopleure confers ventral identity (Figure 1.2. A; Michaud et al., 1997). This early specification of DV polarity ensures the DV axis of the limb matches that of the body. Bmp signalling in the ventral body wall is likely to induce Bmp-expression in the wing bud ectoderm and thus acts as a ventralising factor (Figure 1.2. A; Pizette et al., 2001) to establish DV polarity. In Section 1.3. I will discuss in more detail how this polarity influences DV patterning.

1.2.2. Establishing PD polarity in the limb

Establishment of the DV axis in the limb leads to PD polarity as cells which amalgamate along the boundary between dorsal and ventral ectodermal compartments of the limb will form the AER. *T-box transcription factor 5 (Tbx5)* is activated in the lateral plate mesoderm initiating forelimb outgrowth (Rodriguez-

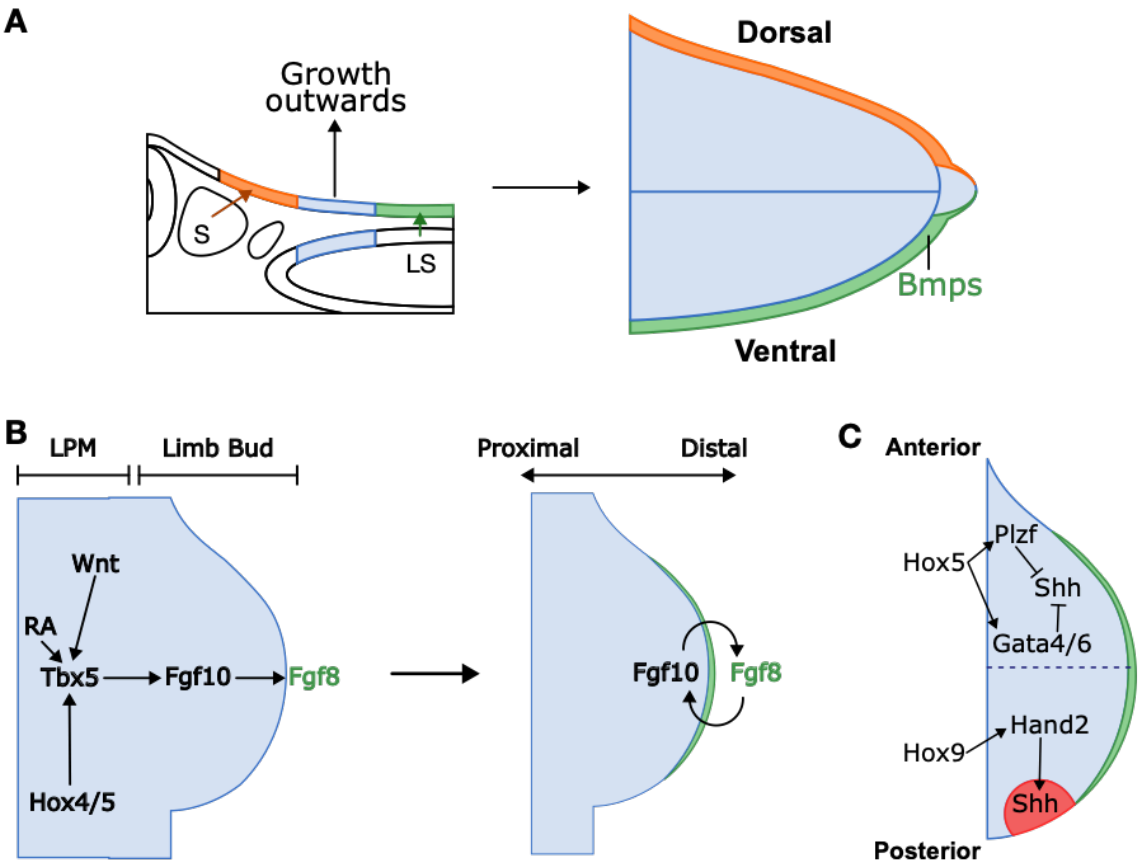

Figure 1.2. Establishment of limb polarity.
A) Schematic demonstrating how DV polarity is established in the limb. Dorsal identity (orange) is conveyed to the ectoderm by signalling from the somites (S), whilst ventral identity (green) is conveyed by signalling from the lateral somatopleure (LS). It is likely that Bmps act as a ventralising factor. B) Schematic showing how PD polarity is established in the limb. Tbx5 is up-regulated in the lateral plate mesoderm (LPM) by RA signalling, Wnt signalling and Hox4/5 paralogues. Tbx5 up-regulates *Fgf10* expression in the mesenchyme, which in turn up-regulates *Fgf8* in the overlying ectoderm. This leads to the establishment of the AER (green) and a feedback loop between Fgf10 in the mesenchyme and Fgf8 in the ectoderm. C) Schematic demonstrating how the AP polarity in the forelimb is established. Hox5 up-regulates and works with Plzf and Gata4/6 to inhibit *Shh* expression in the anterior. In the posterior limb bud Hox9 up-regulates and works with Hand2 to promote *Shh* expression in the PR.

Esteban et al., 1999, Takeuchi et al., 1999). Expression of *Tbx5* in the presumptive forelimb area is likely regulated by Wnt/β-catenin signalling, retinoic acid (RA) signalling, and Hox 4 and Hox5 paralogues (Minguillon et al., 2012, Nishimoto et al., 2014, Nishimoto et al., 2015). Tbx5 then induces the expression of *Fgf10* in the forelimb mesenchyme, which in turn induces *Fgf8* expression in the overlying ectoderm at the DV boundary leading to the formation of the AER (Figure 1.2. B; Agarwal et al., 2003). Fgf8 from the ectoderm then signals to the mesoderm to maintain *Fgf10* expression, initiating an Fgf8-Fgf10 feedback loop which controls limb bud outgrowth (Figure 1.2. B; Ohuchi et al., 1997). Thus, the establishment of the AER confers PD polarity to the limb bud. In Section 1.4. I will discuss in more detail how the AER, AER-Fgfs and other signals pattern the PD axis.

1.2.3. Establishing AP polarity in the limb

As mentioned above, establishing AP polarity in the limb ensures the correct positioning of the PR. Early experiments demonstrated that grafting a piece of HH11 flank tissue which had been rotated 180º along the AP axis results in the host limb developing with reversed AP polarity (Chaube, 1959). This indicated that AP polarity of the limb is specified early during development and in relation to the polarity of the main embryo body (Chaube, 1959). This coincides with when the AP axis of the body has been established by *Hox* genes.

Establishment of the anterior region of the forelimb prevents the PR from forming along the anterior margin. This relies on *Hox5* expression as loss of function in mouse embryos results in the PR being positioned at the anterior margin (Xu et al., 2013). *Shh* expression is restricted to the posterior region of the limb bud by transcription factors binding to a distant cis-regulatory enhancer known as the ZPA regulatory sequence (ZRS; Lettice et al., 2002, Williamson et al., 2016). Hox5 interacts with the transcription factors *Plzf, Gata4* and *Gata6* to inhibit *Shh*

expression in the anterior forelimb, thus restricting PR development to the posterior forelimb (Figure 1.2. C; Xu et al., 2013, Hayashi et al., 2016).

Establishment of the posterior region of the forelimb relies on *Hox9* expression: deletion of *Hox9* paralogous genes in mouse results in the failure to establish Shh signalling at the posterior margin of the forelimb bud (Xu and Wellik, 2011). Transcription factors *Hox9* and *Hand2* (the latter promoted in the posterior limb by Hox9) bind to the ZRS and up-regulate *Shh* expression in the PR (Figure 1.2. C; Xu and Wellik, 2011, Lettice et al., 2017), thus ensuring the PR forms along the posterior margin. Interestingly, there is little evidence that *Hox* genes are required to determine the AP polarity of the hindlimb. Instead, it has been demonstrated that AP polarity is established in the hindlimb by regionalised transcription factors such as Islet1 (Itou et al., 2012) and Sall4 (Akiyama et al., 2015). In Section 1.5. I will discuss how the PR and Shh patterns the AP axis of the limb.

1.3. DV patterning of the limb

The DV axis of the limb is crucial to ensure functional morphology such as nails or claws dorsally on the fingertips, however DV axis patterning has not been as well studied as either AP or PD axis patterning. As discussed in Section 1.2.1., Bmp is thought to be the ventralising factor in the limb. Bmp signalling in the ventral ectoderm induces *Engrailed 1* (*En1;* Figure 1.3.) which acts as a ventral signal, as loss of En1 results in dorsalised limbs (Loomis et al., 1996).

The dorsalising factor is thought to be Wnt7a in the dorsal ectoderm which induces *LIM homeobox transcription factor 1-beta (Lmx1b)* in the underlying mesoderm (Figure 1.3.; Parr and McMahon, 1995, Riddle et al., 1995, Vogel et al., 1995). Loss of Wnt7a function in mouse results in ventralised limbs (Parr and McMahon, 1995) whilst over-expression of *Lmx1b* dorsalises the limb (Riddle et al., 1995, Vogel et al., 1995).

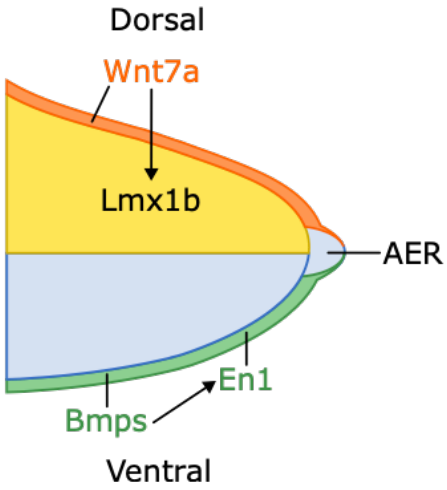

Figure 1.3. DV patterning of the limb.
Bmp signalling in the ventral ectoderm induces En1 which acts as a ventral signal. Wnt7a is expressed in the dorsal ectoderm and acts as the dorsal signal by inducing Lmx1b expression in the underlying mesoderm. The AER forms at the boundary between the ventral and dorsal compartments.

1.4. PD patterning of the limb

The structures of the limb are patterned in a PD sequence (Figure 1.4. A; Saunders Jr, 1948): the stylopod (i.e. the humerus or femur) is laid down first, then the zeugopod (i.e. the ulna/radius or the tibia/fibula) and then the autopod (i.e. the fingers or toes). Across tetrapod species the stylopod and zeugopod remain highly conserved whilst the autopod displays high variability in digit number between species resulting in specific adaptations to fit the environment.

As described above in Sections 1.1. and 1.2.2., the AER is characterised by expression of AER-Fgfs, such as Fgf8 (Vogel et al., 1996) and forms at the boundary between the dorsal and ventral compartments. Importantly, as will be discussed below, the AER is required for growth and patterning along the PD axis (Saunders Jr, 1948).

1.4.1. The 'progress zone' model of PD patterning

Numerous models have been proposed for the mechanism behind PD patterning. The classic model - the 'progress zone' model - came through studies showing that removal of the AER at different time points of chick wing development truncates the limb at different PD levels (Saunders Jr, 1948). For example, early removal of the AER results in a limb consisting of just the stylopod, whilst later removal of the AER results in a limb consisting of the stylopod and zeugopod (Saunders Jr, 1948). This observation was interpreted in terms of positional information and led to the progress zone model (Summerbell et al., 1973). This model suggests that the sequential specification of PD positional values is due to an internal autonomous 'clock' operating in the mesenchyme below the AER (Figure 1.4. B). This area, defined as the 'progress zone', is exposed to signals from the AER which keeps the cells in an undifferentiated, proliferative state. Over time, cells proliferate, and the limb grows, causing cells to exit the 'progress zone' and differentiate with correspondingly more-distal positional values (Figure 1.4. B). Therefore, the 'progress zone' model postulates that specification of PD values is dependent on the length of exposure to AER signals (Summerbell et al., 1973). The theory that the 'progress zone' functions autonomously is supported by findings that distal tips of wing buds continue to autonomously progress through PD positional values when transplanted to wings of different ages (Summerbell and Lewis, 1975). Furthermore, cells in the distal mesenchymal 'progress zone' continue to autonomously progress through PD values when older or younger AERs are grafted in place of the original AER (Rubin and Saunders, 1972). This result also indicates

that the AER does not have a role in specifying PD values and is instead required permissively for the outgrowth of the limb.

The specification of PD positional values in a proximal-to-distal pattern is also supported by the temporal pattern of 5' *Hoxa* and *Hoxd* gene expression, which are

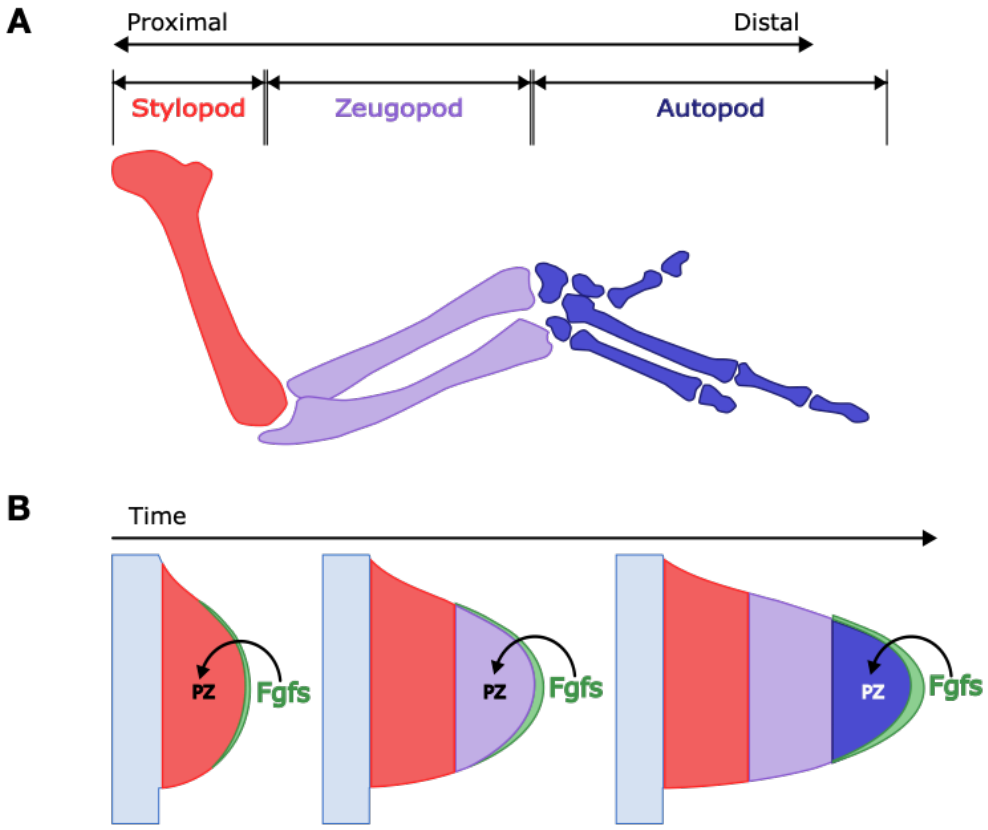

Figure 1.4. The 'progress zone' model of PD patterning.
A) Schematic of the limb showing the stylopod, zeugopod and autopod. The elements of the limb are laid down in PD order. B) Schematic showing the 'progress zone' model - Fgfs from the AER act on the proliferative mesenchyme in the 'progress zone' (PZ). Fates are specified depending on the length of time cells spend in the PZ.

considered to provide cells with positional information. *Hox9* and *Hox10* specify proximal positional values (i.e. the humerus), *Hox11* specifies the intermediate positional values (i.e. the radius/ulna) and lastly *Hox12* and *Hox13* specify the distal values (i.e. the digits; reviewed in Zakany and Duboule, 2007).

1.4.2. The 'two-signal' model of PD patterning

Following experiments in the chick wing an alternative 'two-signal' model was proposed to explain PD axis specification. Unlike the autonomous 'progress zone' model, this model proposes that two opposing signalling gradients - one from the proximal side of the limb and one from the distal side - work cooperatively to specify PD positional values (Figure 1.5. A and B). This model was proposed after the observation that AER-Fgfs antagonise RA signalling (*Meis1* and *Meis2* were used as a read-out of RA signalling) from the body wall of the embryo (Mercader et al., 1999, Mercader et al., 2000). Furthermore, RA signalling was found to be capable of specifying proximal fates (Cooper et al., 2011, Roselló-Díez et al., 2011). Evidence for this model was obtained by ectopically expressing *Meis1* and *Meis2* in chicken embryos which disrupts the formation of distal elements, but not proximal elements (Capdevila et al., 1999, Mercader et al., 1999). On the other hand, in mice, inactivation of *Meis1* and *Meis2* results in the severe reduction or total loss of proximal structures in both hind- and fore-limbs (Delgado et al., 2020), indicating the role of RA signalling in specifying proximal fates.

RA signalling is restricted to the proximal part of the limb bud through inhibition by AER-Fgfs (Figure 1.5. A; Mercader et al., 2000). However, for the 5' Hoxa/d11-13 gene expression programme to be activated, RA needs to be cleared from the developing limb bud (Roselló-Díez et al., 2011). This occurs through degradation of RA, and displacement away from the proximal RA signals through growth (Figure 1.5. A; Roselló-Díez et al., 2011). When AER-Fgfs function is deleted in mouse embryos, *Meis1* expression expands distally (Mariani et al., 2008).

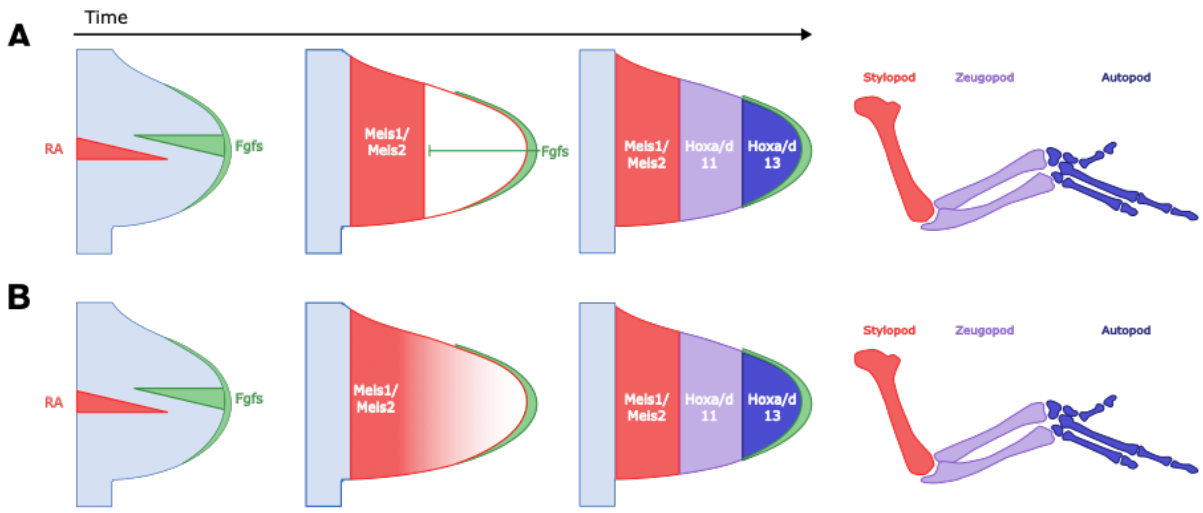

Figure 1.5. The 'two-signal' model of PD patterning.
The 'two-signal' model - Opposing gradients of RA/Meis1/Meis2 (proximal) and AER-Fgfs (distal) specify the PD axis. A) The original 'two-signal' model - RA is cleared from the distal limb through Fgf inhibition and growth. This allows for the activation of the Hoxa/d11-13 pattern which specifies the PD axis. B) The 'two-signal' model proposed by Delgado et al. (2020). The RA to Fgf ratio is interpreted into a gradient of Meis1/2 where high Meis1/2 patterns the proximal values, low Meis1/2 patterns the intermediate value and no Meis1/2 patterns the distal values. This concentration gradient allows for the progressive activation of Hoxa11 and Hoxa13.

More recently, the 'two-signal' model has been suggested to be an instructive model whereby the RA to Fgf ratio is interpreted into the graded distribution of Meis proteins along the PD axis (Figure 1.5. B; Delgado et al., 2020). Thus, high Meis1 and Meis2 specify the proximal values, low Meis1 and Meis2 specify the intermediate values and absent Meis1 and Meis2 specify the distal values (Delgado et al., 2020). The gradient of RA signalling, as interpreted through Meis1 and Meis2, would allow for the progressive activation of *Hoxa11* and *Hoxa13* required to form the limb

(Figure 1.5. B; Delgado et al., 2020). Interestingly, *Hoxa11* and *Hoxa13* continue to be progressively activated when Meis function is inactivated (Delgado et al., 2020), suggesting a level of autonomy in specifying the more distal structures.

1.4.3. The 'signal-time' model of PD patterning

Another model for PD patterning integrates elements of the 'progress zone' model and the 'two-signal' model. In this 'signal-time' model, antagonism between RA and AER-Fgfs patterns the proximal values. A gradient of Meis1/2 arises due to the RA signalling from the flank being degraded distally by the RA-degrading enzyme *Cytochrome P450 26B1 (Cyp26b1)*, which is induced by AER-Fgfs (Yashiro et al., 2004, Delgado et al., 2020). As in the 'two-signal' model, high and low Meis levels are required in the proximal limb to specify the stylopod and zeugopod respectively (Delgado et al., 2020).

Through a series of heterochronic grafting experiments, it was determined that the specification of distal positional values is due to an autonomous timing mechanism. When young (i.e. HH20) distal mesenchyme was grafted under the distal ectoderm of older (i.e. HH24) host wings, the grafted mesenchyme retained the cell cycle kinetics and timing of *Hoxa13* consistent with its age (Saiz-Lopez et al., 2015). This result indicates that *Hoxa13* and the cell cycle parameters are intrinsically timed by the distal mesenchyme and cannot be reset by extrinsic factors. Furthermore, it was demonstrated that AER-Fgfs do not play an instructive role in PD patterning as the intrinsic timing mechanism in the grafts was not affected by the age of the AER (Saiz-Lopez et al., 2015). Moreover, it was demonstrated that the grafted distal mesenchyme dictated the duration of signalling in the host AER (Saiz-Lopez et al., 2015). Thus, AER-Fgfs play a permissive role in PD patterning and are required for the clearance of RA in the distal mesenchyme to create a permissive environment that is required for *Hoxa13* expression (Figure 1.6.; Mercader et al., 2000, Cooper et al., 2011, Roselló-Díez et al., 2011).

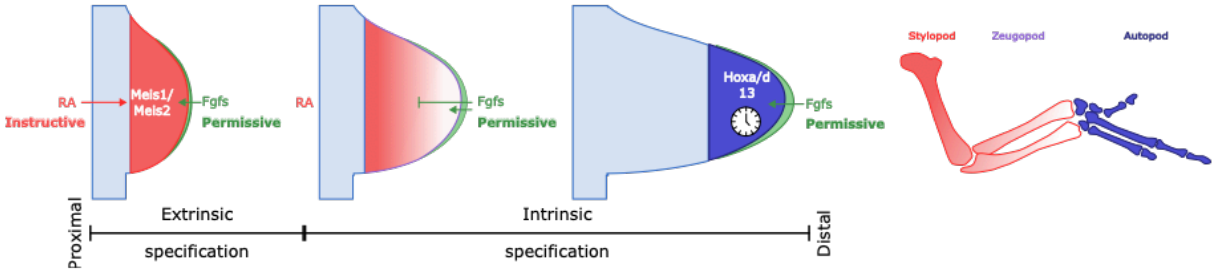

Figure 1.6. The 'signal-time' model of PD patterning.
Schematic showing the 'signal-time' model - A gradient of Meis1/2 arises due to RA signalling being antagonised distally by Fgf signalling. This gradient of Meis1/2 patterns the stylopod and zeugopod. Distally, RA is cleared from the limb by AER-Fgfs which allows for activation of *Hoxa/d13* genes which patterns the autopod. Activation of the *Hoxa/d13* genes also initiates a Bmp-dependent proliferation timer. This timer determines the duration of chick wing patterning.

More recently, it has been demonstrated that activation of *Hoxa/d13* genes results in the initiation of a Bmp-dependent proliferation timer in the distal mesoderm (Figure 1.6.; Pickering et al., 2018). This timer decreases the rate of proliferation by inhibiting the G1-S phase transition through *p57*^{kip2} expression and determines the duration of chick wing patterning (Pickering et al., 2018). Surprisingly, it has been revealed that when Fgf signalling is diminished in *ex vivo* distal limb tissue explants, distal mesoderm cells are capable of maintaining normal proliferation and differentiation (Sedas Perez et al., 2023). It was found that the distal limb tissue explants maintain expression of *Hoxd13* at levels sufficient to initiate the intrinsic distal patterning despite the absence of *Hoxa13* (Sedas Perez et al., 2023). This would suggest that Fgf signalling is dispensable for the intrinsic patterning of distal positional values once it has been activated.

1.5. AP patterning of the limb

The number and structure of the digits varies in the limbs of different species and has enabled adaptation to the environment. For example, most avian species have three digits in their wings, an adaptation which potentially enabled flight (Padian and Chiappe, 1998), whilst mice have the general mammalian pattern of five digits. Much of the work in understanding how the AP axis is patterned has emerged through studies which use the chick embryo as a model organism. Until recently, there had been contention regarding the identities of the three digits in the chick wing (i.e. relative to a 5-digit organ), which contain different numbers of phalanges (i.e. 1 phalange in the most anterior digit, 2 phalanges in the middle digit and 1 phalange in the posterior digit). It had been noted that during embryonic development rudimentary condensations form anteriorly and posteriorly to the true digit condensations. Therefore, it was postulated by developmental biologists that the wing digits were digits 2, 3 and 4 whilst the rudimentary condensations took the place of digits 1 and 5 (Burke and Feduccia, 1997). In addition, the idea that the bird wing had a digit in the fourth position was supported by the idea that a conserved 'primary axis of condensation' runs through the ulna to digit 4 in all limbs (Burke and Feduccia, 1997). This theory postulated that cartilaginous condensations in the limb develop in a highly stereotyped pattern amongst all amniotes, with the first digit condensation to appear having digit 4 identity (Shubin and Alberch, 1986). Thus, the first digit to condense - the most posterior digit in the chick wing - would have digit 4 identity and the latter two anterior digits would be digits 3 and 2 (Burke and Feduccia, 1997). However, there is no direct evidence to support this theory in the fossil record (discussed in more detail in Section 1.8.), which instead suggests that the digits in the chick wing have the identities of digits 1, 2 and 3. This proposal is supported by fate maps of mouse and chicken PRs. In the mouse, PR cells give rise to the cartilage and soft tissue of digits 4 and 5 (Figure 1.7.; Harfe et al., 2004) - the most

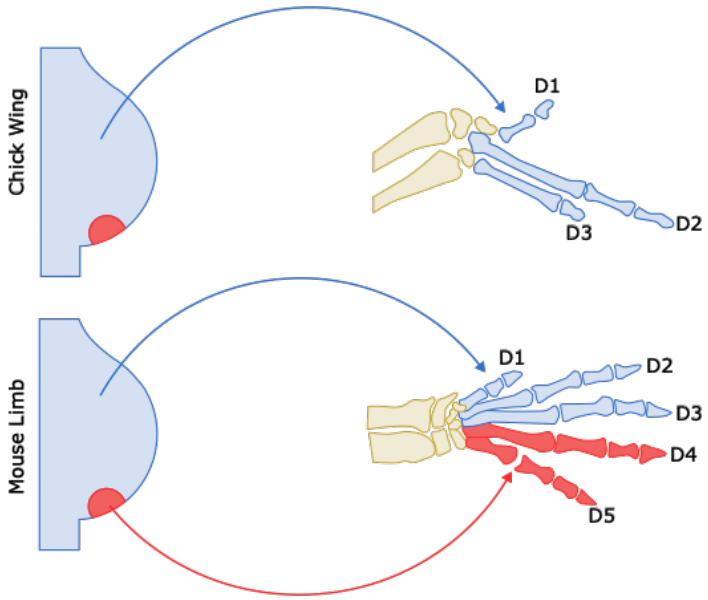

Figure 1.7. The chick wing has lost the two most posterior digits which arise from the PR in mouse limbs.
A) Schematic demonstrating that the digits of the chick wing (D1, D2 and D3) arise from mesenchyme above the PR. B) Schematic demonstrating that D1, D2 and D3 in the mouse paw arise from mesenchyme above the polarising region but D4 and D5 arise from PR cells.

posterior digits - whereas fate maps in the chick indicate that the PR only gives riseto soft tissue along the posterior margin of digit 3 (Figure 1.7.; Towers et al., 2011). Now the field generally accepts that bird wing digit identities are 1, 2 and 3. Thus for this thesis, I will be referring to the three chick wing digits as digits 1, 2 and 3.

1.5.1. The 'morphogen' model of AP patterning

Early embryological experiments on the chick wing identified an area of cells in the posterior margin which influences AP patterning. In these experiments, tissue

from the posterior chick wing was transplanted to the anterior margin of a host chick wing; this resulted in a mirror image duplication of the pattern of digits (i.e. a pattern such as 3 - 2 - 1 - 1 - 2 - 3 instead of the usual 1 - 2 - 3; Saunders Jr and Gasseling, 1968). This area of posterior tissue was termed the PR (also known as the ZPA). Following a detailed series of embryological experiments, it was proposed that the PR produces a signal or chemical morphogen, which forms a concentration gradient that specifies cells' positional values along the AP axis. Cells interpret their positional value from the gradient and differentiate into the correct digit identity (Tickle et al., 1975). Evidence suggested that a low concentration of morphogen in the anterior region of the forming limb specifies digit 1, an intermediate concentration digit 2 and a high concentration of morphogen in the posterior specifies digit 3 (Figure 1.8. A). As described above, fate-mapping has shown that the PR does not produce any digits in the chick wing (Towers et al., 2011) confirming that AP positional values are specified by long-range signal.

It was discovered that Shh is an excellent candidate for a signal involved in specifying AP position. First, *Shh* transcripts localise to the PR (Riddle et al., 1993). Second, grafting *Shh*-expressing cells to the anterior margin of the chick wing bud results in mirror image duplication of the digits (i.e. a pattern of 1 - 2 - 3 - 3 - 2 - 1 instead of the usual 1 - 2 - 3; Riddle et al., 1993), recapitulating the results of the classic grafting experiments performed by Saunders and Gasseling in 1968. Furthermore, transplanting tissue that included only a small number of PR cells or implanting beads soaked in a low concentration of Shh protein gave rise to an additional digit 1 (Tickle, 1981, Yang et al., 1997). Increasing the number of PR cells or the concentration of Shh protein specified an additional digit 2 and finally digit 3 (Tickle, 1981, Yang et al., 1997) indicating that Shh specifies AP identity in a dose-dependent manner. Wings of the *oligozeudactyly (ozd)* chicken mutant, which has undetectable *Shh* expression in the limbs due to a deletion in the ZRS enhancer (Ros et al., 2003, Maas et al., 2011), do not produce any digits in the wing, whereas only

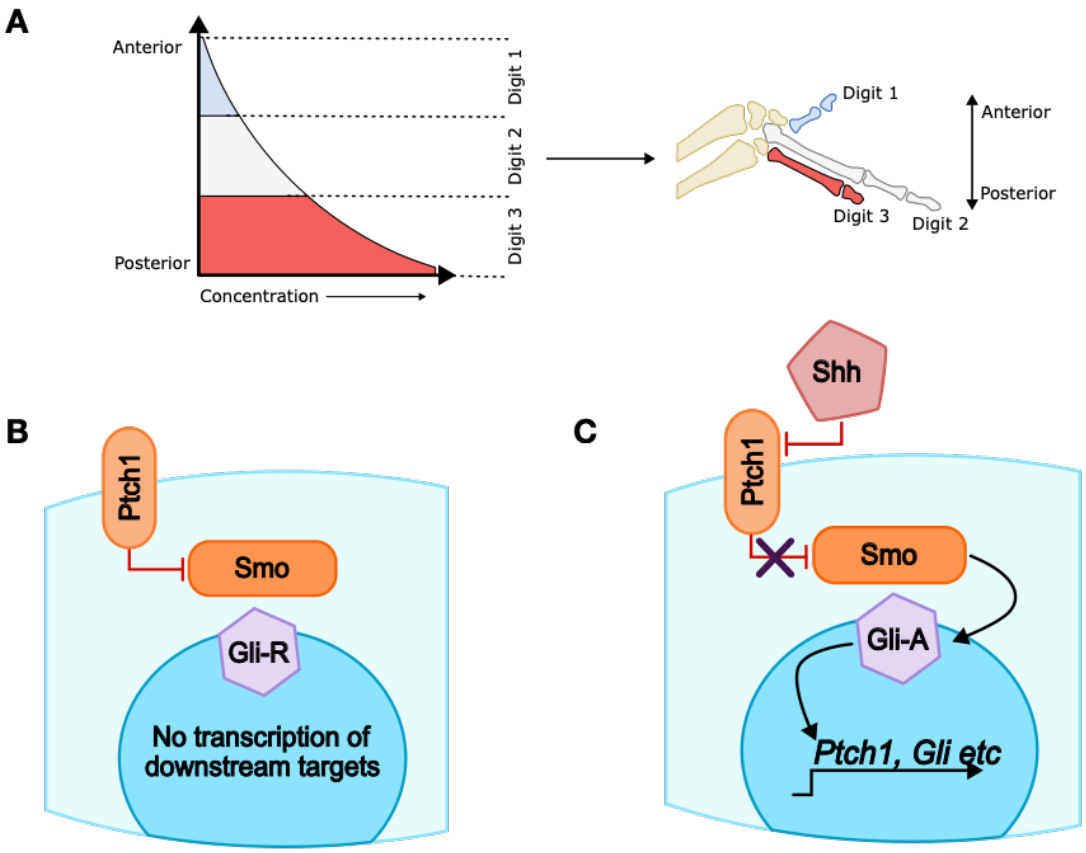

Figure 1.8. The 'morphogen' model of AP patterning and Shh signalling. A) Schematic demonstrating the 'morphogen' model. It was classically thought that the AP axis was patterned by a morphogen which was located at a source in the PR. The morphogen establishes a concentration gradient across the limb bud and different thresholds specify different positional values. A high concentration in the posterior specifies digit 3 (red), a medium concentration specifies digit 2 (grey) and the lowest concentration in the anterior specifies digit 1 (blue). B) In the absence of Shh, Patched 1 (Ptch1) inhibits Smoothened (Smo). Repressor Gli (Gli-R) is not processed and there is no transcription of downstream Shh targets. C) Shh binds to Ptch1 which releases the inhibition on Smo. Smo aids in the processing of Gli-R to the activator form of Gli (Gli-A) which then transcribes downstream targets such as Ptch1 and Gli.

the most anterior digit forms in the leg (Ros et al., 2003). This loss of digits correlates with mouse models in which Shh signalling has been genetically removed, that results in the complete loss of digits in both the forelimbs and hindlimbs (Chiang et al., 1996).

Evidence that Shh acts as a long-range signal in the limb field comes from the distribution of Glioma-associated oncogene (Gli) proteins. Gli proteins are zinc finger transcription factors in the canonical Shh-signalling pathway. In vertebrates there are three paralogs of Gli (Gli1, Gli2 and Gli3; Kinzler et al., 1988, Ruppert et al., 1990) with Gli2 and Gli3 having bi-functionality in the limb as either repressors (Gli-R) or processed into activators (Gli-A; Wang et al., 2000). In the absence of Shh, the transmembrane protein Patched 1 (Ptch1) inhibits the activity of Smoothened (Smo), a G-protein coupled receptor-like protein, which prevents the processing of Gli-R to Gli-A (Figure 1.8. B). In the presence of Shh, Ptch1 releases the inhibition on Smo which allows for the processing of Gli-R to Gli-A resulting in the transcription of Shh target genes including *Ptch1* and *Gli1* amongst others (Figure 1.8. B; Marigo et al., 1996, Lipinski et al., 2006). In the anterior limb bud, there is a high concentration of Gli-R, indicating that it has not received Shh signalling, whilst a gradient of Gli-R/Gli-A is present in the posterior limb bud, reflecting a graded response to Shh signalling (Wang et al., 2000).

1.5.2. The ‘promotion’ model of AP patterning

Although initial studies were interpreted to mean that Shh deriving from the PR acts as a spatial morphogen, early investigations into AP patterning soon established that a morphogen specifies AP positions in both a spatial and time-dependant manner. For example, it was shown that the extent of AP duplication was dependant on the length of time a grafted PR was left in place on the anterior host wing (Smith, 1980). Additionally, when a Shh-soaked bead was implanted in a developing wing bud for a short amount of time, an anterior digit with digit 1 identity developed from

adjacent cells (Yang et al., 1997). However, if the bead was left in the wing for a longer duration, cells gave rise to a digit with a more posterior digit identity (Yang et al., 1997) indicating a temporal requirement in the specification of AP positions. The process through which cells change their positional values over time in response to increasing concentration of morphogen is known as 'promotion'.

More recently, the application of cyclopamine (which inhibits Shh signalling at the level of Smo) to the developing chick embryo has given us a greater understanding into promotion of AP positional values. It was shown that increasingly more posterior digits were lost in both wings and legs the earlier cyclopamine was applied to the embryo (Scherz et al., 2007). More specifically, it was shown that 'promotion' in the chick wing takes place over the first 12 hours of Shh signalling, with more posterior-positional values being promoted every 4 hours (Figure 1.9.; Towers et al., 2011). Thus, application of cyclopamine at 4 hours after the onset of *Shh*

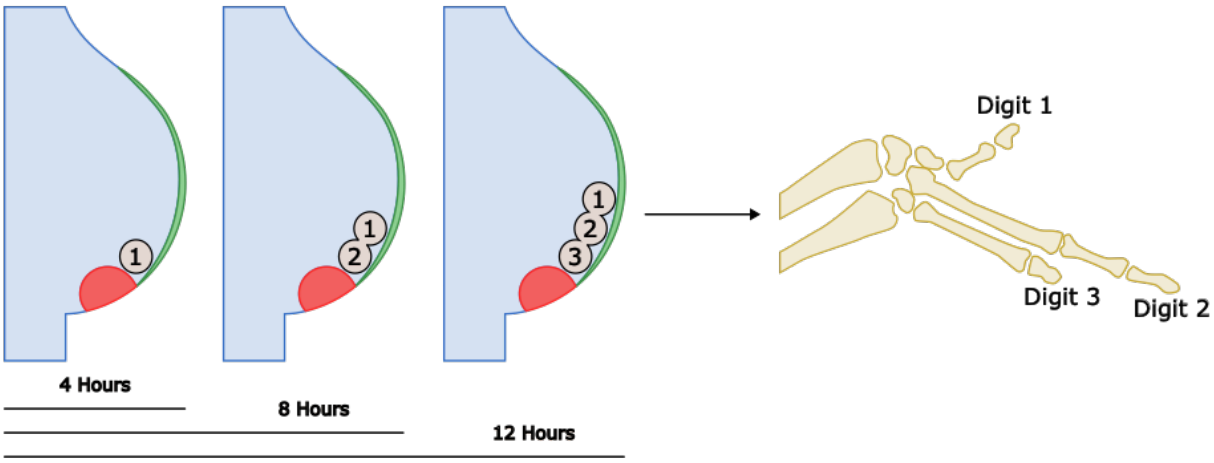

Figure 1.9. The 'promotion model' of AP patterning.
The positional identities of the chick wing are promoted every 4 hours to a more posterior fate. After 4 hours digit 1 has been specified, after 8 hours digit 1 and 2 have been specified and after 12 hours all three digits have been specified.

transcription resulted in wings with only digit 1, at 8 hours wings formed with digits 1 and 2 and at 12 hours wings formed with all three digits (Figure 1.9.; Towers et al., 2011). This result demonstrates that digit identities are promoted from anterior values to more posterior values every 4 hours in chick wing development.

1.5.2.1. Promotion to posterior fates in the chick wing requires the intermediary factor, Bmp2

Shh does not operate directly to promote posterior digits. Instead, early experiments indicated that during 'promotion' Shh signalling is required to induce and maintain *Bmp2* expression and that Bmp2 protein mediates the PR-specific promoting activity of Shh (Drossopoulou et al., 2000). It had previously been shown that Shh signalling induces expression of *Bmps* during limb development (Laufer et al., 1994, Yang et al., 1997). However, it was found that if *Bmp2*-expressing cells were transplanted in place of a Shh-soaked bead in the anterior margin of the chick wing at the beginning of 'promotion' an increased number of digits formed - often including a posterior digit 3. This suggests that Bmp signalling mediates the promoting activity of Shh in the PR (Drossopoulou et al., 2000). This was confirmed in normal development as blocking Shh signalling at the end of 'promotion' results in the loss of *Bmp2* expression and a pattern of anterior digits forming in the wing (i.e. 1 - 2 - 2 - 2 (note that an extra digit also forms when Shh signalling is blocked at this stage which I will discuss in more detail in Section 1.7.; Pickering et al., 2019). Implanting a Bmp2-soaked bead after Shh signalling has been blocked rescues digit 3 identity (i.e. 1 - 2 - 3; Pickering et al., 2019), indicating that Bmp2 is required in the developing limb to promote digit 2 identity to digit 3.

1.5.3. Shh signalling regulates proliferation across the AP axis

One of the earliest observations when grafting PRs to a host wing was that the host wing widens across the AP axis (Cooke and Summerbell, 1980, Smith and

Wolpert, 1981, Summerbell, 1981). This suggests that Shh could have a dual role in determining positional values and in promoting growth across the AP axis. More recent experiments with cyclopamine have found that blocking Shh signalling reduces the AP expansion of the wing bud (Towers et al., 2008, Towers et al., 2011). This can be explained by the observation that Shh regulates the expression of cell-cycle regulators *Cyclin D1, Cyclin D2* and *N-myc*, which all increase cell proliferation by promoting G1-S phase transition during the cell cycle (Towers et al., 2008). Expansion of the AP axis is required to provide enough tissue for positional value specification. Inhibition of growth through D-cyclin inhibitor *p21*^{cip1} results in the formation of a singular posterior digit (Towers et al., 2008). This result indicates that growth is required to expand the limb field to accommodate the full range of anterior to posterior positional values. The posterior identity of the singular digit indicates that Shh-mediated promotion was continued in the limb unaffected. Thus, Shh has a dual role in integrating proliferation and growth with digit specification.

1.5.4. AP patterning in the mouse limb

The mouse limb has the general mammalian pattern of five digits (i.e. 1 - 2 - 3 - 4 - 5) with digits 2 - 5 all having 3 phalanges, making them morphologically very similar. As mentioned in Section 1.5., fate-mapping work demonstrated that the mouse PR gives rise to the two posterior-most digits (digits 4 and 5; Harfe et al., 2004). This has led to some incompatibility between models of AP patterning proposed in the chick wing versus the mouse limb.

1.5.4.1. The ‘temporal-expansion’ model of AP patterning in the mouse limb

A ‘temporal-expansion’ model was proposed that could account for the finding that mouse digits 4 and 5 are derived from the PR (Harfe et al., 2004). In this model, long-range paracrine signalling specifies the positional values of digits 2 and 3 in a

concentration-dependent manner whilst digits 1 forms independently of Shh signalling. This conclusion was drawn as inactivation of *dispatched 1* gene, which is required for the transportation of Shh, results in the reduction of long-range Shh signalling and the loss of digit 2 (Harfe et al., 2004). The authors concluded that the more posterior digits are specified through the duration of autocrine Shh signalling, likely through a mechanism related to the proliferation of PR cells (Harfe et al., 2004). As two digits need to be specified from the same population of cells, an extended period of Shh signalling would be required in the mouse limb. *Shh* is expressed for approximately 60 hours in the mouse limb (Echelard et al., 1993), which could allow digits 4 and 5 to be specified.

1.5.4.2. The 'biphasic' model of AP patterning in the mouse limb

A later 'biphasic' model was proposed by Zhu et al. (2008) following a series of experiments in which *Shh* function was removed at different stages of mouse limb development. In this model, Shh controls limb development in two phases: an early patterning phase and an extended growth phase (Figure 1.10.; Zhu et al., 2008). In contrast to the 'temporal-expansion' model, it was found that *Shh* was required for a limited pulse to provide the mouse digits with their identity. However, it is required at later stages to promote the survival of cells and the expansion of the AP axis to produce enough cells for a full complement of digits (Figure 1.10.; Zhu et al., 2008). This conclusion was reached as the removal of *Shh* outside the patterning phase resulted in digit loss in an order which did not reflect the AP position. Instead, digits were lost in the reverse order in which the condensations arise in the limb (i.e. the first condensation to arise was only lost when *Shh* was removed early in the growth phase; Zhu et al., 2008). However, this conclusion was based on assigning the mouse digits 1 - 4 with unique identities. As mentioned, the mouse digits 2 - 5 have similar morphology, thus it is very hard to truly assign identities to the mouse digits.

More recently it has been shown, by enforcing cell survival through deletion of pro-apoptotic factors, that a 2-3 hour pulse of *Shh* expression is sufficient to produce a full complement of digits in the mouse limb (Zhu et al., 2022). However, Shh is unlikely to pattern the entire mouse limb as digits 4 and 5 (the PR digits), are the only digits responsive to direct Shh signalling during the pulse, indicating that the other three more anterior digits are specified by an unknown intermediary factor (Zhu et al., 2022). The authors do not speculate on what this intermediary factor may be. However, as discussed in Section 1.5.2.1., Bmp2 has been suggested act as an intermediary factor to specify posterior fates in the chick wing (Pickering et al., 2019), thus may have a similar role as an intermediary factor in mouse limb AP patterning.

As mentioned in Section 1.5., the morphology of digits 2 to 5 in the mouse limb are very similar - all containing 3 phalanges. Thus, it is possible to speculate that

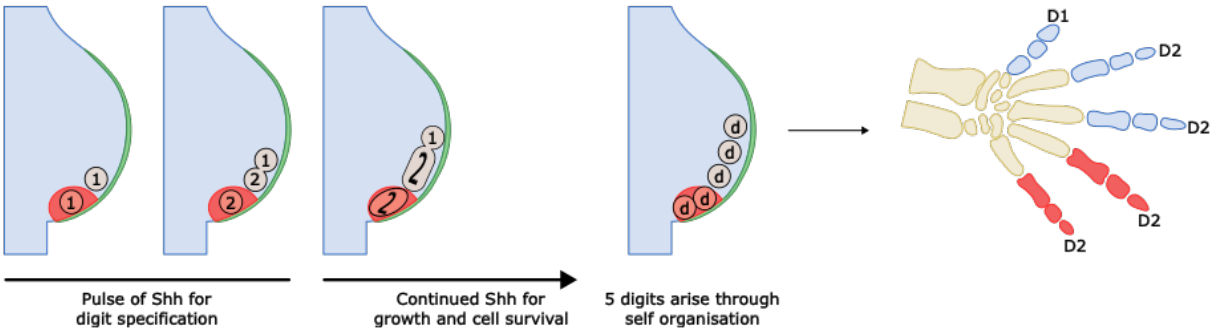

Figure 1.10. The 'biphasic' model of AP patterning in the mouse limb. Initially a short 2-3 hour pulse of Shh signalling specifies the digits with digit 1 and digit 2 identity. Shh signalling is then required to ensure cell survival and promote growth across the AP axis. The growth across the AP axis allows for 5 digits to form through a Turing-type self organisation mechanism, with digits 4 and 5 arising from the PR. Digits 2 to 4 all have three phalanges so can be assumed to have digit 2 identity.

the pulse of Shh specifies a digit 1 and a digit 2 - the 3-phalange identity - whilst continued Shh signalling supports growth across the limb field which in turn allows for the formation of multiple digits with digit 2 identity through self-organisation (Figure 1.10.; see Section 1.5.5. for more information on self-organising to form the digits). Growth across the limb field is also likely to be indirectly supported by AER-Fgfs (Pickering and Towers, 2016).

1.5.5. Forming the digits through a Turing-type self-organisation mechanism

It is important to note that patterning of the AP axis does not confer the number of digits which form from the digit-forming field. Instead, there is evidence that the periodic formation of digit condensations involves a self-organisation mechanism which functions independently of Shh signalling. It was shown that disaggregated single cells from a limb were able to form digits after being re-aggregated and placed back in an epidermal jacket (Zwilling, 1964). Furthermore, recombinant limbs made from disaggregated cells from the anterior mesenchyme of the chick limb - cells which do not normally give rise to digits nor possess PR-activity - gave rise two or three digit-like structures with similar morphology (Hardy et al., 1995, Piedra et al., 2000). These experiments demonstrated that the digits arise due to a self-organisation mechanism which can function independently of Shh signalling.

It has been suggested that the self-organisation mechanism which gives rise to the digit pattern is a Turing-type mechanism. The Turing-type self-organisation model is based upon the interactions between two diffusible molecules - an activator and an inhibitor - which produce stable patterns (Turing, 1952). The activator promotes production of the activator and the inhibitor, whilst the inhibitor inhibits the production of the activator. Thus, if the inhibitor diffuses more readily, waves of concentration differences will be generated (Turing, 1952). In the case of the digits, studies in the mouse limb have elucidated a Turing-type mechanism based on the

interactions between Wnt, Bmp and Sox9 signalling (Raspopovic et al., 2007). Here Wnt signals, which act as an inhibitor of *Sox9,* and Bmp signalling, which acts as an activator of *Sox9*, act concomitantly to modulate *Sox9* expression (Healy et al., 1999, Raspopovic et al., 2007). In the resulting pattern, *Sox9* is expressed in the pre-cartilage mesenchymal condensations which will go on to form digits (Bi et al., 1999), whilst Wnt signalling and *Bmp*, specifically *Bmp2* (Healy et al., 1999)*,* are present in the interdigital space (Raspopovic et al., 2007).

1.6. Integration of the three axes

Growth and pattern formation of the three principal axes is integrated. Not long after the identification of Shh as the signal specifying AP identities, a positive feedback loop between the AER-Fgfs, namely Fgf4, and Shh was identified. In this feedback loop, *Shh* expression is regulated by Fgf4 (Figure 1.11. A and B) with loss of the AER resulting in loss of *Shh* expression (Niswander et al., 1994). In turn, *Shh* up-regulates the AER maintenance factor - the BMP antagonist *Gremlin 1 (Grem1)* - which supports expression of *Fgf4* (Figure 1.11. A and B; Laufer et al., 1994, Niswander et al., 1994, Zúñiga et al., 1999). In addition, it has been shown that another AER-Fgf, Fgf8, is required to support and maintain expression of *Shh* in the PR (Crossley et al., 1996, Mariani et al., 2008).

However, experiments in which Shh signalling was inhibited in chicks has demonstrated that Shh is not required for the maintenance of *Grem1* after early limb bud stages (Pickering and Towers, 2016). Instead, inhibition of Shh signalling results in the expansion of *Grem1* expression into the PR domain (Pickering and Towers, 2016). Expansion of *Grem1* into the PR domain is also observed in the *ozd* mutant, which completely lack Shh function (Ros et al., 2003, Maas et al., 2011). Thus, Shh signalling is not required for *Grem1* expression in the limb bud at later stages of development (Figure 1.11 C), indicating the feedback loop operates at early stages but is then dispensable for limb development.

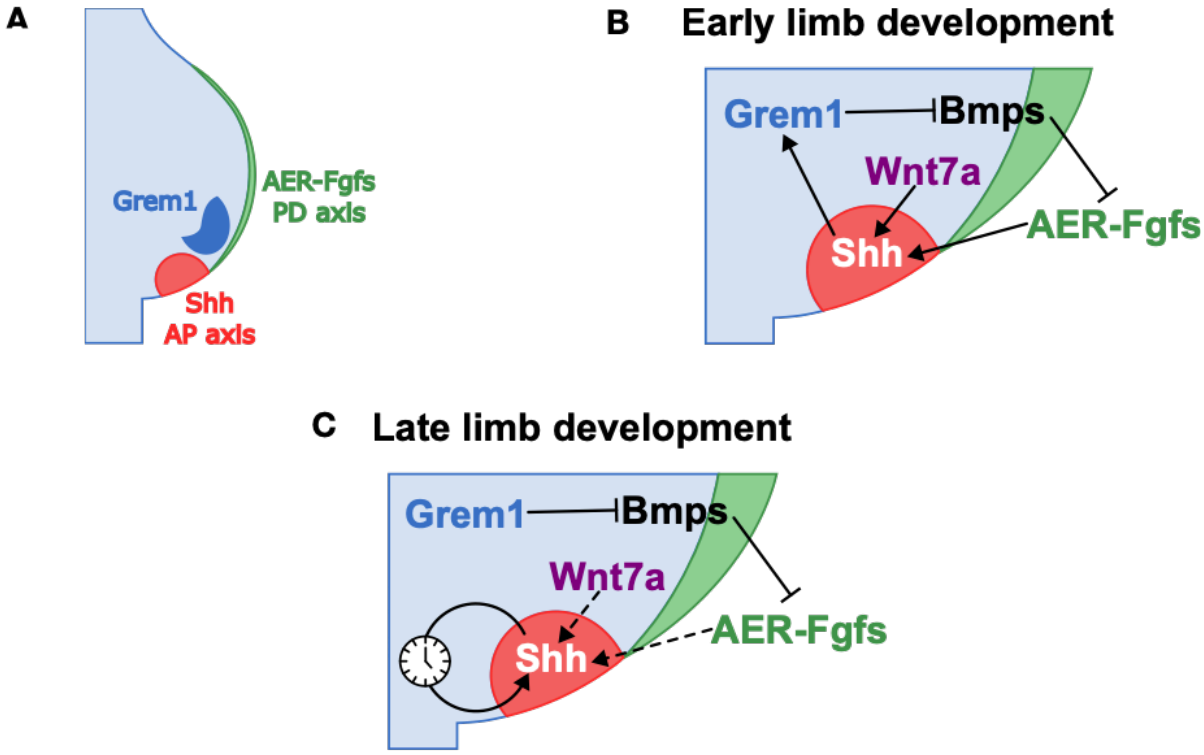

Figure 1.11. The three axes of the limb are integrated.
A) Schematic showing the expression patterns of *AER-Fgfs* (PD axis), *Shh* (AP axis) and *Grem1* (mesenchyme) which form a positive feedback loop in the limb. B) During early limb development a positive feedback loop functions between Shh/ Grem1/AER-Fgfs. In this loop, Shh up-regulates *Grem1* expression which in turn acts as a Bmp antagonist allowing for *Fgf* expression in the AER. AER-Fgfs and Wnt7a (dorsal ectoderm) have been shown to maintain Shh signalling in the PR. C) In later limb development, Shh is no longer required to maintain *Grem1* expression and thus, the Shh/Grem1/AER-Fgf feedback loop is broken. The PR intrinsically maintains *Shh* expression however it is not clear if AER-Fgfs and Wnt7a are required permissively for *Shh* expression in the PR.

It was also noted that implanting beads of *Fgf4* in chick wings results in increased activation of Shh on the dorsal side of the limb compared to the ventral (Yang and Niswander, 1995). Additionally, removal of the dorsal ectoderm dramatically reduces *Shh* expression, however, this could be rescued by the

transplantation of *Wnt7a* expressing cells (Yang and Niswander, 1995). Thus, it was concluded that Wnt7a, the dorsalising factor of the DV axis, is required concomitantly with Fgf4 signalling to maintain *Shh* expression in the limb (Figure 1.11. B; Yang and Niswander, 1995).

1.6.1. Termination of *Shh* expression may be intrinsically regulated by the PR

It had been proposed that the termination of *Shh* expression was a result of the breakdown of Fgf4/Shh/Grem1 feedback loop signalling which would occur due to the expansion of cells. However, as already discussed, the Fgf4/Shh/Grem1 signalling is dispensable for later stages of limb development (Figure 1.11. C). Furthermore, application of deacetylase inhibitor trichostatin A (TSA) - which inhibits proliferation through inducing $p21^{cip1}$ transcription - prolonged *Shh* expression in the chick wing (Towers et al., 2008), indicating that the duration of *Shh* expression is dependent on a timing mechanism. Additionally, heterochronic grafts (i.e. transplanting a PR to a host wing of an older stage chick) have demonstrated that the duration of *Shh* expression in the PR is intrinsically determined, as PR cells continue to express *Shh* consistent with their own age, not the host age (Chinnaiya et al., 2014). This demonstrated that *Shh* expression in the PR is not dependent on signalling from the Shh/Grem1/Fgf4 feedback loop, instead the duration of Shh signalling is intrinsically determined within PR cells (Figure 1.11. C).

1.7. The role of Shh signalling within chick wing PR cells

As described above, a major difference between chick wing and mouse forelimb development is the ability of the mouse PR to produce digits. Fate-mapping of the PR reveals that PR cells in the chick wing only contribute to the soft tissue along the posterior margin of digit 3 (Towers et al., 2011), whilst PR cells in the mouse forelimb form digits 4 and 5 (Harfe et al., 2004). However, application of

cyclopamine to chick wings to inhibit Shh signalling at HH20/21 can result in wings with an extra digit (Figure 1.12. A.; Pickering and Towers, 2016, Pickering et al., 2019). This is surprising as application of cyclopamine to younger embryos results in the loss of digits (discussed in Section 1.5.2.; Towers et al., 2011) and so the authors examined from where this extra digit arose. By grafting *Green-Fluorescent Protein (GFP)*-expressing PRs in place of a wildtype host PR and applying cyclopamine it was determined that the extra digit arose from PR cells themselves (Pickering and Towers, 2016). Furthermore, the additional digit often had the identity of digit 2 (Figure 1.12. A and C.; Pickering and Towers, 2016), indicating that specification of digits 1 and 2 had occurred before Shh signalling was inhibited. As already discussed in Section 1.5.2.1., inhibition of Shh signalling prevents the promotion of digit 2 to digit 3 due to the loss of *Bmp2* expression (Pickering et al., 2019). Thus, the resulting wing had a more mammalian-like pattern of digits (i.e. 1 - 2 - 2 - 2), where digits 2 - 4 were all morphologically similar (Figure 1.12. A and C; Pickering and Towers, 2016, Pickering et al., 2019). In summary, these experiments indicate that while the chick PR does not normally form a digit, it can do so under experimental conditions where Shh signalling is inhibited.

A potential mechanism has been uncovered through the analyses of the cell cycle. Using flow cytometric analysis, it was inferred that during normal development PR cells gradually decrease their cell cycle rate by extending the length of G1-phase of the cell cycle (Figure 1.12. B; Chinnaiya et al., 2014). Interestingly, it has been demonstrated that PR cells intrinsically regulate their own proliferation. Young PRs (i.e. HH20) grafted in place of PRs in older host wings (HH24) and left for 24 hours maintain their ‘young’ rate of proliferation rather than adopting the proliferation rate of

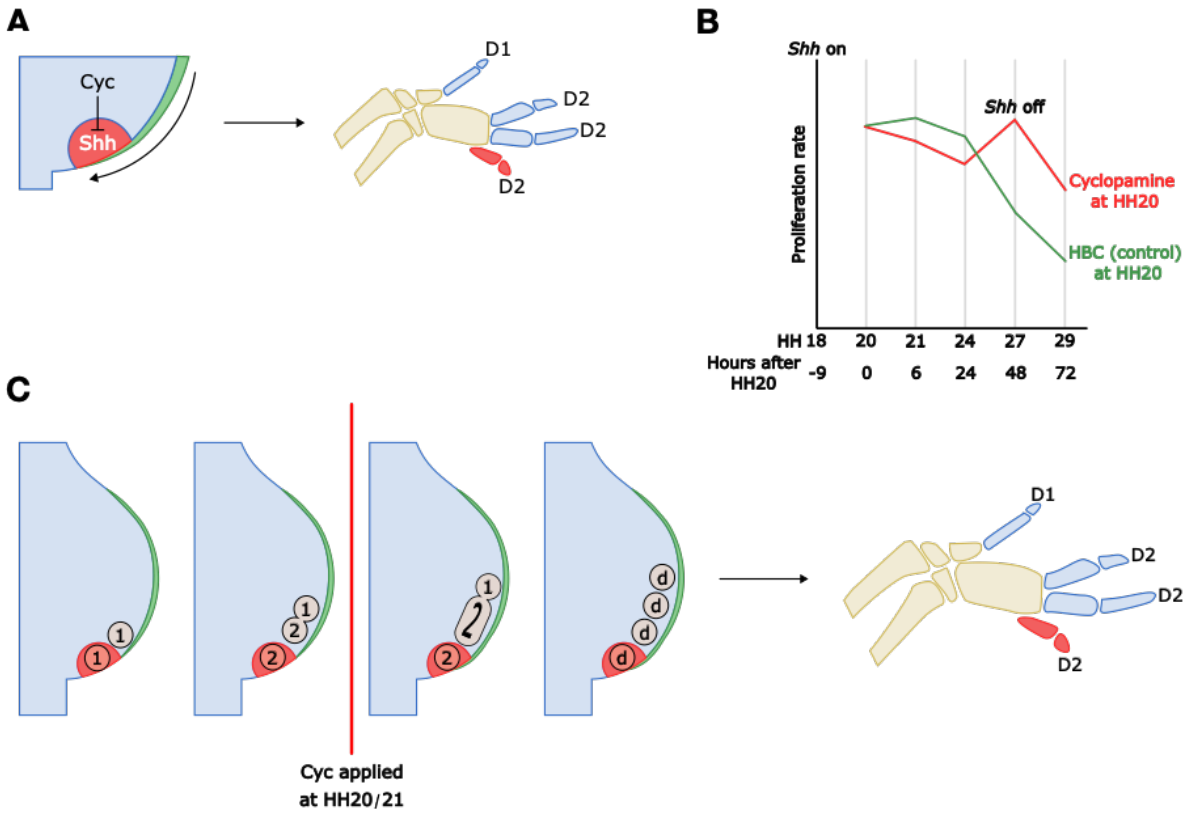

Figure 1.12. Inhibiting Shh signalling in the chick wing PR at HH20/21 results in over-proliferation and the formation of a PR-derived digit.
A) Inhibiting Shh signalling in the PR of a chick wing at HH20/21 results in the extension of the AER over the PR and the formation of a PR-derived digit (red digit). Digits 2 to 4 are morphologically similar so have the same digit 2 identity. B) In control PRs (green), proliferation rates remain high over the first 24 hours after treatment with HBC but then decrease. When Shh signalling is blocked with cyclopamine (red), proliferation rates decrease over the first 24 hours but increase between 24 and 48 hours. After *Shh* expression switches off proliferation rates decrease in both controls and cyclopamine treated PRs. Figure edited from Pickering et al. (2019). C) Applying cyclopamine at HH20/21 stops specification of digits when digit 1 and digit 2 have been specified. The AP axis expands due to the extended AER which allows for two digits with digit 2 identity to form via self-organisation. PR cells, which have been specified as digit 2 identity, over-proliferate and form an ectopic digit. This is also supported by the extended AER. The resulting wing has four digits with a 1 - 2 - 2 - 2 pattern of digits. Wing with extra digit traced from Pickering and Towers (2016).

the older host (Chinnaiya et al., 2014). This indicates that proliferation rates of PR cells are intrinsically regulated. Applying cyclopamine at HH20 initially decreases the rate of PR proliferation over 24 hours followed by an increase between 24 and 48 hours (Figure 1.12. B; Pickering and Towers, 2016, Pickering et al., 2019). Together this indicates that Shh signalling intrinsically regulates the PR proliferation parameters, preventing over-proliferation of cells and the formation of a digit.

The same study noted that application of cyclopamine to chick wings at HH20/21 led to the extension of the AER posteriorly over the PR (Figure 1.12. A; Pickering and Towers, 2016). This indicates that Shh signalling inhibits the formation of an AER over the chick PR. It was also observed that inhibition of Shh signalling results in the expansion of *Grem1* expression into the PR area (Pickering and Towers, 2016), which suggests that *Grem1* expression supports the extension of the AER. It had been previously suggested that the AER supports the development of the PR-derived posterior digits in the mouse limb as here it overlaps the PR (Pickering and Towers, 2016). When the extended region of AER was removed from the cyclopamine-treated wing, a three-digit wing formed. However, the contralateral cyclopamine-treated wing still formed an extra digit (Pickering and Towers, 2016), indicating that the extension of the AER supports the formation of a PR-derived ectopic digit in cyclopamine-treated chick wings. Furthermore, it was found that removal of the extended AER resulted in PR cells proliferating at a slower rate than the PR cells in contralateral wings where the AER was left intact (Pickering and Towers, 2016). This result suggests that the over-proliferation of PR cells in cyclopamine treated wings is supported by the extended AER.

Thus, it was concluded that inhibiting Shh signalling at HH20/21 halts specification when cells have acquired digit 1 and digit 2 identity (Figure 1.12. C). The AP axis subsequently expands due to the extended AER, increasing the field of cells which have been specified digit 2 to a size where two digits can be formed by self-organisation (Figure 1.12. C; see Section 1.5.5. for more information on digit

formation; Pickering and Towers, 2016). At the same time, PR cells - which have been specified as digit 2 - over-proliferate, which is supported by the extended AER. As a result, a PR-derived digit forms with digit 2 identity (Figure 1.12. C; Pickering and Towers, 2016). Thus, in normal chick wing development a PR-derived digit does not form as over-proliferation does not occur. This is in part due to the inhibition of the AER forming over the PR (Pickering and Towers, 2016), however, it has also been suggested that Shh signalling intrinsically prevents the PR from over-proliferating. One potential mechanism is suggested by the observation that regulators of G1-S phase entry are specifically expressed in the chick wing PR (Pickering et al., 2019).

1.7.1. Shh signalling regulates a cell cycle mechanism controlling proliferation of the PR cells in the chick wing

Insight into how Shh signalling may intrinsically regulate proliferation was provided by earlier experiments which demonstrated that Shh controls the expression of genes which promote G1-S phase transition within the PR specifically. As mentioned in Section 1.5.3., Shh controls the expression of *Cyclin D1, Cyclin D2* and *N-Myc*, with *Cyclin D2* being expressed within the PR at HH20/21 and in an area overlapping the PR at HH24 (Towers et al., 2008). Blocking Shh signalling with cyclopamine results in the immediate loss of *Cyclin D2* expression from within the PR which explains the initial decrease in PR proliferation (Pickering and Towers, 2016).

Shh signalling also regulates the expression of D cyclin-dependent kinase inhibitors, which inhibit the activity of D cyclins thus inhibiting the G1-S phase transition and subsequently slowing proliferation (Sherr and Roberts, 1999). Expression of $p27^{kip1}$, a member of cyclin dependent kinase inhibitor (CDKI) family, is specifically restricted to the PR between HH20 and HH27 (Pickering et al., 2019). Intriguingly, $p27^{kip1}$ expression is not lost immediately after cyclopamine is applied but is lost approximately 30 hours after treatment (Pickering et al., 2019). This would

explain the increase in proliferation seen between 24 and 48 hours after cyclopamine treatment (Pickering and Towers, 2016). Additionally, application of PD0332991 - a drug which universally inhibits D cyclin/cyclin-dependent kinase complexes - following cyclopamine treatment prevents over-proliferation and the formation of an extra digit (Pickering et al., 2019). This suggests that D cyclin inhibition through *p27^{kip1}* is crucial for the normal development of the chick wing.

The delay in the attenuation of *p27^{kip1}* expression after blocking Shh signalling may indicate that *p27^{kip1}* is regulated through an intermediary factor. Bmp2 was identified as a possible intermediary factor due to Bmps being capable of regulating *Cip/Kip* family transcription (Nakamura et al., 2003) as well as being known as a transcriptional target of Shh in the limb (Yang et al., 1997). Furthermore, *Bmp2* is expressed in a domain that encompasses the PR from HH16 to HH25/26, when it spreads more distally (Francis et al., 1994). Beads soaked in recombinant Bmp2 protein were able to induce expression of *p27^{kip1}* in the PR of cyclopamine treated wings (Pickering et al., 2019) indicating that Bmp2 is the intermediary factor between Shh and *p27^{kip1}* expression.

The results described above led to the identification of a cell cycle mechanism which explains how Shh intrinsically regulates proliferation parameters in the chick wing PR. In this mechanism, Shh initially up-regulates proliferation through Cyclin D1 and Cyclin D2 (Pickering et al., 2019). Whilst Cyclin D1 promotes proliferation throughout the limb field, Cyclin D2 specifically 'fine-tunes' proliferation of PR cells (Figure 1.13. A; Pickering et al., 2019). In conjunction with this, Shh up-regulates the Bmp2-p27^{kip1} pathway in PR cells. By acting through an intermediary factor, Shh is able to temporally regulate *p27^{kip1}* expression enabling a gradual decrease in the proliferation rate of PR cells (Figure 1.13. A). This Bmp2-p27^{kip1} pathway is crucial in preventing over-proliferation of PR cells, increased growth along the AP axis and the formation of an ectopic PR digit (Pickering et al., 2019). Thus, through G1-S phase

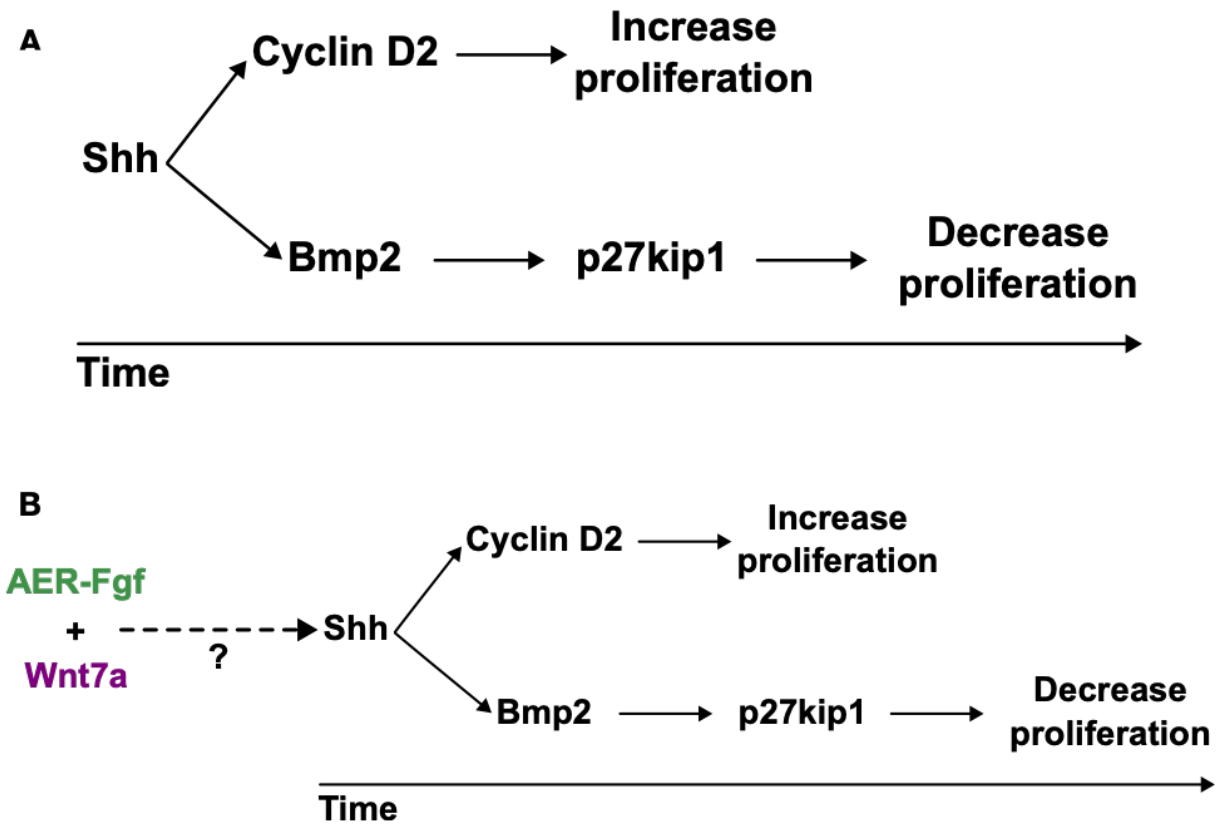

Figure 1.13. Shh temporally regulates proliferation of PR cells.
A) Schematic demonstrating how Shh regulates proliferation in chick wing PR cells. Shh up-regulates Cyclin D2 which causes an increase in proliferation. Additionally Shh up-regulates Bmp2 which in turn up-regulates $p27^{kip1}$ causing a decrease in proliferation. The Shh-Bmp2-$p27^{kip1}$ pathway is slower than the Shh-Cyclin D2 pathway meaning the decrease in proliferation occurs later in PR development. B) It is unknown whether AER-Fgfs/Wnt7a are required to maintain *Shh* expression in the PR and thus their role in this mechanism is unknown.

regulators, Shh signalling intrinsically controls the rate and duration of PR cell proliferation.

1.7.2. Intrinsic regulation and extrinsic factors affecting PR development

Although the PR intrinsically regulates PR proliferation parameters and the duration of Shh signalling, extrinsic factors may also play a role in PR development. As described in Section 1.6., the limb signalling centres do not function independently. Whilst it has been demonstrated that AER-Fgfs and Wnt7a from the dorsal ectoderm are required to maintain Shh signalling during early limb development (Laufer et al., 1994, Niswander et al., 1994, Yang and Niswander, 1995, Crossley et al., 1996, Zúñiga et al., 1999, Scherz et al., 2004, Mariani et al., 2008) it is unlikely that they play the same instructive role during later stages of limb development. Moreover, it is not clear whether AER-Fgfs and Wnt7a play an instructive or permissive role in the proliferation mechanism discussed in Section 1.7.1. (Figure 1.13. B) as more recent experiments in both mouse and chick have indicated that the duration of *Shh* expression and proliferation may be intrinsically regulated (Towers et al., 2008, Chinnaiya et al., 2014) with AER-Fgfs playing a more permissive role (Pickering and Towers, 2016; Figure 1.13. B). However, due to the essential role of AER-Fgfs *in vivo,* studies to elucidate the actual roles of the PR and AER are very difficult.

To truly understand the intrinsic development of the PR, it would need to be studied in isolation, i.e. apart from the AER and *Grem1*-expressing cells. In 2023, to circumvent the essential requirement of the AER *in vivo*, a chick wing tissue explant model was developed by the Towers lab (Sedas Perez et al., 2023). The explants, which consist of the posterior-distal tissue of HH20 chick wings cultured in Matrigel, maintain *in vivo* proliferation and differentiation parameters (Sedas Perez et al., 2023). By utilising the explant system, the authors found that Fgf signalling after HH22 was dispensable for proliferation and differentiation of the underlying

mesoderm (Sedas Perez et al., 2023). It was concluded that AER-Fgfs play an essential role in *in vivo* limb development, but this can be bypassed using an *ex vivo* explant system. Thus, such a system may be useful in understanding the intrinsic development of the PR.

1.8. The evolution of the three-digit bird wing

As discussed above the chick wing utilises Shh signalling to intrinsically and temporally regulate PR cell proliferation to prevent the formation of a PR-derived digit. This is unlike the mouse limb, whereby the PR produces two digits (i.e. digits 4 and 5; Harfe et al., 2004). Since the common ancestor of birds and mammals likely had five digits (Carroll, 1969, Smithson et al., 1993), it is possible that birds evolved this proliferation mechanism to limit the number of digits in their wings to enable flight (Padian and Chiappe, 1998). The reduction of digit number in the avian wing can be traced back through the fossil record to the earliest ancestral dinosaurs of the late Triassic period when Ornithischians, such as *Heterodontosaurus* (Norman et al., 2011) and Saurischians, such as *Herrerasaurus* (Novas, 1994) diverged. Fossils of both *Heterodontosaurus* and *Herrerasaurus* display reduced digits 4 and 5 (Figure 1.14.; Novas, 1994, Norman et al., 2011) indicating that this was a trait in their common ancestor. The stem clade Saurischians diverged into three groups, including Theropoda (Weishampel et al., 2004). Fossils of the late theropod *Dilophosaurus* display forelimbs in which digit 5 has been entirely lost and digit 4 is vastly reduced (Figure 1.14.; Welles, 1984, Marsh and Rowe, 2020). *Dilophosaurus* is thought to be a close ancestor of theropods, the Tetanurans and the Ceratosaurs (Weishampel et al., 2004). The late Tetanuran theropod *Allosaurus* exhibited complete loss of digit 4 in the forelimb and reduction of digit 5 to single metacarpal in the hind limb (Figure 1.14.; Madsen, 1976). From the Tetanuran clade arose the Avialae group which rapidly diversified at the beginning of the Cretaceous period (Godefroit et al., 2013). The Avialae includes the famous *Archaeopteryx* which supports the direct link between modern birds and their dinosaur ancestors (Ostrom, 1974). *Archaeopteryx*

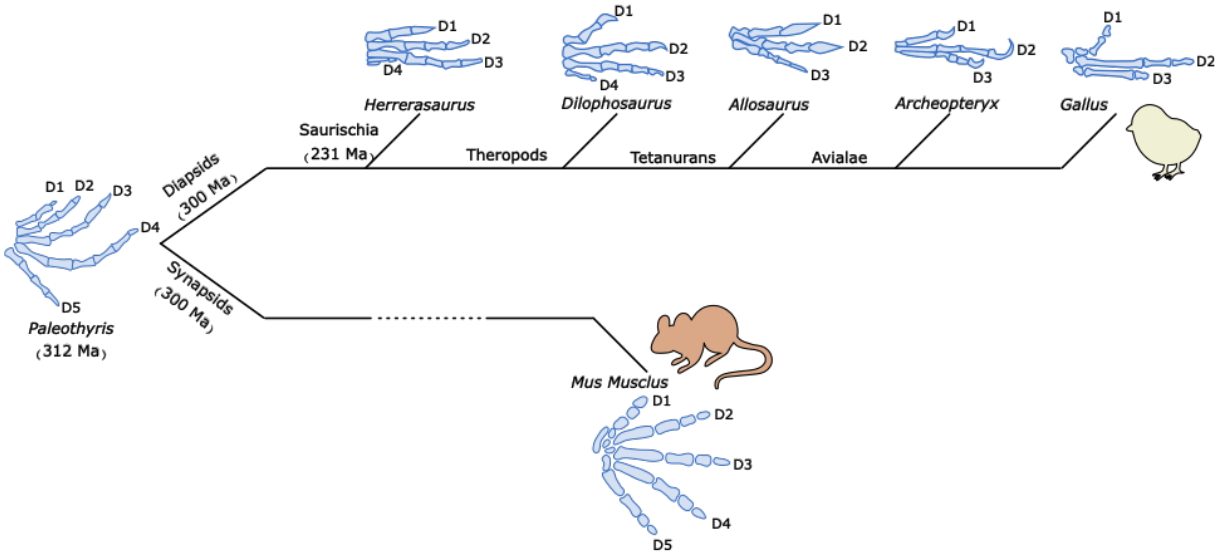

Figure 1.14. Evolution of the bird wing
Schematic demonstrating the evolution of the three-digit bird wing through a selection of fossilised dinosaurs/birds. Approximately 300 million years ago the Synapsid and Diapsid groups diverged. The Synapsid group gave rise to mammals such as the mouse which retains the pentadactyly ancestral state. The Diapsid group gave rise to birds which lost digit 4 and 5 in the wing. Schematic simplified from Towers, 2018

fossils exhibit 3 digits in their forelimbs and 4 digits in their hindlimbs (Figure 1.14.; Ostrom, 1974). This digit configuration is also seen in modern birds and allows for the specialised shape of wings for flight (Padian and Chiappe, 1998). Therefore, by following the loss of digits in the fossil record we can determine that the posterior digits 4 and 5 have been lost in the modern-day bird wing.

1.8.1. A potential evolutionary mechanism functions in the PR of the chick wing

As described in Section 1.5., the PR of mouse limbs, which retain the ancestral pentadactyl ground state, gives rise to digits 4 and 5 (Harfe et al., 2004). By examining the fossil record, it has been determined that digits 4 and 5 are not

present in the chick wing and this has been confirmed by fate-mapping (see Section 1.5.; Towers et al., 2011). We can postulate that the PR of the limbs of the common ancestor of birds and mammals produced two digits, namely digits 4 and 5.

Inhibiting Shh signalling through cyclopamine results in the formation of a digit from the PR cells in the chick wing and a more mammalian-like pattern of digits (see Section 1.7.; Pickering and Towers, 2016). This may suggest that the PR of bird wings has evolved the mechanism described in Section 1.7.1. to prevent the formation of PR-derived digits. In this mechanism, Shh signalling promotes proliferation of PR cells through *Cyclin D2* expression. Subsequently, Shh signalling down-regulates proliferation through a Bmp2-$p27^{kip1}$ pathway which prevents over-proliferation of cells and the formation of an extra digit. Additionally, Shh signalling prevents the extension of the AER posteriorly over the PR, further moderating proliferation of PR cells.

However, this mechanism which prevents the PR cells of the bird wing from producing digits has not been fully resolved. In particular, it is not clear whether the PR is an intrinsic developmental unit regulating Shh signalling duration and proliferation or whether it is influenced by extrinsic factors such as Wnt7a, Grem1 and AER-Fgfs. Furthermore, if the PR is an intrinsic developmental unit, the extent to which Shh intrinsically regulates proliferation through cell cycle regulators is unknown. Furthermore, it is unknown if Shh signalling affects extrinsic factors within the PR cells. Lastly, there has not been any investigation to determine whether the regulation of proliferation through cell cycle regulators in the chick wing PR is an avian-specific trait or if this mechanism is also present in mammalian species.

1.9. Aims of the thesis

- I hypothesise that the PR can function as an intrinsic developmental unit, regulating duration of Shh signalling and proliferation rates as suggested by

Chinnaiya et al (2014; discussed in Section 1.6.1. and 1.7.). Thus, in this thesis I aimed to adapt the chick wing explant model in Sedas Perez et al. (2023) to develop a chick wing PR explant system. This PR explant system would allow me to determine the patterning, proliferation and growth parameters of the developing PR without influence from extrinsic factors which would be present *in vivo*.

- Secondly, I used the chick wing PR explant model to determine the functional consequences of inhibiting Shh signalling pathway during chick wing development. Based on *in* vivo evidence discussed in Section 1.7., I hypothesise that inhibiting Shh signalling would result in the reduction of the Bmp2-$p27^{kip1}$ pathway and the subsequent over-proliferation of cells in the PR explant.

- Lastly, I aimed to determine if the intrinsic control of proliferation in the PR through cell cycle regulators, including Cyclin D2 and $p27^{kip1}$, is an evolutionary adaptation of the avian wing. To do this, I aimed to examine the expression of cell cycle regulators in the PR during the development of the mouse forelimb. By examining the fossil record and fate-mapping studies performed by Towers et al. (2011) and Harfe et al. (2004), I hypothesise that, at the very least, the Bmp2-$p27^{kip1}$ pathway which leads to a decrease in proliferation in the chick wing PR, is greatly reduced or absent in the mouse PR.

CHAPTER 2

Materials and Methods

2.1. Avian embryo husbandry

2.1.1. Incubation of avian embryos

Fertilised wild type chicken eggs (gallus gallus) were obtained from Medeggs Ltd. (formerly Henry Stewart and Co., Norfolk, UK). *GFP*-expressing chicken embryos were obtained from The Roslin Institute (University of Edinburgh, Edinburgh, UK; McGrew et al., 2008).

Eggs were incubated on their side in a Panasonic MIR-262-PE incubator set to 37ºC with 95% humidity. All experiments involving live chick embryos were carried out in accordance with the relevant regulatory standards (University of Sheffield, Sheffield, UK).

At day 3 incubation (72 hours), eggs were windowed. Blunt forceps were used to make a small hole in the base of the egg and approximately 2ml of albumen was removed by syringe. The eggs were laid sideways in an egg tray and another small hole was made by blunt forceps on top of the egg. This small hole was covered over by tape and the eggs returned to the incubator for the remainder of their incubation.

2.1.2. Removal of embryos from the egg

At the appropriate time points, scissors were used to cut a hole in the egg to access the developing embryo. Embryos were then removed from the egg and placed in a petri dish containing phosphate-buffered saline solution (PBS). Membranes were carefully removed using sharp forceps.

The embryos were then staged according to Hamburger-Hamilton system (Hamburger and Hamilton, 1951) to determine if they were the appropriate age. Due to variability in early development stages, some embryos were discarded if deemed underdeveloped, overdeveloped or had notable developmental defects.

2.1.3. Fixation of avian embryos

For embryos fixed straight out of the egg, the head and internal organs were removed, and the embryos were fixed in 4% Paraformaldehyde (PFA) at 4ºC.

2.2. Mouse embryos

Mouse (mus musculus) embryos were obtained from the Mary Lyon centre at MRC Harwell (Oxford, UK). Mouse embryos were also gifted from Marian Ros (Institute of Biomedicine and Biotechnology of Cantabria, Santander, Spain).

2.3. PR explants

2.3.1. Dissecting PRs for explant

PRs were dissected from embryos at approximately HH20/21 at 3.5 days into incubation. To dissect the PR, embryos were transferred to a petri dish containing a bed of 1.5% agarose and PBS topped with 1% Dulbecco's Modified Eagle Medium (DMEM; Gibco). Embryos were laid out, so the dorsal side faced upwards and the limb buds were outstretched. The embryo was secured with insect pins. Using a sharp dissection knife, two small cuts were made into the posterior margin of the wing bud. A further cut was made parallel to the two cuts, so a small square of tissue could be excised from the wing bud. The location of these cuts was based upon the approximate location of *Shh*-expressing cells from in situ hybridisations for *Shh* (see Figure 3.2. in Section 3.2.1.) and diagrams from Maccabe et al. (1973).

2.3.2. Culturing PR explants in Type I Collagen

To prepare the collagen, 135µl Type 1 Collagen (Corning), 30µl 10X DMEM (Gibco) and 7.5µl $NaCHO_3$ was combined. In each well of a four-well plate, a bed of 30µl of the collagen mix was allowed to set at room temperature for another 30 - 40 minutes. Four PR explants were then placed atop each of the collagen beds and covered with another layer of the collagen mix which was allowed to set at room temperature for another 30 - 40 minutes. The explants were cultured in CMRL media (Gibco) supplemented with 10% fetal bovine serum (FBS; Sigma), 1% Pen-strep and 1% L-glutamine in a Sanyo CO_2 MCO-17AI humidified incubator at 37ºC and 5% CO_2.

At the relevant time, explants were removed from the incubator. A square was cut in the collagen around the explant using a sharp knife. Collagen squares containing explants were fixed in 4% PFA and then stored at 4ºC.

2.3.3. Culturing PR explants in Matrigel

In each well of a four well plate, a bed of 20µl Growth Factor Reduced Matrigel (Corning) was prepared and allowed to set for 30 - 40 minutes in an incubator set at 37ºC. Four explants were placed atop each of the Matrigel beds and covered with another layer of Matrigel which was allowed to set for another 30 - 40 minutes in an incubator set at 37ºC. The explants were cultured in CMRL media (Gibco) and supplemented with 10% FBS (Sigma-Aldrich), 1% Pen-strep and 1% L-glutamine in a Sanyo CO_2 MCO-17AI humidified incubator at 37ºC and 5% CO_2.

At the relevant time, explants were removed from the Matrigel by replacing the CMRL media with Cell Recovery Solution (Corning) on ice for 1 hour. Explants were then fixed in 4% PFA and stored at 4ºC.

2.3.4. Shh signalling inhibition

Cyclopamine (Sigma) was dissolved in a control carrier of 45% 2-hydropropyl-β-cyclodextrin (HBC; Sigma) in PBS to a concentration of 1µg/µl. Cyclopamine was further diluted to a concentration of 20µM with supplemented CMRL (see Section 2.3.2.) and applied to explants embedded in Matrigel.

2.3.5. Measuring the size of PR explants

Brightfield images of explants in culture were taken on a Leica MZ16F microscope and LAS X1.1.0.12420 imaging software. Images were taken at 24-hour intervals. The surface area of each explant was calculated using the Record Measurement feature of the Lasso tool in Adobe Photoshop 2024. Statistical analysis was performed in Prism 10.1.0.

2.4. Analysis of gene expression

2.4.1. Conventional *in situ* hybridisation

Conventional *in situ* hybridisation was performed on whole mount embryos prepared as described in Section 2.1.3..

2.4.1.1. Ribonucleic acid (RNA) probe synthesis

Plasmid deoxyribonucleic acid (DNA) in vectors were transformed into *E.coli* DH5α competent cells, plated in LB agar with ampicillin antibiotic and cultured overnight at 37ºC. The following day one colony was selected per transformation and inoculated in LB broth with ampicillin antibiotic and incubated overnight at 37ºC on a shaking platform. Plasmid purification was performed with a QIAGEN mini-prep kit.

DNA templates were subsequently generated using a restriction enzyme reaction or a polymerase chain reaction (PCR).

2.4.1.2. Obtaining a DNA template through PCR

To extract the template and amplify it, M13 forward and reverse primers were used with 25-50ng of plasmid. Biomix (Biotin) was used as the PCR master mix and MilliQ (MQ) water was added to bring the reaction volume to 50µl. PCR machine settings are as follows:

- 94ºC 5 minutes
- 94ºC 1 minute (denature)
- 55ºC 1 minute (anneal primers)

- 72ºC 40 seconds (extension)
- Repeat steps 2-4 34x
- 72ºC 10 minutes (elongation)
- Hold at 4ºC

The resulting template DNA was purified with a GeneJet purification kit with all steps carried out in accordance with the manufacturers protocol.

2.4.1.3. Obtaining a DNA template through restriction enzyme reactions

At least 5µg of plasmid DNA was linearised with the relevant restriction enzyme (see Table 2.1.), Buffer and bovine serum albumin (all NEB) in a reaction totalling 50µl. The reaction was incubated at 37ºC for between 1 and 4 hours. The resulting template DNA was purified with GeneJet purification kit, and all steps were carried out in accordance with the manufacturers protocol.

Table 2.1. Anti-sense probes used in this thesis.

Probe name	Species	Restriction enzyme	RNA polymerase	Source (many thanks to the following labs)
Shh	Gallus gallus	Sal1	Sp6	Cheryl Tickle
Shh	Mus musculus	HindIII	T3	Marysia Placzek
Bmp2	Mus musculus	XbaI	T3	Marysia Placzek
P27	Mus musculus		T7	Matthew Towers
Cyclin D1	Mus musculus	XbaI	T3	Marian Ros
Cyclin D2	Mus musculus	XbaI	T7	Marian Ros

2.4.1.4. Synthesising the digoxigenin (DIG)-labelled riboprobes

DNA templates (1µg) were used to synthesise anti-sense DIG-labelled ribiprobes through *in vitro* transcription in a 20µl reaction. Roche 10x transcription buffer (2µl), RNase inhibitor (1µl; NEB), the appropriate RNA polymerase (2µl; see table 2.1.) and DIG label mix (2µl; Roche) were added to DNA template, which was then topped to 20µl with diethylpyrocarbonate (DEPC)-treated MQ water. Reactions were incubated at 37ºC in a heat block for 2 hours before the probes were purified using the Illustra ProbQuant G-50 Micro Column (GE) in accordance with the manufacturers protocol. Probes were diluted with 5ml of pre-hybridisation buffer (50% formamide / 50% 2X sodium chloride/sodium citrate (SSC)) and stored at -20ºC.

2.4.1.5. Whole mount *in situ* hybridisation for chick embryos

Fixed embryos (see Section 2.1.3.) were washed twice with 0.1% PBS/Tween 20 (PBST) before being taken through a series of dehydrating washes in methanol (25%, 50%, 75% and 100%). These embryos were stored overnight in 100% methanol at -20ºC.

Embryos were rehydrated through a series of methanol washes (75%, 50%, 25%) before two washes in PBST. Proteinase K (1:2000; Sigma) was applied to the embryo. The length of this was dependant on the age/type of tissue being washed:

- 1 minute per stage up to stage 25 for whole mount tissue.
- 10 minutes for limb buds or explants.

Embryos were washed in PBST to halt the proteinase K, post-fixed at room temperature in 4% PFA (30 minutes) and pre-hybridised with pre-hybridisation buffer

(50% formamide / 50% 2X SSC). Antisense DIG-labelled probes in pre-hybridisation buffer (1µg/1ml) were incubated with the embryos at 69ºC overnight.

On the subsequent day, embryos were washed twice in pre-hybridisation buffer at 69ºC, twice in 50:50 pre-hybridisation / malic acid buffer containing Tween 20 (MABT) at 69ºC and then twice in MABT at room temperature. Embryos were then places in blocking buffer (2% blocking reagent (Roche), 20% FBS (Sigma), 80% MABT for 3 hours at room temperature before being transferred to blocking buffer with anti-DIG antibody (1:2000; Roche) and gently rocked overnight at 4ºC.

Embryos were washed with MABT which was replaced every hour at least 5 times and again gently rocked overnight at 4ºC.

To visualise the mRNA distribution, embryos were washes twice in NTMT (100mM NaCl, 100mM Tris-HCl (pH 9.5), 50mM $MgCl_2$) before being transferred to NTMT containing Nitro Blue tetrazolium (NBT) and 5-bromo-4-chloro-3-indolyl-phophate (BCIP; both Roche). This was allowed to develop in the dark at room temperature. When the stain had fully developed, embryos were washed in 5X Tris-buffered saline with Tween 20 (TBST) in PBS and images were taken using a Leica MZ16F microscope and LAS X1.1.0.12420 imaging software.

2.4.1.6. Whole mount *in situ* hybridisation for mice

Fixed embryos were washed twice with 0.1% PBST before being dehydrated through a series of increasing methanol washes (25%, 50%, 75% and 100%) and stores in 100% methanol at -20ºC for at least overnight.

Embryos were rehydrated through a series of decreasing methanol series (75%, 50% and 25%) before being washes twice in PBST and washed further in

Proteinase K (1:2000; Sigma). The length of this wash depended on the age of the mouse embryo:

- 9.5 dpc: 15-minute wash
- 10.5+ dpc: 20-minute wash

Embryos were then rinsed in PBST, post-fixed in 4% PFA and rinsed again in PBST before a 1:1 PBS / pre-hybridisation buffer wash and a pre-hybridisation wash (all washes performed at room temperature). The pre-hybridisation buffer was replaced with fresh pre-hybridisation buffer and incubated for 2 hours at 69ºC before being replaced with pre-warmed pre-hybridisation buffer containing 1µg/ml antisense DIG-labelled probe and incubated for up to 48 hours at 69ºC.

Following this, embryos were washed twice with pre-hybridisation buffer at 69ºC, once with 1:1 pre-hybridisation buffer / MABT at 69ºC and three times with MABT. Embryos were then washed for an hour with MABT / 2% blocking reagent (Roche) and for a following hour with mat / 2% blocking reagent / 20% FBS. Embryos were then incubated overnight in MABT / 2% blocking reagent / 20% FBS containing anti-DIG antibody (1:2000; Roche) at 4ºC.

On the subsequent day, embryos were washed with fresh MABT every 1.5 hours at least 5 times. Embryos were left in MABT for between 24 - 72 hours at 4ºC.

To visualise the mRNA distribution, embryos were transferred to NTMT then to NTMT containing NBT / BCIP and kept in the dark until the colour developed. When the colour had reached the desired effect the embryos were washed with 5X TBST and images were taken using a Leica MZ16F microscope and LAS X1.1.0.12420 imaging software.

2.4.2. Hybridisation chain reaction fluorescence *in situ* hybridisation

Fixed tissue (see Section 2.3.2. and 2.3.3.) was washed twice in 0.1% PBST before being taken through a series of dehydrating washes in methanol (25%, 50%, 75% and 100%). The tissue was stored in 100% methanol overnight at -20ºC.

The following day explants were rehydrated through a series of methanol (75%, 50% and 25%) washes on ice before being washed twice with PBST at room temperature and treated with proteinase K (1:2000) for 3 minutes. The tissue was then post-fixed in 4% PFA at room temperature, washed twice with PBST on ice, once with 1:1 5X SSCT (SSC with Tween 20) on ice. Explants were incubated with hybridisation chain reaction (HCR) hybridisation buffer (molecular instruments) on ice and then at 37ºC for 30 minutes. HCR probes (molecular instruments) were added to HCR hybridisation buffer at a concentration of 4µl probe per 250µl hybridisation buffer then applied to the tissue which was incubated overnight at 37ºC.

Following this, explants were washed four times in HCR wash buffer (molecular instruments) at 37ºC. Whilst washes were ongoing, amplification hairpins (molecular instruments) were snap-cooled by heating them at 95ºC for 90 seconds and allowing them to cool in a dark drawer for 30 minutes. Whilst the hairpins were cooling, the tissue was washed twice in 5X SSCT and pre-incubated with amplification buffer (molecular instruments). Once cool, hairpins were added to fresh amplification buffer (1µl per 100µl) which was then applied to the tissue. The tissue was subsequently incubated in the dark overnight on a gentle shaking platform.

Explants were then washed in 5X SSCT, followed by a wash in SSCT/PBST and a wash in PBST before being imaged on Zeiss Apotome 2 microscope using Axiovision software (Zeiss).

2.5. Analysis of the cell cycle

2.5.1. Measuring cell cycle rate

Embryos were collected at the relevant time and dissected in a Petri dish containing PBS, then transferred to a petri dish containing a bed of 1.5% agarose and PBS topped with 1% DMEM. Embryos were outstretched and pinned with insect pins. Using Maccabe et al. (1973) and *Shh in situ* hybridisations (See Figure 3.1. in Chapter 3) as a guide, 150 - 200µm blocks of tissue were dissected at the approximate location of the PR. Tissue from 12 embryos were pooled for each repeat of the experiment. For explants cell cycle analysis, explants were taken from Matrigel using Cell Rescue Solution. For each repeat, 12 explants were pooled. The tissue was then transferred to 0.05% trypsin (Gibco) and gently pipetted to begin disaggregation. The tissue blocks/explants were then left in trypsin at room temperature for 30 minutes to allow for continued disaggregation. The disaggregated cells were then pelleted at 7000rpm for 5 minutes at 4ºC in a 5417R centrifuge. Trypsin was then removed, and PBS was added to the pelleted cells. The cells were then centrifuged again, and the PBS removed. The pellets were resuspended in 70% ethanol and stored at least overnight at -20ºC.

On the day of the flow cytometry analysis, cells were centrifuged then resuspended in 0.5ml of staining buffer (50µg/µl propidium iodide (Roche), 50µg/µl RNase (Sigma) and 0.1% Triton X (Sigma)).

Analysis of the cell cycle was performed at the Flow Cytometry core facility at the University of Sheffield, the proportion of cells in G1-phase, S-phase and G2-M-phase were determined from 10,000 cells gated for analysis, and statistical analysis was performed in Prism 10.1.0.

2.5.2. EdU labelling

Explants were removed from Matrigel (described in Section 2.3.3.) and incubated in 0.5mM ethynyl-2'-deoxyuridine (EdU) in CMRL for 4 hours at 37ºC. The explants were then post-fixed with 4% PFA (15 minutes) and washed with 3% FBS / PBS at room temperature. The explants were permeabilised with 0.5% Triton X-100 in PBS before being incubated in a click-kit reaction cocktail containing Azide Dye (Molecular Probes) in the dark and washed with 3% FBS/PBS counterstained with DAPI (1:1000). This was followed by three washes in 3% FBS/PBS before imaging. Fluorescent images the explants labelled with EdU/DAPI were taken on a Zeiss Apotome 2 microscope using Axiovision software (Zeiss).

Quantification of the percentage of Edu positive area compared to the DAPI area was performed using a macro created for ImageJ v 2.14.0 (FIJI). Binary masks of the DAPI and EdU positive area in the Z-stack (approximately 25 - 35 slices) were created using the Moments Auto Threshold function, then the area of DAPI in the Z-stack was measured using the Analyse Particles in the EdU mask. Another Analyse Particles command in the EdU mask measured the area of EdU within the area of DAPI. Finally, statistical analysis was performed using Prism 10.1.0.

2.6. Explant grafts

Explants made from either wildtype or *GFP*-expressing chicken embryos were removed from Matrigel after 24 hours incubation (described in Section 3.1.2.). Explants were kept on ice in Cell Rescue during the procedure.

In a petri dish containing 90% ethanol, 25µm platinum wire was cut into small lengths and bent into "L" shape using two pairs of forceps. Explants and "L"-shaped pins were placed together into a petri dish containing DMEM. The "L"-shaped pins are used to skewer the explants.

A small hole was cut in the top of the HH21/22 wild type chick egg using scissors. The vitelline membrane and amnion above the wing bud was removed with forceps. A block of tissue of approximately 200μm by 200μm was removed either in the anterior or in the posterior margin of the limb bud with a sharpened tungsten needle.

The explant affixed to the “L”-shaped pin was lifted into the host egg and then manoeuvred with the pin using forceps. The explant was pushed into the hole made in the limb bud and secured with the “L”-shaped pin. If necessary, another “L”-shaped pin was added to secure larger explants to the limb. A few drops of DMEM containing ampicillin were added to the host egg which was then resealed with Sellotape and returned to the incubator for 6 days.

2.7. Cartilage staining

Embryos were collected on day 10 of incubation and dissected in PBS. The head and internal organs were removed from the embryo. The embryo was then fixed overnight in 90 - 100% ethanol.

The following day, the embryos were placed into 0.05% Alcian blue staining solution (0.05% Alcian blue powder (Sigma) / 20% acetic acid / 80% ethanol; pH 2.5) and left overnight.

The Alcian blue stain was replaced with 100% ethanol for 2 hours, then this was replaced with 50% ethanol for 2 hours which was subsequently replaced with 100% water for 2 hours. The embryos were then placed in 0.1 - 1% KOH which was refreshed over the following 1 - 3 days until the embryo cleared. Embryos were then imaged on a Leica MZ16F microscope using LAS X1.1.0.12420 imaging software before being stored in 50% glycerol in PBS.

CHAPTER 3

Developing an *in vitro* chick wing PR explant model

3.1. Introduction

As outlined in the Introduction Section 1.6., during limb development the PR and the AER maintain each other's activity via reciprocal signalling. Furthermore, the AER plays an essential role in maintaining outgrowth of the limb. For example, removal of the AER results in the truncation of the chick wing along the PD axis (Saunders Jr, 1948, Mariani et al., 2008). Moreover, Fgf signalling from the AER is essential for the maintenance of the PR, with the mechanical removal of the AER resulting in the loss of *Shh* expression (Niswander et al., 1994). This essential requirement for the AER in PR development means that these organisers cannot easily be studied in isolation *in vivo* and, thus understanding their relative roles and contributions is very difficult.

Recently, a chick wing tissue explant system was developed to investigate if the essential role of AER-Fgfs for *in vivo* development could be bypassed (Sedas Perez et al., 2023). To achieve this, the posterior-distal third of HH20 chick wings were dissected and cultured as explants in Matrigel. It was shown that explants maintain *in vivo* proliferation and differentiation parameters. In addition, important patterning genes including for instance, *Hoxa13, Hoxd13, Shh* and *Bmp2* maintain *in vivo* expression timing in explants (Sedas Perez et al., 2023). Furthermore, it was revealed that Fgf signalling after HH22 is disposable for proliferation and differentiation timing of the underlying mechanism (Sedas Perez et al., 2023). This was revealed by the mechanical removal of the AER and the addition of SU5402, which blocks Fgf signalling. However, the removal of Fgf signalling also results in a loss of *Shh* expression (Sedas Perez et al., 2023), again indicating the important role that the AER-Fgfs plays in maintaining PR activity. Nonetheless, the authors concluded that although AER-Fgf-PR-Shh signalling plays essential roles in *in vivo* development they can be bypassed in an *ex vivo* system.

Whilst useful in demonstrating the power of the explant system to bypass essential *in vivo* requirements, this study did not directly examine PR development. In my thesis, I aimed to develop a chick wing PR explant system without adjacent mesoderm and the AER. I hypothesised that the PR could operate as an intrinsic developmental unit as an explant thereby allowing me to determine its patterning and growth parameters.

3.2. Results

3.2.1. Dissection of the chick wing PR to make explants

Previous studies have shown that the chick wing bud becomes visible as a small swelling on the flank of the embryo at HH16 (2.5 DOI) and that expression of *Shh* can be detected in the PR mesoderm at HH18 (3.0 DOI). *Shh* is then

Figure 3.1. In vivo *Shh* marks the PR from HH1 to HH28.
A) Schematic demonstrating the approximate location of the PR in the chick wing bud between HH17 and HH22. Schematic enhanced from Maccabe et al. (1973) and not to scale. B) Whole mount *in situ* hybridisation for *Shh* was performed on chicken embryos at various Hamburger-Hamilton stages. Expression of *Shh* in cells along the posterior edge of the is present at HH20/21 and is down-regulated at approximately HH27/28. Scale bars: Whole embryo = 1mm, inset limb buds = 500μm

continuously expressed for approximately 72 hours until HH27/28 (5.5 - 6.0 DOI) when it is down regulated, becoming completely undetectable in the posterior margin of the wing bud by HH28/29 (6.0 - 6.5 DOI; Riddle et al., 1993). My first aim was to determine a time point at which I might be able to routinely and cleanly dissect out the PR. I therefore analysed the expression of *Shh* by whole mount chromogenic *in situ* and examined published schematics of the PR in the chick wing (Figure 3.1. A and B; Maccabe at al., 1973). Between HH16 and HH19 the wing bud is very small and has not expanded sufficiently across the AP axis. Thus, I concluded that it would be very difficult to cleanly remove the PR from surrounding mesenchyme and AER between these stages via mechanical dissection (Figure 3.1. A). By HH20/21 the

wing bud is larger and has a convex shape with a distinct posterior margin on which the PR is located (Figure 3.1. A and B). The larger size and the distinct posterior margin made it easier to locate and dissect the PR cleanly. Thus, I concluded that the earliest stage at which I might be able to routinely dissect the PR from surrounding tissues was HH20/21 (Figure 3.1. A and B). Note for the remainder of this thesis, I will refer to HH20/21 as the 0-hour time point for PR explants.

To further aid with pinpointing the PR - with a view to isolating it cleanly - I next performed RNA-fluorescence *in situ* hybridisation using hybridisation chain reaction (HCR RNA-FISH), simultaneously examining expression of *Shh* and *Fgf8* in HH20/21 wing buds. This revealed that the distal edge of the *Shh*-expressing PR abuts the *Fgf8*-expressing AER (Figure 3.2. A and B). These markers would therefore allow me

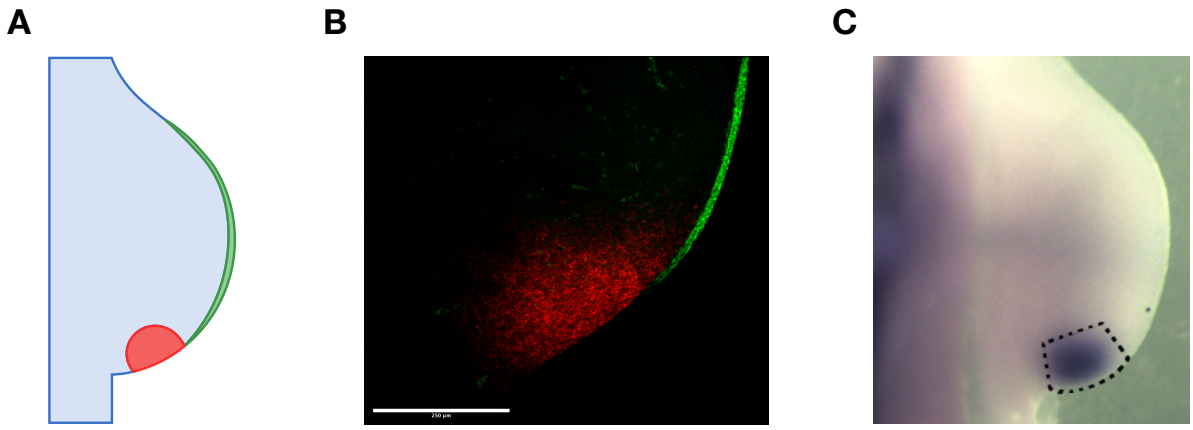

Figure 3.2. Relative positions of the PR and AER.
A) Schematic of the relative positions of the PR (red) and AER (green)). B) HCR RNA-FISH demonstrating the relative positions of *Shh*-expressing PR cells (red) and *Fgf8*-expressing AER cells (green) in a HH21 chicken embryo. Scale bar = 250 µm. C) Whole mount *in situ* hybridisation for *Shh* at 0 hours. Dashed black line indicates domain explanted in future experiments.

to ascertain that I could obtain a clean dissection of the PR at 0 hours, with reference to the adjacent AER (Figure 3.2. C).

Using the approach outlined above, I dissected the PR from the surrounding mesoderm and adjacent AER. To confirm that my dissection was clean, a subset of such explants were analysed immediately post-dissection (i.e. 0 hours; Figure 3.3. A). Simultaneous HCR RNA-FISH of *Shh* and *Fgf8* expression of the explanted region indicates that the PR was cleanly dissected (Figure 3.3. B). Thus, although the dissected tissue consistently expressed *Shh* (Figure 3.3. C'; n = 13/13), *Fgf8* expression was undetectable in the majority of explants (Figure 3.3. C' and Table 3.1; n = 10/13). To determine if I was dissecting the PR independently of more-anterior mesoderm, I analysed *Grem1* expression. *Grem1* is not expressed in mesoderm immediately adjacent to the PR, but it is found in more central regions of the wing bud (Merino et al., 1999). *Grem1* expression was undetectable in the PR explants (Figure 3.3. C'; n = 13/13). However, when I took a slightly larger explant (as a positive control) containing more-anterior tissue there was clear expression of *Grem1* anterior to *Shh* expression (Figure 3.3. C''; n = 4/5). These results therefore indicate that I can cleanly dissect the HH20/21 PR, in a manner that excludes more-anterior mesenchyme and the AER, most of the time.

Table 3.1. Quantification of the number of explants *Shh*+/- and *Fgf8*+/-.

	Shh+ / Fgf8-	***Shh+ / Fgf8+***	***Shh- / Fgf8+***	***Shh- / Fgf8-***
Tissue at dissection	10/13	3/13	0/13	0/13

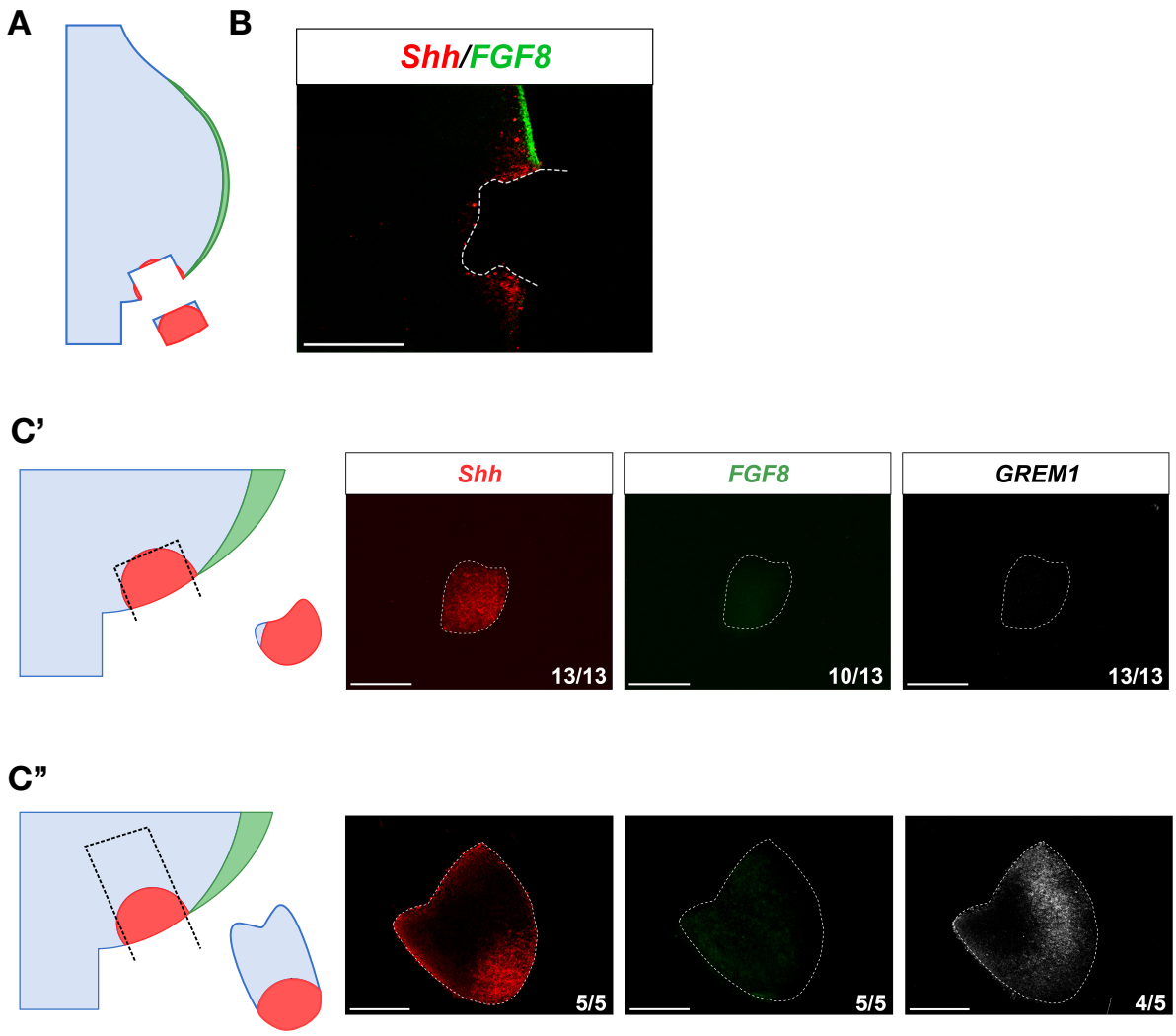

Figure 3.3. Dissecting the PR.
A) Schematic demonstrating the dissecting of the PR from a HH21 chick wing. B) HCR RNA-FISH of *Shh* (red; PR cells) and *Fgf8* (green; AER cells) in the limb bud after the PR has been removed. C) HCR RNA-FISH of PR cells after dissection from a HH20/21 limb bud. C' - PRs dissected correctly express *Shh* (n=13/13) and do not express *Grem1* (n=13/13). The majority of the PR dissections do not have visible *Fgf8* expression (n=10/13). C" - Dissections which include more-anterior mesoderm express *Shh* along the posterior edge (n=5/5), *Grem1* in a domain more anterior to the PR (n=4/5) and do not express *Fgf8* (n = 5/5). All scale bars = 250μm.

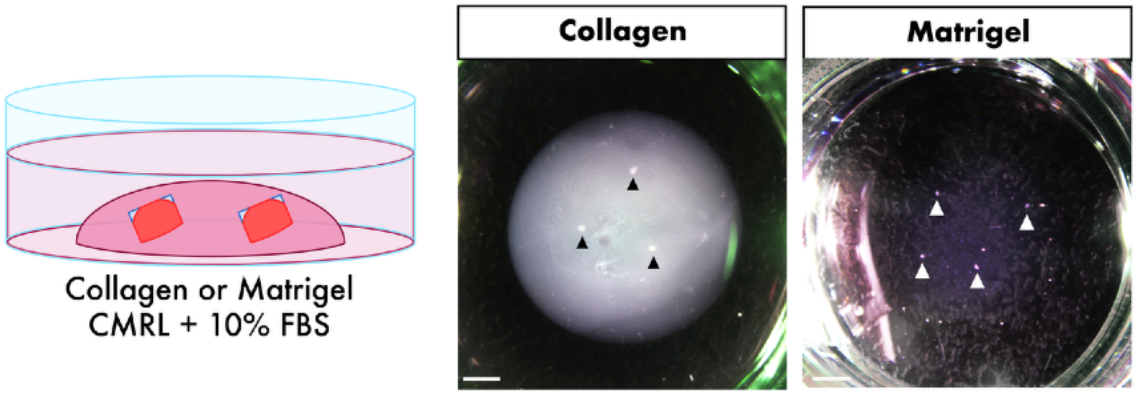

Figure 3.4. Culturing the dissected PR.
Schematic showing dissected PR embedded in Collagen/Matrigel and incubated with CMRL + 10% FBS/1%L-glutamine/1%Penstrep. Brightfield images show explants embedded in culture. Scale bar = 1mm.

I next set out to culture PR explants. In the original explant procedure (Sedas Perez et al., 2023) explants were cultured in Matrigel. However, due to the worldwide shortage of Matrigel after the Covid-19 pandemic, I initially cultured the explants in Type 1 Collagen. However, Matrigel became my preferential culturing matrix when it became available, due to the ease with which explants could be removed with Cell Rescue Solution for further analysis. Thus, most of the work was performed in Matrigel and I will note whenever PR explants have been cultured using Type 1 Collagen. In both cases, explants were incubated with an aqueous CMRL media supplemented with 10% FBS / 1% L-glutamine / 1% Pen Strep (Figure 3.4.).

I first examined if PR explants are viable and are able to grow, by measuring their surface area every 24 hours. When incubated in Type 1 Collagen, there was a significant increase in the size of explants over the first 24 hours of incubation (Figure

3.5. B; $p = 0.0141$), however there was no significant change in explant size between 24 and 48 hours ($p > 0.05$). Similarly, when PR explants were cultured in Matrigel there was a significant increase in the size of explant in the first 24 hours of incubation (Figure 3.5. C; $p = 0.0342$) and there was no significant change in explant size between 24 and 48 hours ($p > 0.05$). To examine whether there was a significant difference in explant size between culturing conditions, I compared the results of Matrigel and Collagen. There was no significant difference in the surface area of the PR explants cultured in either matrix at 0 hours (n = 7 - 28, $t(33) = 0.8594$, $p = 0.3963$), at 24 hours (n = 7 - 30, $t(35) = 0.0025$, $p = 0.9980$) or at 48 hours (n = 7 - 15, $t(20) = 0.4490$, $p = 0.6583$). Therefore, it appears that PR explants are equally viable in Type 1 Collagen and Matrigel.

3.2.2. Comparing *in vivo* and *ex vivo* PR development

To determine if PR explants maintain *in vivo* developmental timing parameters, I determined if they express *Shh* for the same duration as is seen *in vivo* and if they maintain proliferation rates in a manner that mimics that *in vivo*. I therefore cultured explants for a period of 24 hours (bringing them to the equivalent HH24), 48 hours (equivalent to HH27/28) or 72 hours (equivalent to HH29).

I then performed HCR RNA-FISH assays on explants cultured Type 1 Collagen. My results showed that *Shh* is strongly expressed in PR explants at 24 hours - equivalent to HH24 (Figure 3.6. A and B; n = 42/42). Similarly, at 48 hours - equivalent to HH27/28 - *Shh* expression is present in PR explants (n = 15/15). Interestingly, *Shh* expression is restricted to an increasingly smaller proportion of the PR explant over time. By 72 hours - equivalent to HH29 - *Shh* is undetectable in PR explants (Figure 3.6. A and B; n = 12/12). Therefore, in the explants, *Shh* is

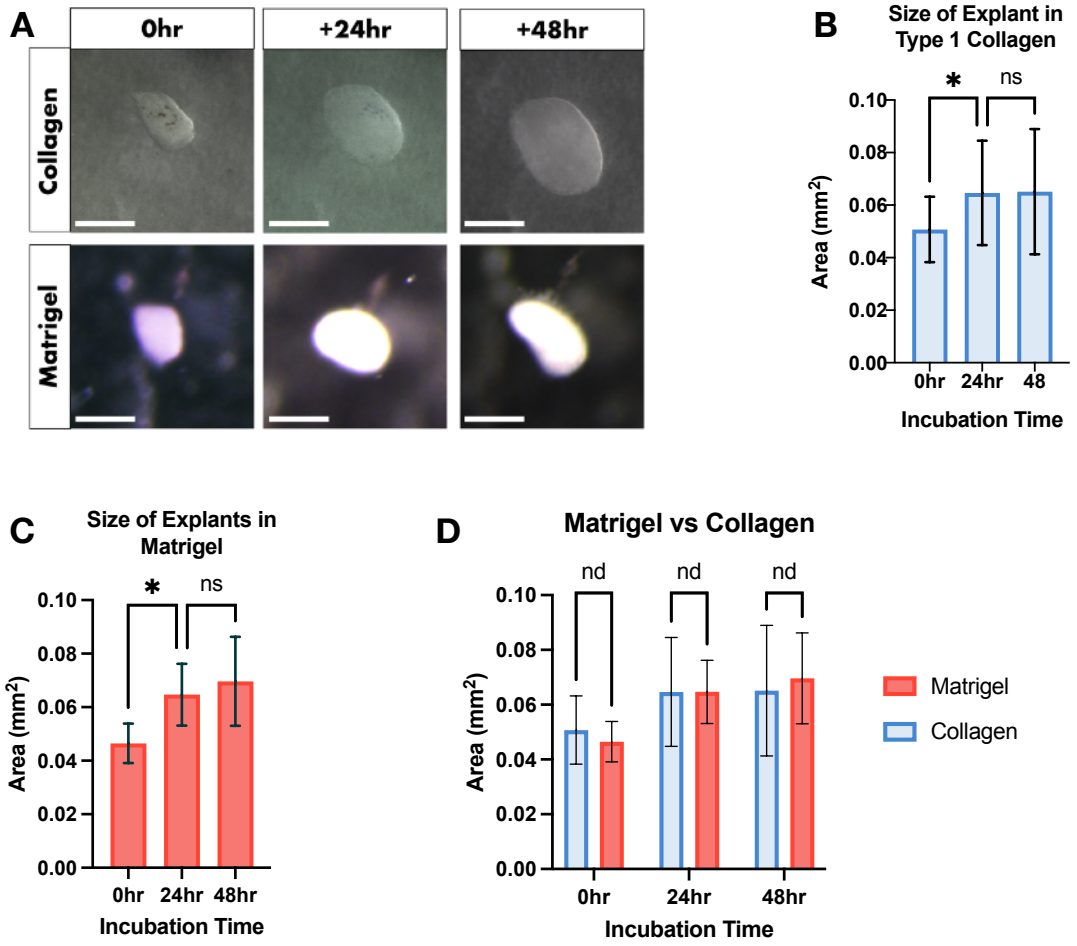

Figure 3.5. PR Explants grow in culture.

A) Brightfield images of PR explants in culture (Collagen or Matrigel) taken at 24 hour intervals. Scale bars = 250µm. B) Graph of explant sizes after 24 hours and 48 hours of growth in Collagen. There was a significant increase in size of explants [$F(2,70) = 5.082$, $p = 0.0087$] with significant increase in size between 0hr and 24hr ($p = 0.0141$). However, there was no significant increase in size between 24hr and 48hr ($p > 0.05$), n = 15-30. C) Graph of explant sizes after 24 hours and 48 hours of growth in Matrigel. There was a significant increase in size of explants [$F(2,18) = 6.744$, $p = 0.0065$] with significant increase in size between 0hr and 24hr ($p = 0.0342$). However, there was no significant change to explants size between 24hr and 48hr ($p > 0.05$), n = 7. D) Graph showing size differences between explants grown in Matrigel and explants grown in Collagen. There is no significant difference in size between explants grown in Matrigel and explants grown in Collagen at 0 hours (n = 7 - 28, $t(33) = 0.8594$, $p = 0.3963$), at 24 hours (n = 7 - 30, $t(35) = 0.0025$, $p = 0.9980$) or at 48 hours (n = 7 - 15, $t(20) = 0.4490$, $p = 0.6583$). *p* values: *=<0.05, **=<0.01, ***=<0.001, nd/ns = no difference. Error bars = SD.

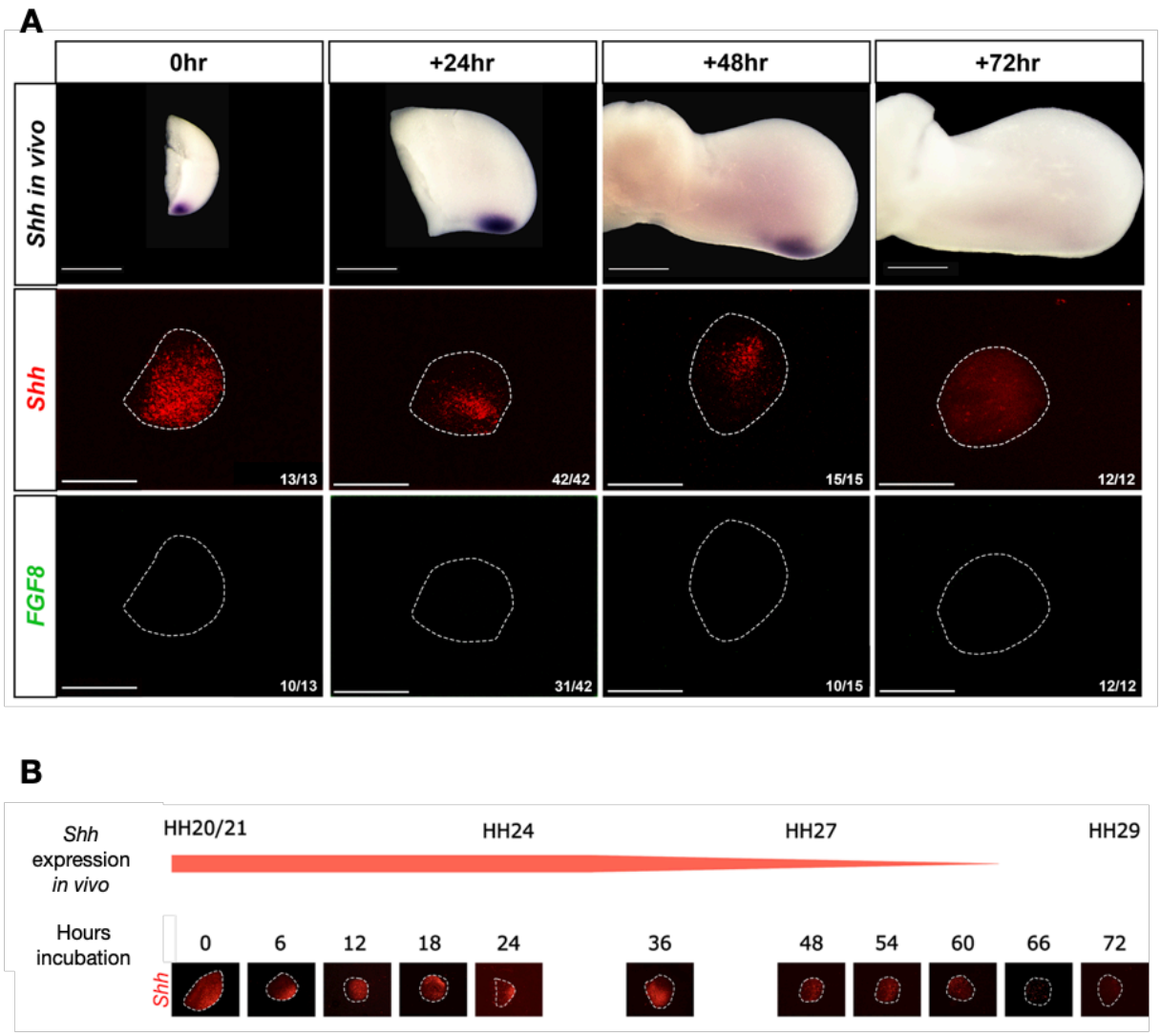

Figure 3.6. PR explants maintain timing of *Shh* expression.
A) Top row: In situ hybridisation of *Shh* in chick wing buds - *Shh* is expressed at HH21 (0hr) and continues to be expressed for the following 48 hours. *Shh* is not detectable in the wing bud after 72 hours. Scale bar = 1mm. Middle row: HCR RNA-FISH of *Shh* in PR explants. *Shh* is expressed at time of dissection (0hr) and continues to be expressed for the following 48 hours. *Shh* is not detectable in the PR explant at 72 hours incubation. Scale bar = 250μm. Bottom row: *Fgf8* is undetectable in the majority of PR explants (0hr = 10/13, 24hr = 31/42, 48hr = 10/15) and is undetectable after 72 hours incubation. B) Timeline of *Shh* expression in PR explants. Shh is expressed strongly when the tissue is dissected at HH20/21. This strong expression is maintained until 36 hours incubation. Shh expression has weakened by 48 hours incubation and is undetectable at 72 hours incubation which mimics the *in vivo Shh* expression parameters. Scale bar = 250μm.

expressed for a similar duration to that observed *in vivo* (Figure 3.6. A and B). The fact that Shh expression is maintained for the correct duration in explants is unexpected because my dissections excluded the *Fgf8*-expressing AER (see Figure 3.3. C') and - as outlined in the Introduction Section 1.6. - the general consensus is that *Shh* is maintained AER-Fgfs. To confirm the absence of *Fgf8*, I performed HCR RNA-FISH assays for *Fgf8* over the explant time-course. The results revealed that *Fgf8* was undetectable in the majority of explants cultured for 24 to 72 hours (Figure 3.6. A; 24 hours, n = 31/42 were *Fgf8*-negative, i.e. 73.8%; 48 hours, n = 10/15 were *Fgf8*-negative, i.e. 66.7%; 72 hours n = 12/12 were *Fgf8*-negative, i.e. 100%). Thus, *Shh* can maintain its correct duration independent of the AER and the Fgf signals that it produces.

Next, I asked whether explants maintain the same proliferation rates as is seen in the PR *in vivo*. To do so I used flow cytometry to quantify the percentage of cells in G1 phase of the cell cycle, which provides an accurate stage-specific read out of cell proliferation rates (Chinnaiya et al., 2014, Pickering et al., 2019, Stainton and Towers, 2022, Sedas Perez et al., 2023). A lower percentage of cells in G1-phase is indicative of a faster rate of cell cycle due to G1-phase being the rate-limiting phase of the cell cycle (Crowley et al., 2016). PR explants were incubated for 24 or 48 hours, pooled into groups of 12, and the pooled explants then trypsinised and 10,000 cells were processed (Figure 3.7. A; see Section 2.4. for more detail). Two biological repeats of the procedure were undertaken, and the results were collated and analysed with a Student's t-test. For controls, PRs were dissected from embryos at the associated-relative time points (i.e. HH24 for 24-hour explant and HH27/28 for 48-hour explant), pooled and processed (Figure 3.7. A). At 24 hours, there was no significant difference in the percentage of cells in G1-phase between *in vivo* and *ex vivo* PRs (Figure 3.7. B; 2 replicates, $t(2) = 1.595$, $p = 0.252$). Similarly, at

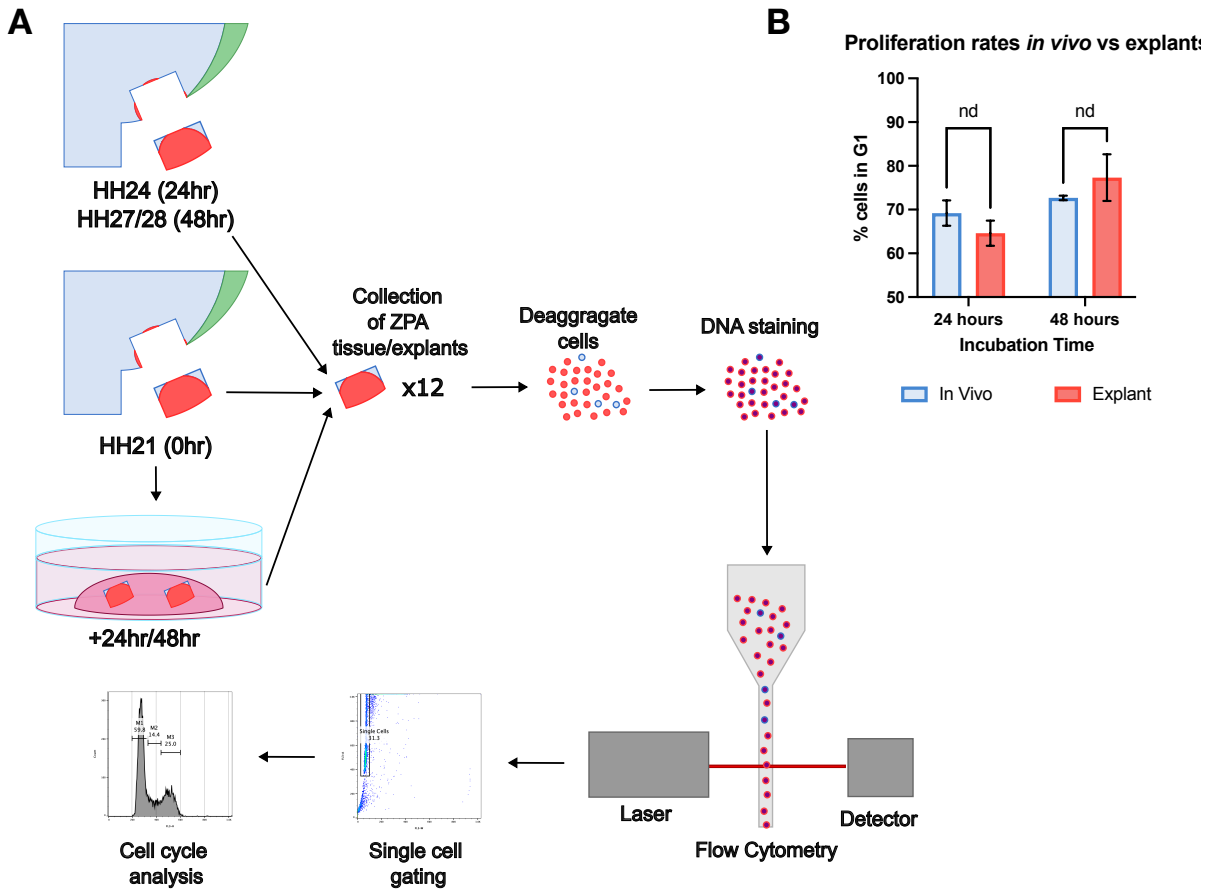

Figure 3.7. Examining proliferation rates of *in vivo* and *ex vivo* PRs
A) Schematic of the process of analysing PR cells using Flow cytometry. PR cells are collected from embryos at HH21, HH24 and HH27/28. 12 PR explants are pooled for each condition, deaggregated, stained with Propidium Iodide and passed through a FACs sorting machine. Output from the machine is analysed. For controls, PRs were dissected from embryos at the associated-relative time points, pooled and processed. B) Graph showing percentage of cells in G1, the rate-limiting stage of the cell cycle. Results from flow cytometry were analysed with a Student's t-test. At 24 hours and 48 hours there was no significant difference between the percentage of cells in G1 between *in vivo* PRs and PR explants (24 hrs: $t(2) = 1.595$, $p = 2.881$; 48 hrs: $t(1.02) = 1.226$, $p = 0.433$). *p* values: *=<0.05, **=<0.01 ***=<0.001, nd = no difference.

48 hours there was no significant difference in the percentage of cells in G1-phase between PR explant and *in vivo* PR cells (Figure 3.7. B; 2 replicates, $t(1.02) = 1.226$, $p = 0.433$). Thus, PR explants intrinsically maintain their proliferation parameters over time.

Taken together, the results in this section indicate that PR explants can maintain the correct duration of *Shh* expression, and the correct proliferation parameters seen in *in vivo* PR development.

3.3. Discussion

In this Chapter, I have described how I developed an *ex vivo* PR explant system. The results I have presented indicate that PR explants mimic/replicate *in vivo* temporal parameters, in particular the duration of *Shh* expression and the rate of proliferation.

3.3.1. Generating PR explants

To generate PR explants, I used a sharp dissection knife to excise the PR from surrounding tissue, including the AER and more-anterior mesenchyme. This technique has long been the sole method of dissecting PRs from the limb bud (reviewed in Stainton and Towers, 2018). Other methods of dissection, such as laser-assisted micro-dissection, might be beneficial in the future for more precise dissections of the PR, i.e. to dissect PRs at a younger stage. Currently, however, protocols for laser-assisted micro-dissection require that tissue is fixed or frozen which would affect the viability of the cells and thus not be beneficial for creating explants. Therefore, manual dissection remains the optimal method for isolating the PR for explants.

The PR explants exhibited growth in both Matrigel and Type 1 Collagen, indicating their viability in either culturing matrices. It is interesting to note that as the explant increased in size the proportion of explant expressing *Shh* appeared to decrease, indicating that the PR gives rise to non-*Shh* expressing cells. This has been observed previously in both chick and mouse embryos where PR-descendent cells do not express *Shh* themselves (Harfe et al., 2004, Towers et al., 2011, Chinnaiya et al., 2014). To quantify this change, HCR RNA-FISH assays could be combined with DAPI staining to determine how the percentage of cells expressing *Shh* in the PR explants change over time. A HCR RNA-FISH/DAPI assay in both PR explant and wing bud could be used to determine whether the size of the PR explant matches that of the PR *in vivo* at different time points. Furthermore, it would be intriguing to examine whether the PR explants maintain the predetermined axes of the limb and whether these axes are used to instruct growth as they are *in vivo,* i.e. along the PD axis. To examine this, a membrane dye could be injected prior to dissection at a known location and visualised at certain intervals. The injection could then be repeated *in vivo,* and the two results compared. This experiment would reveal whether the PR explants maintain the axes of the limb and how this may influence the shape of the PR.

3.2.2. PR explants mimic *in vivo* parameters

Interestingly, I have shown that carefully dissected PR explants can maintain *Shh* expression for the correct duration independent of the AER and more-anterior mesenchyme. This result is unexpected because previous studies indicate a strict requirement for Fgf signalling by the AER to maintain *Shh* in the PR (Niswander et al., 1993, Niswander et al., 1994, Crossley et al., 1996). However, it is important to note that the culturing media which was supplemented with FBS may have contained Fgfs which I could not control for. Furthermore, Fgfs such as Fgf10 are present in the mesoderm which I did not examine for. To negate the effects of these

Fgfs, I began an experiment in which I applied SU4502 - an inhibitor of Fgf receptors - to PR explants at 0 hours. However, this experiment was unsuccessful, and I was not able to repeat it in time. Nevertheless, my results indicate that *Shh* expression in the PR can likely be maintained in the absence of AER cells.

To determine whether PR explants maintain the duration of *Shh* expression I compared HCR-FISH in situs of explants to *in vivo* chromogenic in situs. Whilst this was sufficient to show that *Shh* expression in PR explants is maintained for the same duration in explants as it is *in vivo,* it did not reveal whether the quantity of *Shh* expression was equivalent. This is due to chromogenic *in situs* not being an accurate quantitative measure as the stain can darken depending on the length of time the sample is in the staining solution. Therefore, to quantify whether PR explants express *Shh* equivalent to that *in vivo*, HCR RNA-FISH assays for *Shh* expression would need to be performed on limb buds too, with the level of fluorescence being directly compared.

Lastly, my results indicate that PR explants maintain their intrinsic proliferation parameters for the duration of *Shh* expression independently of AER-Fgfs. This confirms that the PR intrinsically regulates its own proliferation rate through a cell cycle timer (Chinnaiya et al., 2014, Pickering et al., 2019). Thus, PR explants *ex vivo* should be, and indeed are, capable of maintaining their proliferation parameters.

CHAPTER 4

Determining the functional roles of Shh signalling in PR explant development

4.1. Introduction

As discussed in Section 1.7, previous work in the chick wing has demonstrated that inhibiting Shh signalling with cyclopamine at HH20/21 *in vivo* results in extension of the AER over the PR (Pickering and Towers, 2016) and the over-proliferation of PR cells (Chinnaiya et al., 2014, Pickering et al., 2019). Together, this results in the formation of an ectopic digit from PR cells (Pickering et al., 2019). By examining changes in expression patterns of cell cycle regulators after inhibition of Shh-signalling, it was proposed that Shh intrinsically regulates proliferation in PR cells. Shh initially up-regulates proliferation in the PR, likely via the regulation of *Cyclin D2* (Pickering et al., 2019). However, Shh also up-regulates $p27^{kip1}$ through an intermediary factor, Bmp2, which leads to a decrease in

proliferation (see Figure 1.12. in Section 1.7. and Figure 1.13. in Section 1.7.1. for more detail; Pickering et al., 2019).

Nevertheless, due to the essential *in vivo* requirement of the AER for PR development and limb outgrowth, it is difficult to discern the relative contributions that intrinsic mechanisms and extrinsic signals, such as AER-Fgfs, play in PR development. Specifically, it is unknown to what extent intrinsic mechanisms and extrinsic signals affect the regulation of the proliferation mechanism described above.

Since, in Chapter 3, I showed that normal *Shh* expression timing and cell proliferation parameters are maintained in PR explants in the absence of Fgf signalling from the AER, in this chapter I aimed to determine the functional consequences of inhibiting the Shh signalling pathway in isolated PR explants. As described above, inhibiting Shh signalling *in vivo* with the drug cyclopamine affects the proliferation rate and results in the extension of the AER over the PR. Therefore, I used cyclopamine to inhibit Shh signalling in the PR explants and then examined how this affected various developmental parameters including growth, gene expression timing and cell proliferation. Based on *in vivo* evidence, I hypothesised that applying cyclopamine to the PR explants would cause an increase in growth because of an increase in proliferation. Furthermore, I hypothesised that expression of *Bmp2* and *p27^{kip1}* would be greatly reduced in the PR explant when treated with cyclopamine.

4.2. Results

4.2.1. Blocking Shh signalling affects growth of PR explants

I determined the concentration of cyclopamine that would effectively block Shh signalling in the PR explants. Cyclopamine inhibits Shh signalling by binding to Smo (Chen et al., 2002), which prevents Gli-R from being processed into Gli-A, thus

preventing the transcription of downstream targets (Figure 1.8. A; Marigo et al., 1996, Wang et al., 2000, Lipinski et al., 2006). *Ptch1* is a downstream-target of Shh-signalling (Goodrich et al., 1996), therefore I examined expression of *Ptch1* after the application of cyclopamine to determine at what concentration Shh signalling is effectively inhibited. Cyclopamine concentrations of 10μM to 25μM have been used to effectively inhibit Shh signalling in mouse testis explants (Yao and Capel, 2002), mouse kidney explants (Hu et al., 2006) and HH32 chick limb explants (Minina et al., 2001). I tested both 10μM and 20μM cyclopamine and found that concentration of 20μM was sufficient to prevent *Ptch1* expression in PR explants after 24 hours (Figure 4.1. B; n = 3/3). A concentration of 10 μM did weaken expression of *Ptch1* (Figure 4.1. B; n = 4/5) when compared to expression in PR explants treated with

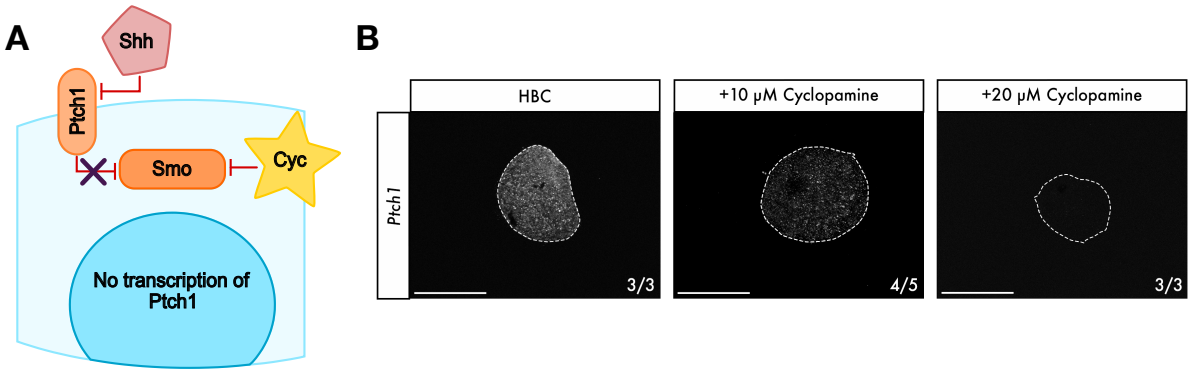

Figure 4.1. 20μM cyclopamine blocks Shh signalling.
A) Schematic demonstrating effect of cyclopamine on Shh signalling. Cyclopamine (Cyc) inhibits Smoothened (Smo) activity which prevents the transcription of *Patched1* (*Ptch1*) and other Shh target genes, even if Shh is present. B) HCR RNA-FISH of *Ptch1* in PR explants cultured with either HBC (control) or cyclopamine for 24 hours. *Ptch1* expression is strong in control PR explants (n = 3/3), but weak in PR explants treated with 10μM cyclopamine (n = 4/5). Expression of *Ptch1* is undetectable in PR explants incubated with 20μM cyclopamine (n = 3/3). All scale bars = 250 μm.

hydroxy-beta-cyclodextrin (HBC), the carrier for cyclopamine (control). Control explants expressed *Ptch1* throughout (Figure 4.1. B; n = 3/3). Thus, I used a concentration of 20μM cyclopamine throughout the subsequent experiments.

To determine if blocking Shh signalling influences PR explant growth, I took brightfield microscopy images of cultured explants at 24-hour intervals and measured their surface area. As previously observed in Section 3.2.1., PR explants treated with HBC increase in size over 48 hours (Figure 4.2. A; n = 7, $p = 0.0071$) with a significant increase in size over the first 24 hours (Figure 4.2. A; n = 7, $p = 0.0342$). The control explants did not have a visible change in shape, remaining in a more 'ball'-like shape (Figure 4.2. B and Table 4.1; n = 14/16). However, by contrast, the majority of the PR explants exposed to cyclopamine exhibited a pronounced change in size and shape over 48 hours incubation, growing into an elongated tear-drop shape with a wider 'head' and longer 'tail' (Figure 4.2. B, C (n = 7, $p = 0.0098$) and Table 4.1 (n = 14/17)). Comparing measurements of surface area at 24-hour intervals between HBC and cyclopamine treated PR explants demonstrated that there was no significant difference in size of explants at 0 hours (Figure 4.2. D; n = 7-8, $p = 0.8292$) and 24 hours (n = 7-8, $p = 0.2940$). However, at 48 hours incubation there was a significant difference in the size of explants (Figure 4.3. D; n = 7-8, $p =$

Table 4.1. Table showing number of explants in a ball shape or an elongated shape after 48 hours incubation with either HBC (control) or cyclopamine

	Ball shape ●	Elongated shape
HBC	14/16	2/16
Cyclopamine	3/17	14/17

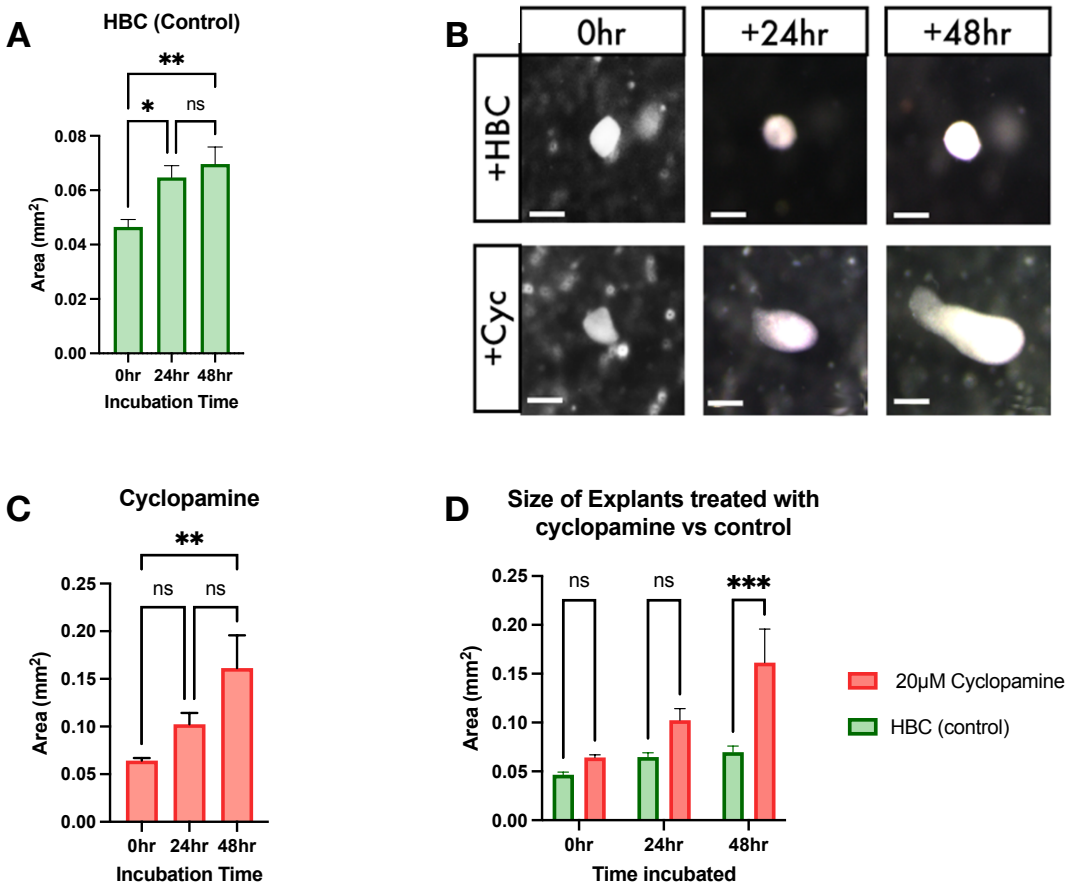

Figure 4.2. Blocking Shh signalling affects the growth of the PR explants. A) Graph showing change in size of PR explants exposed to HBC analysed with one-way ANOVA which found significant interaction ($F(2,18) = 6.744$, $p = 0.0065$). Multiple comparisons revealed that there is an increase in size between 0hr and 48hr ($p = 0.0071$) and 0hr and 24hr ($p = 0.0342$) but no significant increase in size between 24hr and 48hr ($p = 0.7398$). B) Brightfield images of the same PR explant in culture taken at 24-hour intervals. Explants were treated with either HBC or cyclopamine. All scale bars = 250 μm. C) Graph showing change in size of PR explants exposed to cyclopamine analysed with one-way ANOVA which showed significant interaction (n=8,8,8, $F(2,21) = 5.431$, $p = 0.0126$). Multiple comparisons revealed that there is a significant increase in size between 0hr and 48hr ($p = 0.0098$) but no significant increase in size between 0hr and 24hr ($p = 0.4198$) and 24hr and 48hr ($p = 0.1401$). D) Graph comparing size of PR explants exposed to cyclopamine vs HBC analysed with a two-way ANOVA which found significant interaction between treatments and time incubated ($F(2,26) = 4.1$, $p = 0.0278$). Multiple comparisons found that there was no significant difference in size at 0hr (n = 7-8, $p = 0.8292$) or at 24hr (n = 7-8, $p = 0.2940$). However, there was a significant difference in size of explant at 48 hours (n = 7-8, $p = 0.0008$). p values: * = <0.05, ** = <0.01, *** = <0.001. Error bars = SEM.

0.0008), i.e. between PR explants exposed to cyclopamine (M = 0.161 mm^2, SD = 0.097) and PR explants exposed to HBC (M = 0.07 mm^2, SD = 0.017).

4.2.2. Blocking Shh signalling affects the proliferation rate of PR explants

To determine if blocking Shh signalling affects the proliferation rate of PR explants, I used flow cytometry to analyse the DNA content of cells at 24-hour intervals. Groups of 12 PR explants were pooled to produce 10,000 cells per three biological repeats. *In vivo* application of cyclopamine results in the over-proliferation of PR cells (Chinnaiya et al., 2014, Pickering et al., 2019) and thus I asked whether the same over-proliferation also occurs when Shh-signalling is blocked in the PR explants. Furthermore, I aimed to determine whether the increased growth observed in cyclopamine treated PR explants described in Section 4.2.1. could be partly explained by an over-proliferation caused by the inhibition of Shh signalling.

At 24 hours, there was no significant difference in the percentage of cells in G1-phase between PR explants treated with cyclopamine and control PR explants (Figure 4.3. A, n = 3, t(2.168) = 0.516, $p = 0.654$). However, after 48 hours incubation, PR explants exposed to cyclopamine had a significantly lower percentage of cells in G1-phase compared to control PR explants (Figure 4.3. A, n = 3, t(2.383) = 5.221, $p = 0.024$). This indicated that PR explants treated with cyclopamine had a faster rate of proliferation at 48 hours than control PR explants. I also compared the percentage of cells in S-phase and G2-M-phase of the cell cycle 48 hours after treatment with either HBC or cyclopamine. The percentage of cells in S-phase was significantly increased in PR explants treated with cyclopamine compared to the control explants (Figure 4.3. B, n = 3, t(3.918) = 8.439, $p = 0.001$). This indicates that PR explant cells had passed through the G1-S phase transition at a faster rate when Shh signalling was inhibited than under normal conditions. However, there was no

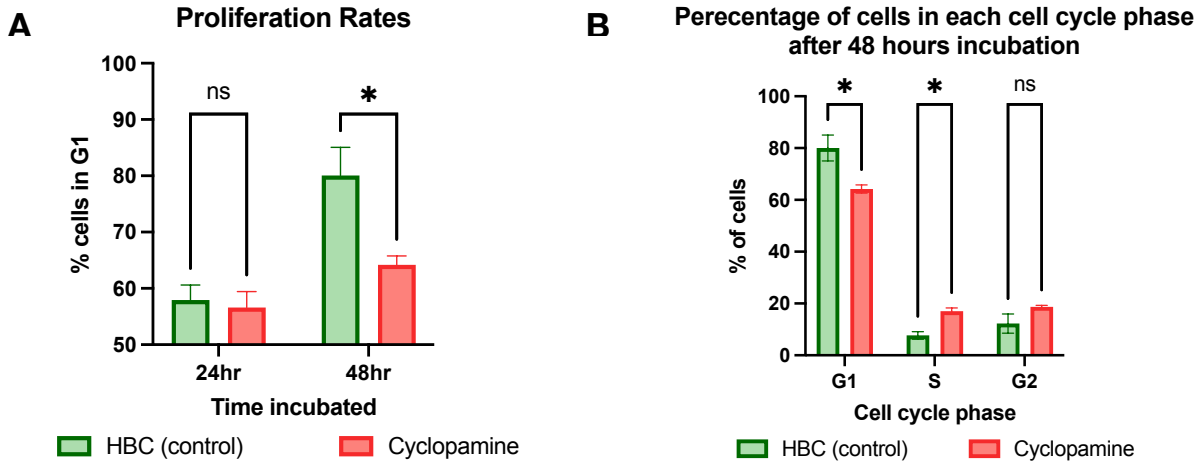

Figure 4.3. Blocking Shh-signalling affects the cell cycle rate of PR explants. A) Graph showing the percentage of cells in G1, the rate-limiting stage of the cell cycle. Results from flow cytometry were analysed with a Student's T-test. At 24 hours there was no significant difference between the percentage of cells in G1 between PR explants treated with cyclopamine versus HBC ($t(2.168) = 0.516$, $p = 0.654$). However, there was a significant difference at 48 hours ($t(2.383) = 5.221$, $p = 0.024$) in the percentage of cells in G1 between cyclopamine treated explants ($M = 64.193$, $SD = 1.562$) and HBC treated explants ($M = 80.047$, $SD = 5.022$). B) Graph showing the percentage of cells in each stage of the cell cycle between explants treated with cyclopamine and HBC following 48 hours incubation. Results from flow cytometry were analysed with a Student's T-test. There was a significant difference in the percentage of cells in G1 ($t(2.383) = 5.221$, $p = 0.024$) between explants treated with cyclopamine and HBC. There was also a significant difference in the percentage of cells in S-phase ($t(3.918) = 8.439$, $p = 0.001$) between explants treated with cyclopamine ($M = 17.07$, $SD = 1.261$) and those treated with HBC ($M = 7.677$, $SD = 1.459$). However, there was no significant difference reported in the percentage of cells in G2 phase ($t(2.08) = 2.982$, $p = 0.092$). All error bars = SD.

significant difference in the percentage of cells in G2-M phase between the two treatments (Figure 4.3. B, n = 3, t(2.08) = 2.982, *p* = 0.092).

Another method of determining changes in proliferation rate is to examine the uptake of EdU (5-ethynyl-2'deoxyuridine). EdU is incorporated into the DNA during S-phase, and this can be used to quantify the amount of cells progressing through this stage of the cell cycle (Flomerfelt and Gress, 2016). Thus, to further analyse the effect of blocking Shh signalling on PR explant proliferation, I performed an EdU assay. PR explants cultured with either HBC or cyclopamine were incubated to 48 hours before being stained with EdU and DAPI. Images were passed through a Fiji macro, which examined the z-stack and determined the area of the DAPI staining

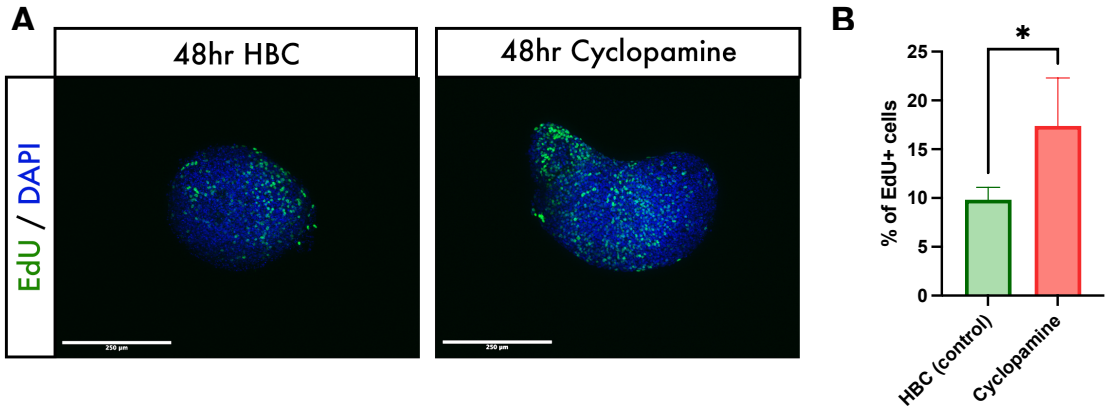

Figure 4.4. Blocking Shh-signalling affects the cell cycle rate of PR explants after 48 hours.
A) EdU labelling in PR explants incubated with either HBC or cyclopamine for 48 hours (n = 4,4). B) Graph quantifying the percentage of cells stained with EdU after 48 hours incubation. Results were analysed with a Student's t-test. There is a significant difference between the percentage of cells stained with EdU when explants were treated with cyclopamine (n = 4) versus HBC (n = 4, t(6) = 2.975, p = 0.0248). Error bars = SD. Scale bars = 250μm

and subsequently the area of EdU staining within the DAPI area. These two results were compared to determine the percentage of the explant that was EdU-positive. PR explants exposed to cyclopamine had a significantly higher percentage area of EdU-positive staining than control PR explants (Figure 4.4. B, n = 4-4, t(6) = 2.975, *p* = 0.0248). Taken with the flow cytometry analysis, these results indicate that inhibiting Shh signalling causes PR explants to maintain a faster rate of proliferation between 24 and 48 hours resulting in more cells passing through from the G1-phase to the S-phase of the cell cycle at 48 hours.

4.2.3. Blocking Shh signalling affects gene expression in PR explants

To determine if Shh signalling affects gene expression in PR explants, I performed HCR RNA-FISH assays on PR explants exposed to cyclopamine or HBC for 48 hours. I analysed G1-S phase regulators, markers of the AER and markers of digit development. My aim was to ask if inhibiting Shh signalling affects the intrinsic mechanism and extrinsic factors during PR development in the absence of the AER. A key aim was to compare my results with those reported in a previous study where Shh signalling was inhibited *in vivo* (Pickering et al., 2019).

As shown in Chapter 3, control explants expressed *Shh* at 48 hours (Figure 4.5. A; n = 15/15) in a manner consistent with *in vivo* development (Figure 4.5. B; see also Figure 3.6.). However, application of cyclopamine resulted in a loss of *Shh* expression in PR explants (Figure 4.5. C; n = 14/15). Again, as previously described in Chapter 3, *Fgf8* is not expressed at 48 hours (Figure 4.5. C; n = 7/9; see also Figure 3.6.), again consistent with *in vivo* development (Figure 4.5. B). Intriguingly, application of cyclopamine to PR explants caused *de novo* expression of *Fgf8* in a small circular group of cells in the ‘head’ of the explant (i.e. the wider region) at 48 hours (Figure 4.5. C, n = 5/8). To better understand Fgf signalling in the PR explants, I examined the expression of *MAP-kinase phosphatase 3 (Mkp3)*, a marker of Fgf

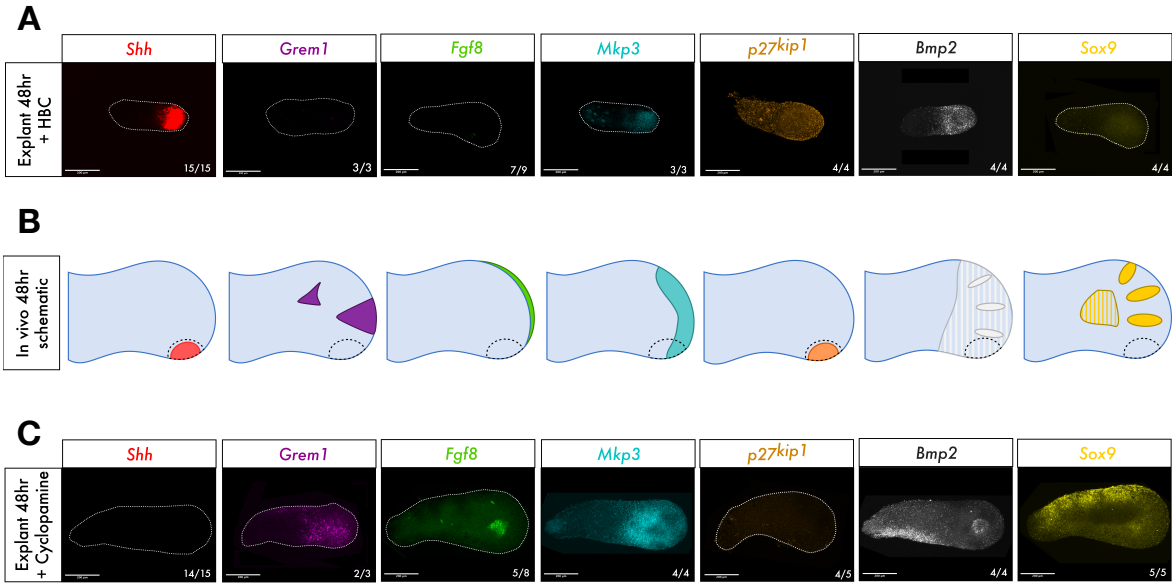

Figure 4.5. Blocking Shh signalling affects expression patterns within PR explants.

A) HCR RNA-FISH of polarising region explants incubated with HBC for 48 hours (controls). B) Schematic of RNA expression in the limb bud at approximately HH27. Dashed black indicates PR area and striped colour indicates areas of weaker expression. C) HCR RNA-FISH of PR explants incubated with cyclopamine for 48 hours. *Shh* expression is present in control explants (n =15/15), consistent with *in vivo* expression. However, *Shh* expression is absent in cyclopamine-treated explants (n = 14/15). Conversely, *Fgf8* expression is absent in control explants (n = 7/9) and *in vivo* but there is *de novo* expression in the cyclopamine treated explants (n = 5/8). *Mkp3* is expressed weakly in the control explants (n = 3/3) and present *in vivo*, but explants incubated with cyclopamine have much stronger expression (n = 4/4). *Grem1* is absent in the control explant (n =3/3) and *in vivo*, however it is expressed in explants treated with cyclopamine (n = 2/3). In control explants, *Bmp2* is expressed at one end of the explant (n = 4/4) consistent with expression *in vivo.* Explants are treated with cyclopamine have altered expression of *Bmp2,* with it now being expressed in a circle of cells in the wider part of the explant and in a stripe along the side (n = 4/4). *P27^{kip1},* which is expressed throughout the control explant (n = 4/4), is only expressed in differentiating myogenic tissue at HH27/28. Application of cyclopamine results in the loss of *p27^{kip1}* expression in the PR explant (n = 4/5). Lastly, *Sox 9* is not expressed in either the control explant (n = 4/4) nor *in vivo*, however, PR explants incubated with cyclopamine express *Sox 9* in a stripe along one side (n = 5/5). All scale bars = 250 μm.

activity (Eblaghie et al., 2003). At 48 hours, control PR explants expressed *Mkp3* weakly in approximately one third of the total area (Figure 4.5. A, n = 3/3), whilst *in vivo Mkp3* is expressed in the mesenchyme under the AER (Figure 4.5. B). However, at 48 hours PR explants treated with cyclopamine expressed *Mkp3* at higher levels in the 'head' of the explant (Figure 4.5. C, n = 4/4) corresponding to the *de novo* expression of *Fgf8* in the same area. As described in Section 1.6., PR-Shh and AER-Fgfs form a feedback loop with *Grem1* (see Figure 1.6.; Laufer et al., 1994, Niswander et al., 1994, Zúñiga et al., 1999). In this feedback loop, Grem1 maintains the AER by acting as a Bmp-antagonist (Zúñiga et al., 1999). Therefore, as a key extrinsic signal, I examined its expression pattern in the treated PR explants. In control PR explants, *Grem1* is not expressed at 48 hours (Figure 4.5. A, n = 3/3) consistent with *in vivo* development at this time-point (Figure 4.5. B). However, application of cyclopamine resulted in *Grem1* expression in the 'head' of the explant at 48 hours (Figure 4.5. C, n = 2/3). Thus, inhibition of Shh-signalling in the PR explants allows for the *de novo* expression of *Grem1* and *Fgf8*, substantiated by an increase in *Mkp3* signalling in the same area.

As discussed in this chapter's introduction, Shh signalling is thought to intrinsically regulate proliferation in PR cells. Importantly, it is thought to prevent the over-proliferation of PR cells through the up-regulation of $p27^{kip1}$ through Bmp2, which inhibits the G1-S phase transition. My results in Section 4.2.2., indicate that inhibiting Shh signalling in PR explants causes an over-proliferation of cells. Therefore, I asked if inhibition of Shh signalling in PR explants has affected the Bmp2-$p27^{kip1}$ pathway. In the control explants, *p27 kip1* is expressed throughout the explant (Figure 4.5. A, n = 4/4). This is consistent with *in vivo* expression as *p27 kip1* is maintained for approximately the same duration as *Shh* expression (Figure 4.5. B; Pickering et al., 2019). Application of cyclopamine, however, resulted in an almost complete cessation of *p27 kip1* expression (Figure 4.5. C, n = 4/5). These results would indicate that inhibition of Shh signalling regulates *p27 kip1* expression, which may go some way to explain the loss of proliferation control observed in Section

4.2.2.. I also examined *Bmp2,* which, in the control explants, is expressed in a region overlapping the *Shh* domain (Figure 4.5. A, n = 4/4).This is in a manner consistent with the *in vivo*, where *Bmp2* is expressed within and beyond the PR (Figure 4.5. B). However, application of cyclopamine resulted in *Bmp2* being robustly detected in a stripe along the 'tail' (i.e. the narrower region) and in a small group of cells in the 'head' of the explant (Figure 4.5. C, n = 4/4). During *in vivo*, development *Bmp2* is expressed in the interdigital space (See Section 1.5.5. for more detail; Healy et al., 1999) thus, it is possible that the stripe of *Bmp2* in the 'tail' of the explant is related to chondrogenesis.

As application of cyclopamine *in vivo* can result in the formation of an extra digits from PR cells, I asked whether blocking Shh signalling in the PR explants could promote chondrogenesis. To do so, I examined the expression of *SRY-Box Transcription Factor 9 (Sox9)*, which marks pre-cartilage mesenchymal condensations *in vivo* (Bi et al., 1999). At 48 hours, control PR explants did not express *Sox9* (Figure 4.5. A, n = 4/4) consistent with the lack of expression of this gene in the PR region *in vivo* (Figure 4.5. B). However, applying cyclopamine to PR explants resulted in a stripe of *Sox9* expression along one edge of explant through the 'head' and 'tail' (Figure 4.5. C, n = 5/5). It is important to also note that Bmp2 is expressed in the inter-digital mesenchyme and regulates expression of *Sox 9* (Healy et al., 1999). Therefore, taken with the results above, the expression of *Sox 9* and *Bmp2* may indicate that the PR explant is beginning to make a cartilaginous condensation, perhaps one that produces a digit.

4.3. Discussion

In this chapter, I have demonstrated that blocking Shh signalling in PR explants through the application of cyclopamine affects PR explant development. Application of cyclopamine is the predominant method of inhibiting Shh signalling in

chick embryology experiments (Chen et al., 2002, Scherz et al., 2007, Towers et al., 2008, Towers et al., 2011, Pickering and Towers, 2016, Pickering et al., 2019). However, the dosage of cyclopamine to cells *in vivo* varies as, once applied, the molecules diffuse into and across the egg. Thus, by applying cyclopamine in culture I could control the dose of cyclopamine the explants were receiving. Nonetheless, advances in chicken genetic models and electroporation may allow for future experiments in which Shh signalling is inhibited in explants through other methods, such as optogenetics.

Importantly, my results demonstrate that Shh signalling inhibition affects the growth, proliferation parameters and gene expression of PR explants. Below I will discuss how this is likely achieved through intrinsic and extrinsic factors.

4.3.1. Inhibition of Shh signalling affects the intrinsic proliferation mechanism

PR explants show a significant change in size and shape after 48 hours incubation with cyclopamine compared to control explants. The cyclopamine treated explants are much larger in size and have an elongated 'head-and-tail' shape. This change in size may be explained by their significant increase in proliferation rates by 48 hours when exposed to cyclopamine. Thus, I have shown that the percentage of cells in G1-phase, the rate limiting stage of the cell cycle, is significantly lower in explants treated with cyclopamine compared to those treated with HBC. This is indicative of proliferation rates being faster in cyclopamine treated PR explants compared to control explants after 48 hours incubation. This result is consistent with previous studies which have examined the proliferation rate of PR cells *in vivo* and found that application of cyclopamine results in a faster proliferation rate (Chinnaiya et al., 2014, Pickering et al., 2019).

I also found that PR explants treated with cyclopamine have altered expression of *Bmp2* and lose *p27^{kip1}* expression, consistent with results of experiments *in vivo* (Pickering et al., 2019). In these experiments, *p27^{kip1}* expression is lost after the application of cyclopamine, which, the authors propose, results in the over-proliferation of PR cells (Pickering et al., 2019). This loss of *p27^{kip1}* expression in the PR explants treated with cyclopamine may explain the over-proliferation described above. Furthermore, the control explants continued to express both *Bmp2* and *p27^{kip1}.* These results would therefore suggest that *Bmp2* and *p27^{kip1}* expression is regulated by Shh signalling and crucial in the PR explants to prevent, in some part, over-proliferation of the cells. This conclusion is consistent with the conclusions reached by Pickering et al. (2019) after applying cyclopamine *in vivo.*

4.3.2. Inhibition of Shh signalling affects extrinsic factors

In Section 4.2.3., I found that blocking Shh signalling with cyclopamine affects the expression of extrinsic factors. Unexpectedly, I found that inhibition of Shh signalling allows for the *de novo* expression of *Fgf8* in a small group of cells in the 'head' of the explant. This suggests that AER-like cells formed *de novo* in the PR explants. The AER lies distally on the limb bud; therefore, it is likely that the head of the explant has a more distal identity. I also observed increased *Mkp3* expression in the distal region of the explant. This is congruent with the expression of *Fgf8*, as *Mkp3* is a marker of Fgf activity (Eblaghie et al., 2003), and therefore, it is likely that the *de novo* expression of *Fgf8* resulted in the increased *Mkp3* distally in the PR explant. Interestingly, it has been reported that application of cyclopamine *in vivo* results in the extension of the AER over the PR (Pickering et al., 2019)

I also observed an increase in *Grem1* expression in the distal region of the PR following Shh inhibition. As discussed in Section 1.6., Shh signalling is required for *Grem1* expression in early limb development in the Shh/Grem1/AER-Fgf feedback

loop (Ros et al., 2003, Maas et al., 2011). However, application of cyclopamine *in vivo* has demonstrated that by HH20/21 *Grem1* expression is independent of Shh signalling. Thus, as the PR is dissected at HH20/21, it is likely that *Grem1* expression is no longer being up-regulated by Shh signalling in the PR explant. The increased expression of *Grem1* in the distal explant after Shh signalling inhibition therefore indicates that *Grem1* is likely inhibited by Shh in the PR after HH20/21. This is consistent with findings that *Grem1* expression expands into the PR after wings are treated with cyclopamine (Pickering and Towers, 2016). Lastly, *Grem1* and *Fgf8* were consistently expressed in the wider distal region of the explant. This indicates that the increased expression of *Grem1* may be important for maintaining expression of *Fgf8* as it occurs *in vivo* (Zúñiga et al., 1999).

Taken together, these results demonstrate that inhibition of Shh signalling results in changes to the expression of extrinsic factors, namely *de novo* expression of *Fgf8* and *Grem1* as well as increased expression of *Mkp3* in the distal region of the PR explant. This may suggest that Shh signalling in the chick PR prevents the formation of the overlying AER by inhibiting the expression of *Fgf8* and/or *Grem1*.

4.3.3. Inhibition of Shh signalling may cause PR explants to produce cartilage

Lastly, I observed that PR explants treated with cyclopamine also have increased expression of *Sox 9* and altered expression of *Bmp2* compared to control explants. This may indicate that the PR explant is beginning to form a cartilaginous condensation, akin to a digit condensation *in vivo* (Francis et al., 1994, Healy et al., 1999). Thus, this change in expression pattern may be indicative of PR explants attempting to form a digit. This supports the findings that blocking Shh signalling in the chick embryo at HH20/21 causes the PR to produce an ectopic digit (Pickering et al., 2019).

CHAPTER 5

Determining the developmental potential of PR explants following Shh signalling inhibition

5.1. Introduction

In Chapter 4, I demonstrated that blocking Shh signalling in PR explants affects their growth, proliferation and gene expression patterns. In this chapter, I determined the developmental potential of cyclopamine-treated PR explants and examined whether inhibiting Shh signalling leads to the production of cartilaginous condensations.

As discussed in Section 1.7., when Shh signalling is blocked at HH20/21 *in vivo,* the AER extends over the PR as determined by *Fgf8* expression (Pickering and Towers, 2016) which supports the over-proliferation of PR cells (Chinnaiya et al., 2014, Pickering et al., 2019). This combination of extended AER and increased proliferation cause an ectopic digit to form from PR cells (Pickering et al., 2019).

Similarly, in the previous chapters, I demonstrated that blocking Shh signalling in PR explants results in over-proliferation and the *de novo* expression of *Fgf8* at the more bulbous distal end of the explant 48 hours after treatment. Finally, I demonstrated that blocking Shh signalling in PR explants increases the expression of *Sox9* and *Bmp2* along the edge of the explant into the more proximal tail. This is interesting as both *Sox9* and *Bmp2* are required to produce digit condensations *in vivo* (Healy et al., 1999). Taken together, these results suggest that inhibiting Shh signalling in PR explants could result in the formation of a digit condensation.

However, to allow a digit condensation to develop would require an explant to be incubated for much longer than 72 hours. This is difficult to achieve, as explant viability decreases over time. As the explants increase in size, the central portions tend to become necrotic (personal observation and personal communication with Placzek lab).

In this chapter, I determined whether blocking Shh signalling is sufficient to allow PR explants to produce a digit condensation. To achieve this aim, I grafted cyclopamine-treated PR explants into chick wing buds and allowed them to develop to HH36 when all phalanges will have condensed (Hamburger and Hamilton, 1951).

5.2. Results

5.2.1. Grafting PR explants

To determine if blocking Shh signalling in PR explants results in the formation of a cartilaginous condensations, I needed to develop PR explants to a stage where condensations could be formed (i.e. HH36; Hamburger and Hamilton, 1951). However, maintaining PR explants in culture beyond 72 hours is very difficult, due to the core of the explant becoming necrotic (personal observation and personal communication with Placzek lab). Thus, to enable the PR explants to form any

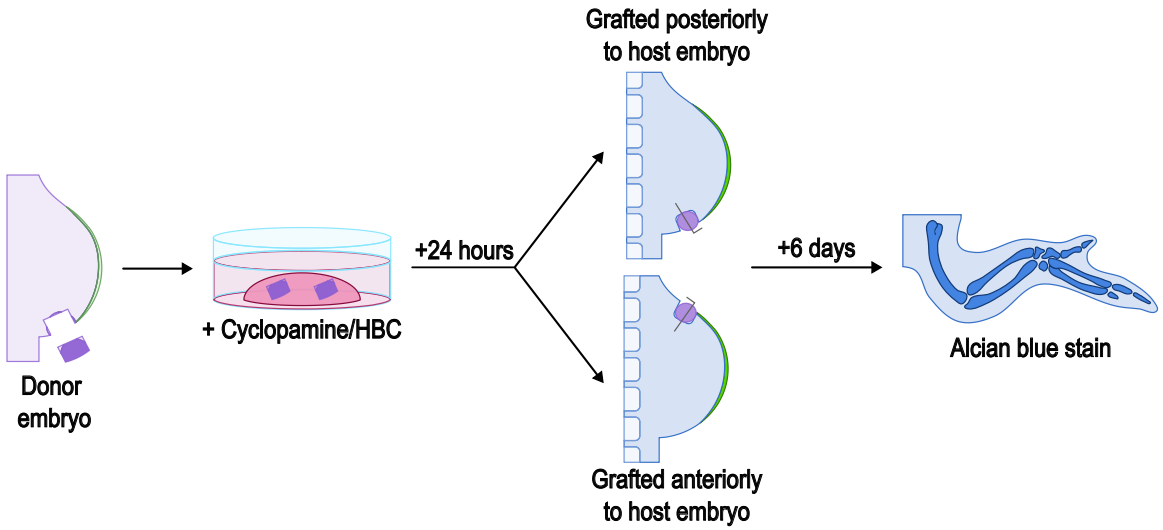

Figure 5.1. Grafting PR explants to HH21/22 host chick wings.
A) Schematic of the grafting process. PR explants are taken from a donor embryo (green), cultured for 24 hours with either cyclopamine or HBC, then removed from culture and grafted to a either the anterior or posterior margin of a host embryo wing (blue). The host embryo is allowed to develop for 6 days before it is sacrificed and the cartilage is stained with alcian blue staining.

cartilaginous condensations, I grafted them into a host chick wing. Grafting PRs between chicks is a well-established technique (Stainton and Towers, 2018), which I adapted for the PR explants. For this experiment, I incubated PR explants with either HBC (control) or cyclopamine for 24 or 48 hours before collecting and transplanting them into either the anterior or posterior margin of HH21/22 chick wings (Figure 5.1.), after which the host embryos were allowed to develop for another 6 days before being collected and the cartilage stained with Alcian blue. I initially attempted to graft explants which had been incubated for 48 hours, however due to the size of cyclopamine-treated explants (see Figure 4.2. for size of 48-hour cyclopamine-treated PR explant) approximately one third of the wing needed to be removed in order to securely position the graft. On the other hand, I found that less tissue

needed to be removed to secure PR explants which had been incubated for 24 hours. Furthermore, the 24-hour PR explants were less unwieldy compared to 48-hour PR explants and generally could be secured into the wing more easily. Thus, I decided to graft PR explants which had been incubated with either HBC (control) or cyclopamine for 24 hours to the host wings of HH22 chicks.

I grafted 38 PR explants which had been incubated with cyclopamine for 24 hours to HH21/22 host chicks, of which 22 survived the first 48 hours and only 8 survived to 10 DOI. As a control, I grafted 11 PR explants which had been incubated with cyclopamine for 24 hours to HH21/22 host chicks with 7 surviving the initial 48 hours and 3 surviving to 10 DOI. I found that all the chick wing with a control graft developed the normal pattern of three digits (n = 3/3; Table 5.1. and Figure 5.2. A). When a PR explant which had been incubated with cyclopamine for 24 hours was grafted to a host wing, however, extra cartilaginous condensations formed in almost all wings (n = 7/8; Table 5.1.). However, these additional cartilage structures varied between embryos. For example, grafting a cyclopamine treated PR explant to the anterior margin of a host wing bud resulted in the formation of a cartilaginous condensation forming anterior to the elbow (Figure 5.2. B and B'). In another case, grafting a cyclopamine treated PR explant to the posterior margin of a host wing bud

Table 5.1. Number of chicks that developed extra cartilage in the wing after receiving a cyclopamine or HBC treated PR explant graft.

	Normal Development	Extra Cartilage
+ Cyclopamine PR explant	1/8	7/8
+ HBC PR explant	3/3	0/3

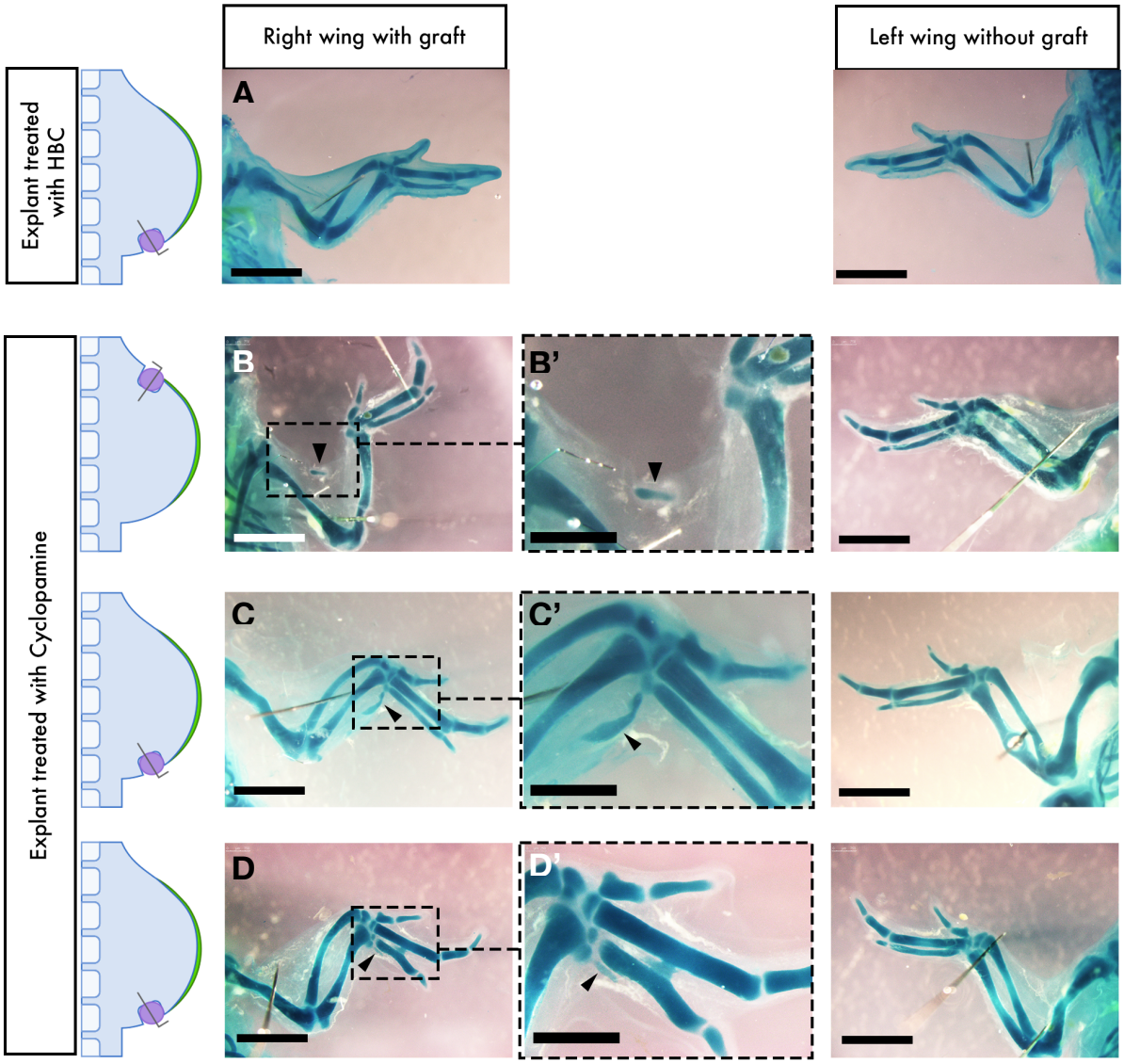

Figure 5.2. Grafting PR explants incubated with cyclopamine produces additional cartilaginous condensations.

Images of chicks collected at incubation day 10 stained with alcian blue which marks the cartilage. Embryos right wings with graft are compared to their left wing without graft to determine if the right wing has developed normally. Grafting a HBC-treated PR explant resulted in the normal development of the host wing (A). Grafting Cyclopamine-treated PR explants resulted in an array of extra cartilage developing (B,C,D). All left wings developed normally. B and B') PR explant was grafted anteriorly and an extra cartilaginous condensation formed anterior to the elbow between two grafting pins. C and C') PR explant was grafted posteriorly and an extra cartilaginous condensation formed at the wrist. D and D') PR explant was grafted posteriorly and an extra cartilaginous condensation formed adjacent to the digits. Scale bars A,B,C,D and all left wings = 2mm, B',C' and D' = 1mm.

resulted in the formation of cartilaginous condensation forming off the wrist (Figure 5.2. C and C'). Another graft to the posterior margin resulted in the formation of cartilaginous condensation adjacent to the digits (Figure 5.2. D and D'). The cartilaginous condensations which form off the wrist and adjacent to the digits are reminiscent of the single phalanx of digit 3, the most posterior digit in the chick wing. All contralateral wings had a normal cartilaginous structure (Figure 5.2.).

5.2.2 Utilising *GFP*-expressing chicks to map condensations after PR explant grafts

To determine if the ectopic cartilaginous structures are derived from PR explants, I utilised *GFP*-expressing chicks (McGrew et al., 2008). Grafting GFP tissue into a wildtype chick wing enables the identification of structures and tissues which arise from the graft as they continue to express *GFP* (Towers et al., 2011, Pickering and Towers, 2016). Thus, I used *GFP*-expressing chicks to create the PR explants which could then be treated with HBC/cyclopamine and grafted into wildtype host chicks (Figure 5.3. A and B).

Again, I found that grafting PR explant which had been incubated with HBC resulted in the normal development of the host wing (Figure 5.4. A). *GFP* was expressed in the soft tissue of the stylopod and zeugopod (Figure 5.4. B and C) indicating that the PR explant was incorporated into the developing wing without producing any additional cartilaginous structures. However, when a PR explant which had been incubated with cyclopamine for 24 hours was grafted into a wing, an extra cartilaginous structure formed at the elbow (Figure 5.4. D). This structure consisted of one long cartilaginous condensation originating from near the elbow which split into two smaller condensations at the tip (Figure 5.4. G). Importantly, this structure at the elbow expressed *GFP* (Figure 5.4. E and F) indicating that these additional

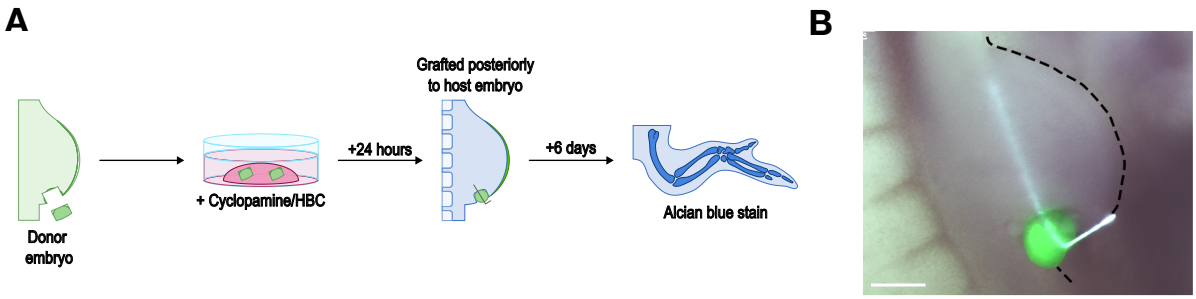

Figure 5.3. Grafting *GFP*-expressing PR explants to HH21/22 host chick wings.
A) Schematic of the grafting process. Polarising region explants are taken from a donor *GFP*-expressing embryo (green), cultured for 24 hours with either cyclopamine or HBC, then removed from culture and grafted to a either the anterior or posterior margin of a host embryo wing (blue). The host embryo is allowed to develop for 6 days before it is sacrificed and the cartilage is stained with alcian blue staining. B) *GFP*-expressing polarising region explant (green) grafted into the posterior host limb bud. All scale bars = 250μm.

cartilaginous condensations arose directly from the cyclopamine-treated PR explant. The left wing without a graft had a normal cartilage structure (Figure 5.4. H).

Unfortunately, as mentioned above, the survival rate of embryos with grafts was low and thus only one chick with GFP-expressing cyclopamine treated PR explant graft has survived to day 10 of incubation. Further surviving grafts would be required to definitively determine whether cyclopamine-treated PR explants give rise to additional cartilaginous condensations as my results here would indicate.

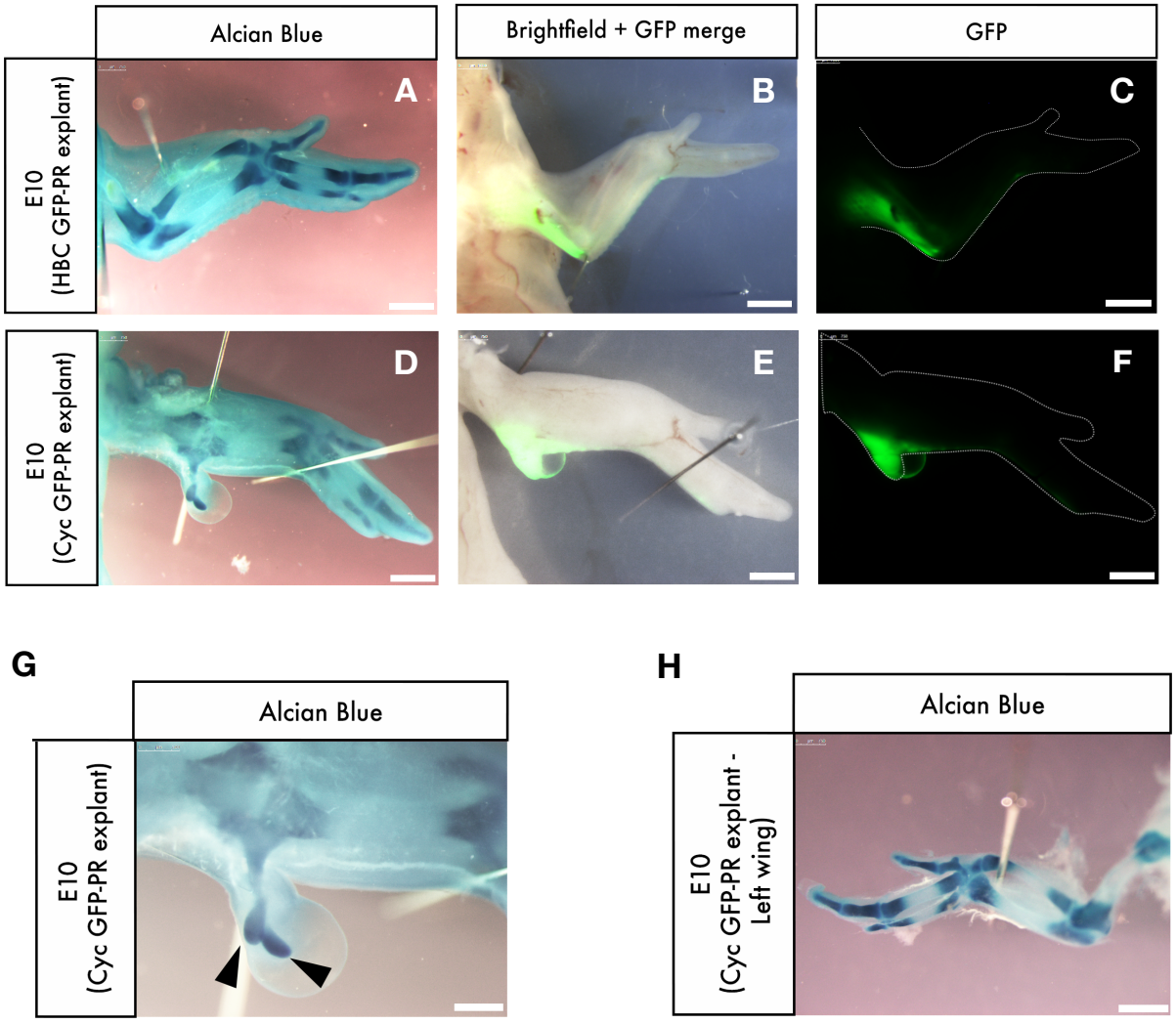

Figure 5.4. Cyclopamine treated PR Explants form cartilaginous condensations.

A-F) Wings at incubation day 10 (E10) with posteriorly grafted GFP-expressing PR explants (GFP-PR explants). The PR explants have been incubated with either cyclopamine or HBC for 24 hours. The wing with the HBC treated GFP-PR explant has not developed any additional cartilaginous condensations (A) with the GFP-PR explant contributing to soft tissue along the stylopod and zeugopod (B,C). The wing with the cyclopamine treated GFP-PR explant has developed a GFP-expressing growth at the elbow (E,F) which consists of two cartilaginous condensations (D, G (arrows)). The cartilaginous condensation consists of one long condensation and two small condensations. The left wing (control) without a cyclopamine treated GFP-PR explant has developed normally (H). Scale bars: A,B,C,D,E,F,H = 1mm, G = 500µm.

5.3. Discussion

In this chapter I have demonstrated that inhibiting Shh signalling in PR explants leads to the formation of additional cartilaginous structures when grafted into HH21/22 host chick wings. Furthermore, I have begun the show that these additional cartilaginous structures are derived from the PR explants themselves. Thus, the results here suggest that inhibiting Shh signalling in PR explants results in the formation of PR-derived cartilaginous condensations. Furthermore, the cartilaginous condensations that form after the grafting of a cyclopamine-treated PR explant are very similar to the single phalanx digit condensations that form after a wing PR is grafted to a chick leg (Towers et al., 2011). Additionally, single phalanx digit condensations, very similar to the cartilaginous condensations in Figure 5.2. C and D, form from the wrist region after the implantation of an Fgf-soaked bead (Nikbakht and McLachlan, 1999). In both cases, the authors term these additional single phalanx structures as rudimentary digits (Nikbakht and McLachlan, 1999, Towers et al., 2011), and thus the cartilaginous condensations that arise after a PR explant graft may be a rudimentary digit. It may be interesting to note that grafting the PR explants resulted in an array of cartilaginous structures throughout the wing (see Figure 5.2. and Figure 5.3.) which may be due to the location and orientation of the grafts differing between embryos.

Combined with the results from Chapter 4, my studies indicate that increased proliferation and *de novo* expression of *Grem1* and *Fgf8* leads to the formation of a digit-like single phalanx cartilaginous condensation. Furthermore, the increased expression of *Sox9* and *Bmp2* indicates that this cartilaginous condensation arises due to the Turing-type self-organisation mechanism which forms the digits *in vivo* (see Section 1.5.5. for more detail on digit formation). This is consistent with observations *in vivo* in which the inhibition of Shh signalling led to an increase in proliferation rate of PR cells and the extension of the AER over the PR which,

combined, led to the formation of a PR-derived digit (Pickering et al., 2019). However, as already mentioned, the application of a Fgf-soaked bead results in the formation of a single phalanx condensation (Nikbakht and McLachlan, 1999). Additionally, it has been demonstrated that prolonged exposure to Fgfs signalling *in vivo* can result in the formation of additional phalanges on digits (Sanz-Ezquerro and Tickle, 2003). Therefore, the phalanx-like structure may be a result of the increased *Fgf8* expression in the cyclopamine-treated explants.

Due to time constraints and the poor survival rate of embryos with grafts I have not been able to generate enough data to conclusively determine whether the additional cartilaginous structures are derived from PR-explant cells. Further grafts of *GFP*-expressing cyclopamine-treated PR explants into wildtype host chicks would be required in the future.

CHAPTER 6

Expression of cell cycle regulators in the mouse limb

6.1. Introduction

The results in the previous chapters indicate that Shh signalling in the chick wing PR prevents the formation of digits, in part, by intrinsically regulating proliferation parameters over time. As discussed in the main Introduction, evidence suggests that Shh signalling intrinsically controls cell cycle regulators in the PR to adjust proliferation rates (Towers et al., 2008, Pickering et al., 2019). This is a two-step process in which Shh signalling promotes G1-S phase entry via *Cyclin D2,* and then inhibits G1-S phase entry via a Bmp2-$p27^{kip1}$ pathway (Pickering et al., 2019). The inhibition of proliferation, at least in part, prevents the PR from producing a digit (Pickering et al., 2019).

As discussed in the main Introduction (see Section 1.8.), the common ancestor of birds and mammals had five digits (Chatterjee, 1998). Therefore,

comparing chick and mouse limbs may give insight into how digits 4 and 5 were lost during the evolution of the bird wing. For instance, the mouse PR gives rise to digits 4 and 5 (Harfe et al., 2004) whereas the chick PR only contributes to soft tissue along the posterior margin of the wing (Towers et al., 2011). Additionally, the AER in the mouse limb extends posteriorly over the PR; however, there is little overlap in the chick wing (Pickering and Towers, 2016; see also Figure 3.2.). Lastly, the chick wing has an area of cell death along the posterior margin known as the necrotic zone (Saunders Jr et al., 1962) which is not present in the developing mouse limb (Martin, 1990). Therefore, in this chapter, I aimed to analyse mouse limb development to determine if the expression of regulators of the G1-S phase transition in the PR is an avian-specific trait. I hypothesised that in the mouse limb *Cyclin D2,* which promotes G1-S phase entry, would be expressed in the posterior limb bud, as it is in the chick wing and thus proliferation is promoted in the mouse PR. However, I hypothesised that *p27^{kip1},* which inhibits G1-S phase entry, would not be detectable in the mouse limb, unlike in the chick wing where is expressed in the PR. A lack of p27^{kip1} in the mouse PR would suggest that proliferation of PR cells is not inhibited through G1-S phase regulators as it is in the chick.

6.2. Results

6.2.1. Correlating mouse forelimb and chick wing development

To analyse any potential differences in mouse forelimb development and chick wing development, I needed to understand the timing of mouse forelimb development in comparison to chick wing development. A staging system for mouse limb development based on morphological changes has already been established, during which the authors compared mouse limb stages to chick HH stages (Wanek et al., 1989).

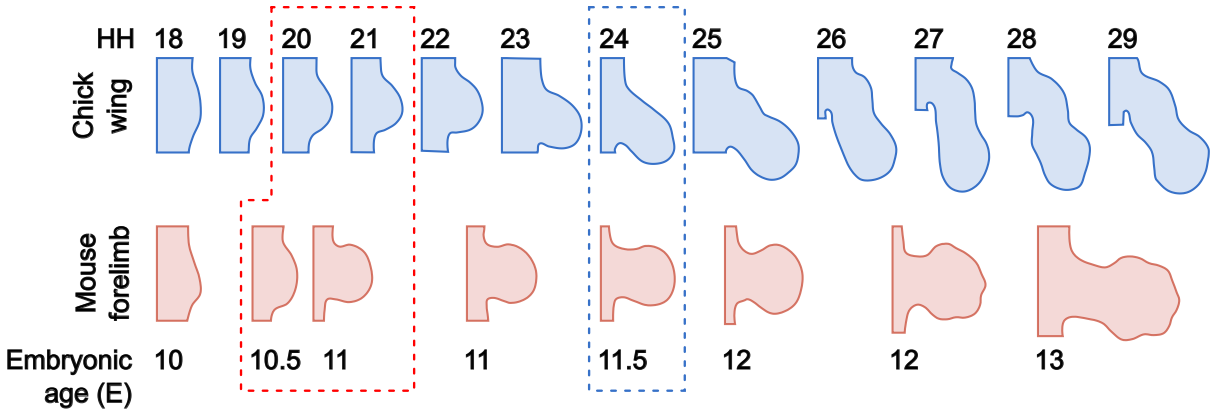

Figure 6.1. Comparing the relative ages of chick wing and mouse forelimb development.
Schematic showing chick wing (blue) and mouse forelimb development (red) at equivalent stages. Chick embryos are staged according to the Hamburger-Hamilton stages (HH), whereas mouse embryos are staged according to embryonic age. Red box: HH20/21 chick wings correlate with E10.5/E11 mouse forelimbs due to length to width ratio (Wanek et al., 1989). Blue box: HH24 chick wings correlate to E11.5 mouse forelimbs due to length to width ratio (Wanek et al., 1989). Images traced from Maccabe et al., 1973 and Wanek et al., 1989. Schematic limbs are not to scale.

During this thesis, I have primarily focussed on examining chick wing development at HH20/21 and HH24/25, therefore I intended to examine mouse limbs at equivalent stages of development. According to Wanek (1989), mouse forelimbs at E10.5 to E11 correlate with chick wing development at HH20/21 (Figure 6.1. red box) as judged by the length to width ratio of the developing wing bud and the presence of the AER. The authors also concluded that mouse forelimbs at E11.5 to E12 correlate with wing development at HH24/25 (Figure 6.1. blue box), judged again by the length to width ratio of the developing limb buds (Wanek et al., 1989).

6.2.2. Comparing expression patterns of *Shh* and *Cyclin D2* in the chick wing and mouse forelimb

As mentioned, it is suggested that Shh signalling initially promotes G1-S phase entry via Cyclin D2 in the chick wing PR, and both *Shh* and *Cyclin D2* are detected in the avian PR from HH20/21 (Towers et al., 2008, Pickering et al., 2019). As outlined above, I hypothesised that in the mouse forelimb, *Cyclin D2*, which promotes G1-S phase entry would be expressed in the posterior limb bud. I therefore began by analysing the expression of *Shh* and *Cyclin D2* in the developing mouse forelimb and comparing the results to expression in the chick wing bud.

Previous studies have shown that *Shh* is expressed in the mouse forelimb from approximately E9.75 but is undetectable by E12.5 (Echelard et al., 1993). I initially analysed expression at E10.5 and E11.5, stages that equate to HH20/21 and HH24, respectively. As a control, whole mount chromogenic *in situ* hybridisations showed that *Shh* is expressed in the mouse PR at E10.5 (Figure 6.2. A; n = 4/4) and E11.5 (Figure 6.2. B; n = 4/4), corresponding to *Shh* expression in the chick wing at equivalent ages of HH20/21 (Figure 6.2. C) and HH24/25 (Figure 6.2. D) respectively (Wanek et al., 1989, Echelard et al., 1993, Riddle et al., 1993).

To determine whether Shh may promote G1-S phase entry through Cyclin D2 in mouse forelimb PR cells, as proposed in the chick wing (Towers et al., 2008, Pickering et al., 2019), I performed whole-mount *in situ* hybridisation for *Cyclin D2* expression in mouse forelimbs at E10.5 and E11.5. *Cyclin D2* is weakly expressed in a horse-shoe shape around the distal half of the mouse forelimb bud at E10.5 (Figure 6.2. E; n = 5/6). At E11.5, *Cyclin D2* is expressed throughout the limb bud with higher levels detectable in the posterior-distal part of the limb (Figure 6.2. F arrow; n = 4/4). This expression of *Cyclin D2* in the mouse forelimb diverges from what is known in the chick wing. It has been demonstrated that between HH20 and HH22 in the chick wing, *Cyclin D2* is restricted to the PR (Figure 6.2. G (arrow); Towers et al., 2008,

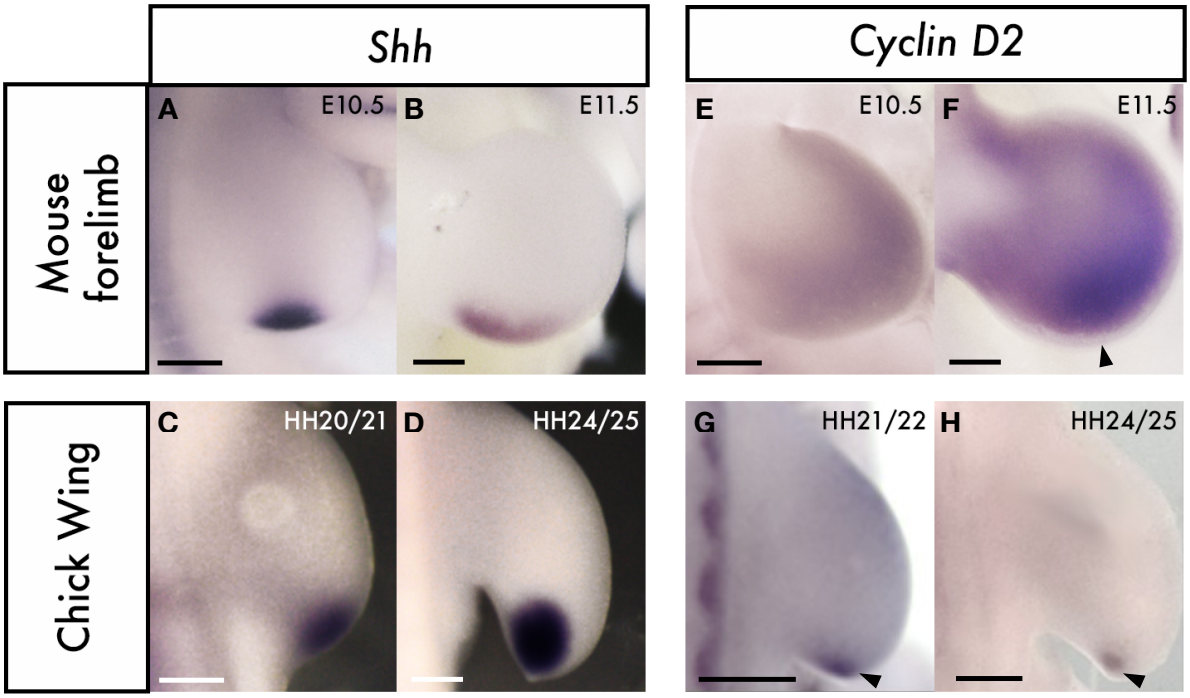

Figure 6.2. *Shh* and *Cyclin D2* expression in the developing mouse forelimb and chick wing.

Whole mount in situs for *Shh* and *Cyclin D2.* A - D) *Shh* is present in the posterior mesenchyme of the mouse forelimb at E10.5 (A; n = 4/4) and E11.5 (B; n = 4/4). *Shh* is also present in the posterior mesenchyme of chick wing at HH20/21 (C; n = 6/6) and HH24/25 (D; n = 4/4). E - H) *Cyclin D2* is present in the distal half of the mouse forelimb at E10.5 (E; n = 4/4). *Cyclin D2* expression spreads throughout the mouse forelimb at E11.5, but higher levels are detectable in the posterior-distal limb bud (F; n = 4/4). In the chick wing, *Cyclin D2* expression is restricted to the posterior mesenchyme at both HH21/22 (G; black arrow) and HH24/25 (H; black arrow; images for G and H taken from Pickering et al., 2019). All scale bars = 250 μm.

Pickering et al., 2019). This expression continues to be restricted to the PR at HH24/25 (Figure 6.2. H (arrow); Towers et al., 2008, Pickering et al., 2019).

These analyses show that, while *Shh* is expressed similarly in the PR in chick and mouse, *Cyclin D2* expression diverges in mouse compared to the chick; in chick C*yclin D2* expression is restricted to PR cells, however in the mouse *Cyclin D2* is expressed throughout the distal limb field, including, but not restricted to, the PR.

6.2.3. Comparing expression patterns of *Bmp2* and p27^{kip1} in the chick wing and mouse forelimb

It has been suggested that Shh signalling inhibits G1-S phase entry via a Bmp2-p27^{kip1} pathway in the chick wing PR (Pickering et al., 2019). As outlined above, I hypothesise that this might be an avian-specific trait. To determine this, I examined the expression of *Bmp2* and *p27^{kip1}* in the mouse forelimb through whole mount in situ hybridisation and compared it to expression in the chick wing.

It has been previously reported that transcripts of *Bmp2* can be found in the mouse forelimb as early as E9.5 (Lyons et al., 1990), and that at E10.5, it is weakly expressed in the posterior limb and under the AER (Lyons et al., 1990, Büscher et al., 1997). I attempted to confirm the expression pattern at E10.5 (Figure 6.3. A; n = 2/4), however, I found that in some embryos expression of *Bmp2* at this stage was too weak to be detectable (n = 2/4). I extended these studies, by analysing expression of *Bmp2* at E11.5. At this time point, *Bmp2* is strongly expressed in the posterior limb bud (Figure 6.3. B white arrow; n = 6/7) and more weakly in the distal limb under the AER Figure 6.3. B black arrow; n = 6/7). This expression pattern of *Bmp2* in the mouse limb is not identical to that in the chick wing where *Bmp2* is restricted to the posterior mesenchyme at both HH20/21 (Figure 6.3. C; n = 8/8) and HH24/25 (Figure 6.3. D; n = 7/7; Francis et al., 1994). Importantly, the expression of *Bmp2* in the mouse limb is too proximal to be associated with the PR.

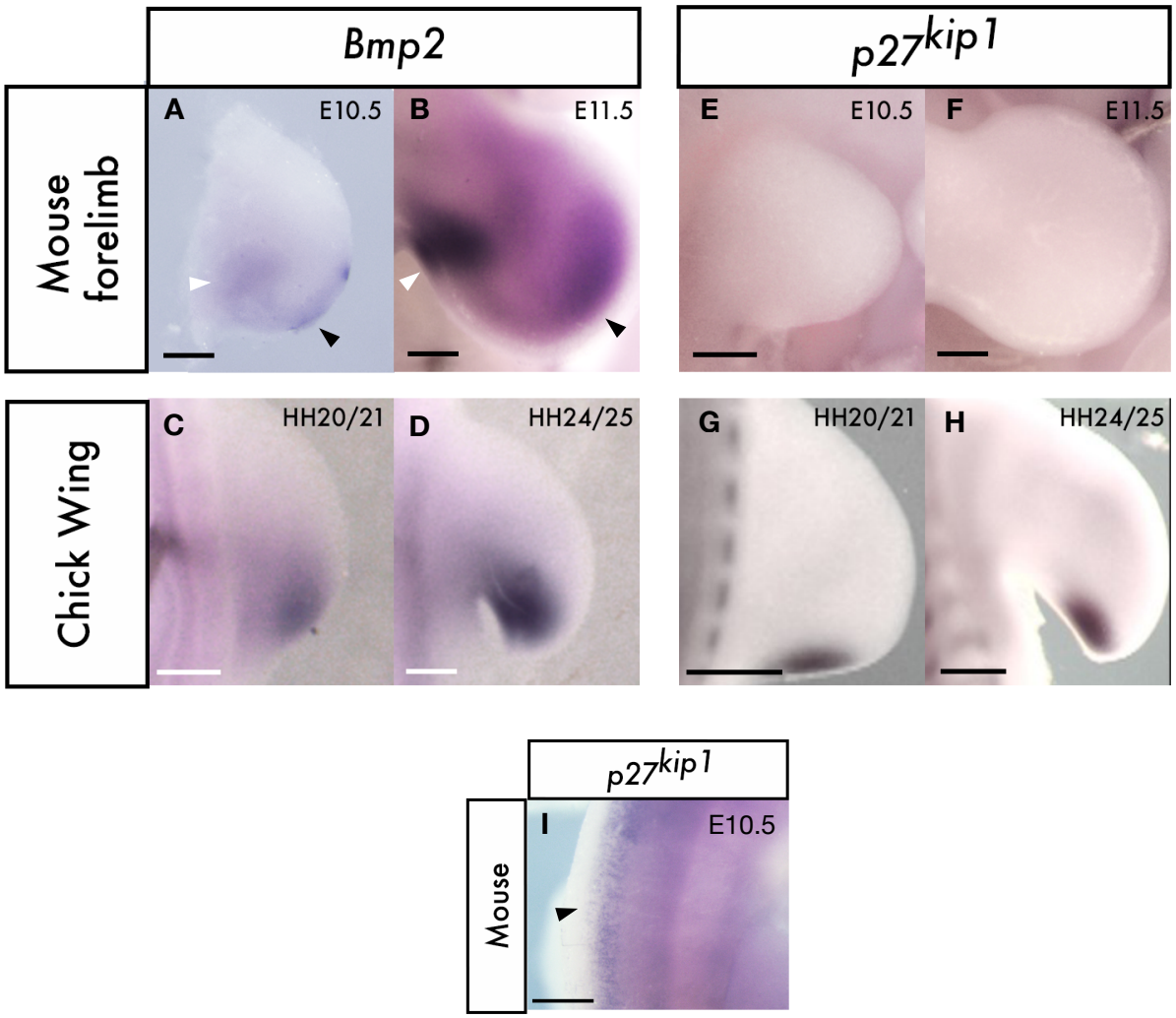

Figure 6.3. *Bmp2* and *p27^{kip1}* expression in the developing mouse forelimb and chick wing.

Whole mount in situs for *Bmp2* and *p27^{kip1}.* A - D) In the mouse forelimb *Bmp2* at E10.5 is expressed in the very weakly in both the posterior mesenchyme (A; white arrow; n =2/4) and distally under the AER (A black arrow; n = 2/4), however this expression is often too weak to pick up. At E11.5 *Bmp2* is present in the posterior mesenchyme (B white arrow) and under the AER (B black arrow; n = 6/7). *Bmp2* is present in the posterior mesenchyme of chick wing at HH20/21 (C; n = 8/8) and HH24/25 (D; n = 7/7). E - H) *p27^{kip1}* is not present in the mouse forelimb at E10.5 (E; n = 4/4), nor is it present at E11.5 (F; n = 5/5). In the chick wing, *p27^{kip1}* expression is restricted to the posterior mesenchyme at both HH21/22 (G) and HH24/25 (H; images for G and H taken from Pickering et al., 2019). *P27^{kip1}* is expressed in the neural tube of E10.5 mouse embryos providing a positive control (I). All scale bars = 250 μm.

Interestingly, I found that *p27^{kip1}* is not detectable in the mouse limb at E10.5 (Figure 6.3. E; n =4/4) nor at E11.5 (Figure 6.3. F; n = 5/5). This is remarkably different to the expression of *p27^{kip1}* in the chick wing, which has been found to be restricted to the posterior mesenchyme at both HH20/21 (Figure 6.3. G) and HH24/25 (Figure 6.3. G; Pickering et al., 2019). As a positive control, I examined the expression of *p27^{kip1}* elsewhere in the E10.5 embryo. Previous immunohistochemistry studies have found that p27^{kip1} protein is expressed in the spinal cord of the E10.5 mouse embryos (Gui et al., 2007, Iulianella and Stanton-Turcotte, 2019). I identified expression of *p27^{kip1}* in the spinal cord of E10.5 mouse embryos (Figure 6.2. I). Thus, the lack of *p27^{kip1}* in the mouse PR indicated that this component of the proliferation regulatory system may diverge in chick and mouse.

6.3. Discussion

In this chapter, I analysed the expression of key regulators of the G1-S phase transition during mouse forelimb development and compared the results to the expression already identified in chick wing development. Whilst expression of *Shh* maintains a similar pattern during mouse forelimb and chick wing development, expression of *Cyclin D2, Bmp2* and *p27^{kip1}* is inconsistent between the two species.

In the developing chick wing, *Cyclin D2* expression is restricted to the posterior mesenchyme, and it is suggested that this promotes G1-S phase transition in PR cells (Pickering et al., 2019). I hypothesised that in the mouse forelimb *Cyclin D2* would also be expressed in the posterior mesenchyme, however I have now revealed that *Cyclin D2* is expressed throughout the distal part of the developing limb bud.

It is also theorised that in the developing chick wing G1-S phase entry is inhibited through a Bmp2-p27^{kip1} pathway. As discussed in this chapter, *Bmp2* is known to be expressed in different parts of the mouse forelimb and chick wing; In the mouse forelimb *Bmp2* is expressed in the posterior mesenchyme and under the AER

(Büscher et al., 1997), whereas in the chick wing, it is only expressed in the posterior mesenchyme (Francis et al., 1994). Importantly, it appears that *Bmp2* is not expressed in the PR of the developing mouse forelimb. The results in this chapter also reveal that there is no expression of *p27^{kip1}* in the developing mouse limb which contrasts with the developing chick wing where *p27^{kip1}* is expressed in the posterior mesenchyme (Pickering et al., 2019). Therefore, it is unlikely that the PR in the mouse forelimb inhibits proliferation through a Bmp2- p27^{kip1} pathway as is seen in the chick wing PR.

The results in this chapter demonstrate differences in expression of *Cyclin D2, Bmp2* and *p27^{kip1}* between developing mouse forelimbs and chick wings. Crucially, expression of *Cyclin D2* and *Bmp2* are not restricted to the posterior mesenchyme of the mouse forelimb whilst *p27^{kip1}* is entirely absent. Taken together, the data presented in this chapter suggests that the expression of regulators of the G1-S phase transition in the PR is an avian-specific trait.

CHAPTER 7

Discussion

7.1. Summary

In this thesis, I have presented a PR explant model which I have used to reveal that cells intrinsically maintain *in vivo* temporal parameters, in particular the duration of *Shh* expression and the rate of proliferation. This occurs in the absence of more anterior *Grem1*-expressing mesenchyme and AER-Fgfs. By inhibiting Shh signalling through cyclopamine, I have shown that PR explants establish *Grem1* expression in the wider end of the explant which likely supports the re-establishment of AER-like *Fgf8*-expressing cells. Additionally, I demonstrated that $p27^{kip1}$ expression, which is maintained in the control PR explants, is lost following the inhibition of Shh signalling. Furthermore, application of cyclopamine to PR explants has shown that Shh signalling temporally regulates proliferation. Thus, it is likely that the over-proliferation of PR cells following Shh signalling inhibition is a direct result of

the loss of *p27^{kip1}* expression and is permissively supported by the re-emergence of AER-like cells.

In addition, I demonstrated that after inhibition of Shh signalling, PR cells begin to adopt digit precursor identities and express *Sox9* and *Bmp2* in the narrower end of the explant. Once transplanted into a host wing, these explants form phalanx-like cartilaginous condensations, demonstrating that Shh signalling prevents the formation of a PR-derived digit in the chick wing.

Moreover, I demonstrated that expression of *Cyclin D2* is not restricted to the PR of mouse limbs as it is in the chick wing. Instead, *Cyclin D2* is expressed throughout the limb with higher levels detectable in the posterior-distal part of the limb. This indicates that *CyclinD2* in mouse limbs is not required for specifically regulating proliferation in the PR. I also demonstrated that expression of *p27^{kip1}* is absent in the mouse forelimb indicating that expression in the PR is an avian specific trait that prevents digit formation.

7.2. Insights into PR development using a chick wing PR explant model

7.2.1. PR cells intrinsically time the duration of *Shh* expression and regulate proliferation parameters

One of the key aims of this thesis was to develop a chick wing PR explant model to determine the patterning and growth parameters of PR cells in the absence of signals that could be essential for *in vivo* development. The PR is a key developmental organiser in the limb and the extent to which it is able to function autonomously has been pondered in previous studies. Additionally, limb explants have recently been used to demonstrate how the essential role for AER-Fgfs can be bypassed *ex vivo* (Sedas Perez et al., 2023). In my thesis, I demonstrated that explanted PR cells maintain the normal duration of *Shh* expression and proliferation

parameters in line with *in vivo* development. Crucially, my results indicate that the PR maintains *in vivo* parameters intrinsically, as the PR explants at the time of dissection did not contain *Fgf8*-expressing AER cells or *Grem1*-expressing anterior mesenchymal cells. These results are supported by a previous study which demonstrated, through heterochronic grafts, that the duration of *Shh* expression is intrinsically regulated (Chinnaiya et al., 2014). In this study, it was found that when PRs from young chick wings (i.e. HH20) were grafted to older chick wings (i.e. HH24), they maintained *Shh* expression consistent with their own age, rather than the age of the host (Chinnaiya et al., 2014). Thus, as the PR does not alter the duration of *Shh* expression in response to extrinsic factors from the host, this result supports my data indicating that the PR intrinsically times the duration of *Shh*. Furthermore, it was found that the young grafted PRs maintained proliferation rates consistent with their age when transplanted to older host wings (Chinnaiya et al., 2014). In addition, PRs grafted between chick and quail wings maintain proliferation rates consistent with both their species and their age (Stainton and Towers, 2022). These studies support my data as they indicate that the proliferation rates are intrinsically timed in PR cells and are not reset or altered by extrinsic factors in host limbs. Thus, my results add to previous studies to demonstrate that the duration of *Shh* expression and proliferation parameters are intrinsically regulated by PR cells after HH20/21.

It was interesting that *Shh* expression was maintained in the complete absence of *Fgf8*-expressing AER cells and *Grem1*-expressing anterior mesenchymal cells, as it had been suggested that *Shh* expression in the chick PR is maintained by AER-Fgfs in an AER-Fgf/Shh/Grem1 positive feedback loop. In this loop, AER-Fgfs maintain *Shh* expression, Shh then induces *Grem1* expression and Grem1 suppresses Bmp signalling which would inhibit AER-Fgfs (Figure 7.1.; Laufer et al., 1994, Niswander et al., 1994, Zúñiga et al., 1999). It is important to note that Shh signalling is established approximately 12 hours before the time of dissection at HH20/21. Thus, whilst this loop may be essential for establishing Shh signalling in

the PR and maintaining the expression during the early stages of limb development, my data suggests that it is dispensable after *Shh* expression has been established (Figure 7.1.). This theory is supported by experiments that demonstrate that inhibiting Shh signalling at HH20/21 results in the expansion of *Grem1* into the PR area (Pickering and Towers, 2016). This result corroborates that after HH20, the AER-Fgf/Shh/Grem1 loop is dispensable in the developing limb. Thus, my data indicates that once Shh signalling has been established, AER-Fgfs are not required to maintain *Shh* expression in PR cells. Instead, the duration of *Shh* expression and the

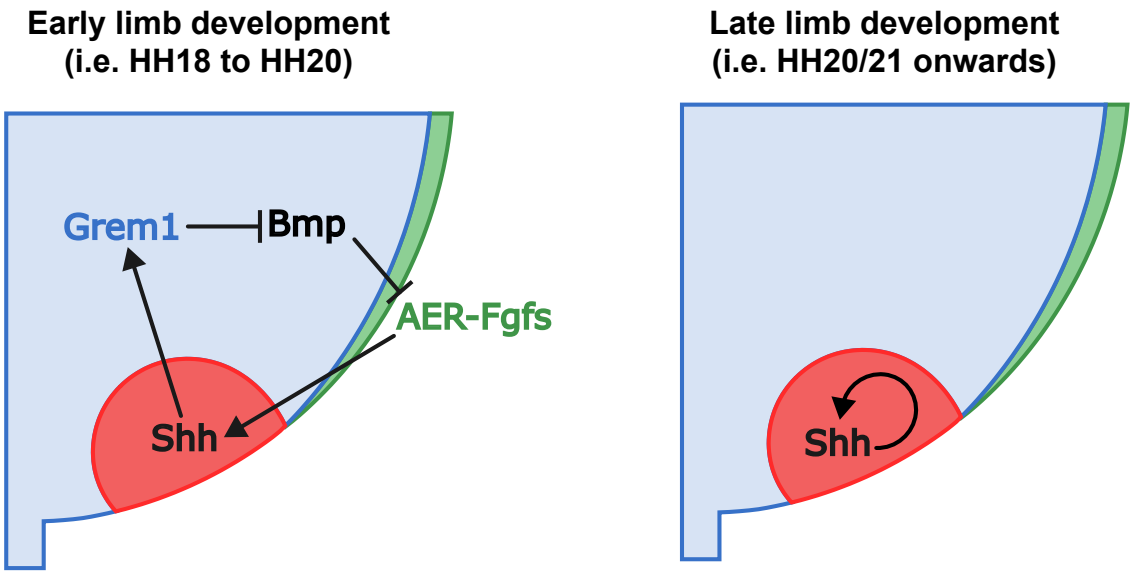

Figure 7.1. The AER-Fgf/Shh/Grem1 feedback loop is dispensable for late limb development.
During early limb development AER-Fgfs promote and maintain *Shh* expression in the PR. In turn, Shh up-regulates *Grem1* in the anterior mesenchyme. Grem1 antagonises BMP which permissively supports AER-Fgfs. Thus an AER-Fgf/Shh/ Grem1 feedback loop is established. This feedback loop is dispensable after HH20/21 when the PR intrinsically maintains the duration of *Shh* expression.

proliferation parameters of the PR are intrinsically timed and regulated by PR cells (Figure 7.1.).

Interestingly, in HH20 distal limb explants, which contain AER cells, anterior mesenchymal cells and PR cells, attenuating Fgf signalling leads to a loss of *Shh* expression after 24 hours (Sedas Perez et al., 2023). However, RNA-sequencing found that the explants with attenuated Fgf signalling up-regulated *Alx4* (Sedas Perez et al., 2023), which is known to repress *Shh* expression in the anterior region of the limb (Takahashi et al., 1998). Combined with the results presented in this thesis, it could be suggested that, whilst *Shh* expression can be intrinsically regulated and maintained by PR cells, Fgf signalling is required to prevent the repression of *Shh* in PR cells by extrinsic factors, such as Alx4. However, this possibility has not been fully explored.

There are some caveats to bear in mind with this research. Firstly, it is possible that Fgfs were present in the culturing matrix/media and in the mesenchymal cells. To account for this, I performed a preliminary experiment where I applied SU4052, a drug which inhibits Fgf signalling, to the explants, however none of the explants survived and I was not able to repeat this experiment during my PhD timeline. Nonetheless, my results still demonstrate that an AER is not required to maintain PR parameters as the majority of my explants did not contain *Fgf8*-expressing cells. Additionally, it is unlikely that defined concentrations of Fgfs in the culturing media/matrix are required to support the PR development. Secondly, the PR explants contained dorsal and ventral ectoderm. This is relevant as it has been suggested that Wnt7a is required to maintain Shh expression in the PR (Yang and Niswander, 1995). However, the study did reveal that *Wnt7a* expressing cells could not induce *Shh* expression when the AER was removed (Yang and Niswander, 1995), thus it is likely that Wnt7a has a negligible effect on maintaining *Shh* expression in the PR explants.

7.2.2. *Fgf8*-expressing cells arise due to self-organisation after Shh signalling is inhibited in the PR

During *in vivo* chick wing development, the AER lies distally to, but not covering, the PR. However, when Shh signalling is inhibited in the chick wing, the AER extends posteriorly over the PR (Towers et al., 2011). Similarly, I demonstrated that inhibiting Shh signalling leads to the re-emergence of a small population of cells which express *Fgf8* in the wider region of the PR explant. Thus, this indicates that the wider region of the explant has a more distal identity whilst the narrower region has a more proximal identity (Figure 7.2. A). Furthermore, I demonstrated that, following Shh inhibition, the distal explant expressed higher levels of *Mkp3,* a marker of Fgf activity. Thus, my results suggest that PR Shh signalling inhibits the formation of posterior AER in the chick wing. This is consistent with findings that both grafts of PRs and beads soaked in Shh-protein cause the AER to regress in *in vivo* chick wings (Saunders Jr and Gasseling, 1968, Bouldin et al., 2010).

Interestingly, I demonstrated that inhibition of Shh leads to increased *Grem1* expression in the distal PR explants. Grem1 is a Bmp-antagonist and is necessary for up-regulating and maintaining expression of AER-Fgfs (Michos et al., 2004). The expansion of *Grem1* is consistent with *in vivo* development, as application of cyclopamine causes the extension of the *Grem1* expression domain into the posterior margin of the limb bud (Pickering and Towers, 2016). Thus, I speculate that the increased *Grem1* expression leads to the up regulation of *Fgf8* in a small population of epithelial cells in the PR explant. Furthermore, Grem1 antagonises Bmps in the mesenchyme and promotes the expression of *Bmp2* in the AER (Michos et al., 2004). *Bmp2* is expressed in the proximal explant and within a small population of cells in the distal region. The results in my thesis, therefore, suggest that the PR explants have the ability to self-organise and re-establish a population of AER-like cells following Shh inhibition. In this mechanism, *Grem1* expression is up regulated in the distal explant, which in turn restricts *Bmp2* expression to the proximal explant.

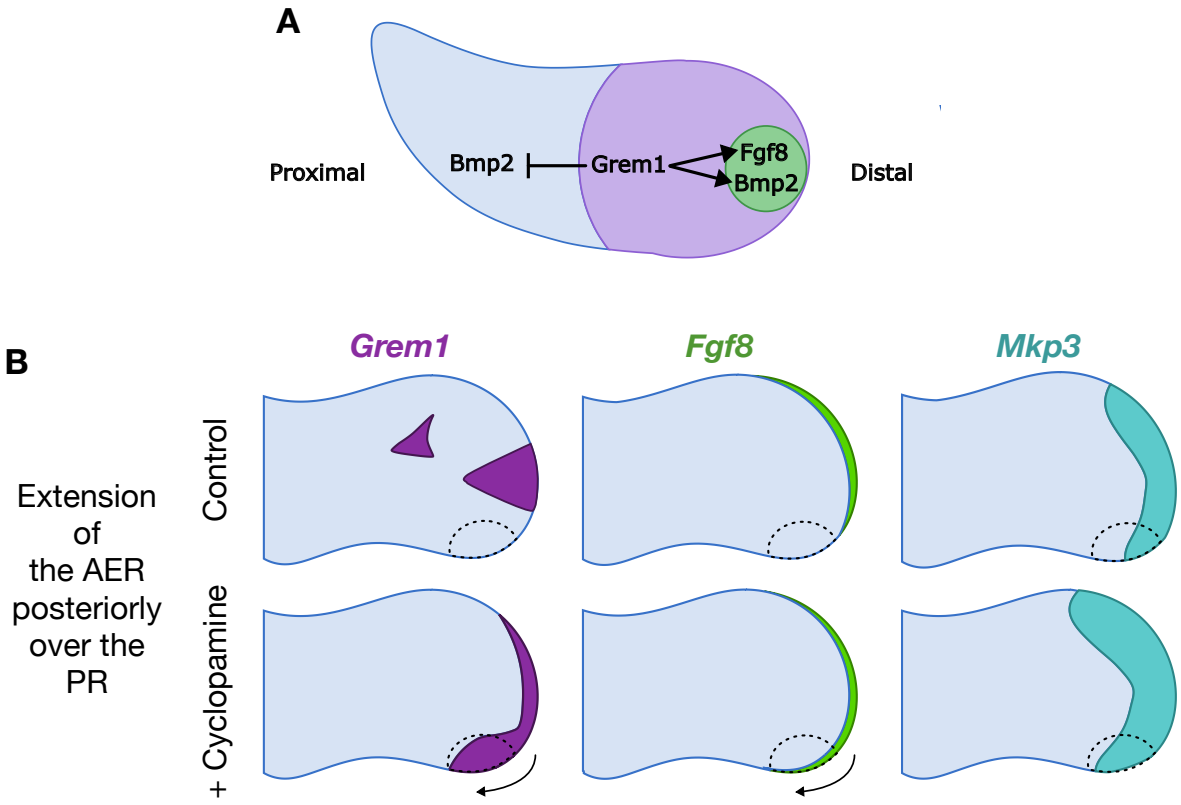

Figure 7.2. PR explants self-organise and express *Grem1* to produce AER-like cells after Shh inhibition.

A) Schematic showing the self-organising ability of the explant. The proximal end of the explant is wider and expresses *Grem1*. It is likely that Grem1 antagonises Bmp signalling in the proximal, restricting the expression of *Bmp2* to the distal explant. The antagonism of Bmps allows for the formation of an AER-like group of cells (green) which expresses *Fgf8*. Grem1 likely up-regulates expression of *Bmp2* in the AER-like cells. B) I suggest that, in the chick wing *in vivo*, Shh signalling inhibits the expression of *Grem1* in the PR to prevent the formation the AER. C) Therefore, *in vivo*, I predict that inhibiting Shh signalling allows for the extension of *Grem1* expression into the PR which leads to the formation of *Fgf8*-expressing AER over the PR. As a result, there is increased *Mkp3* within the PR area. Dashed line = approximate PR location.

The Bmp antagonism allows for the *de novo* expression of *Fgf8* in a small population of epithelial cells causing an increase in *Mkp3* expression in the distal explant. Grem1 up-regulates *Bmp2* in the population of *Fgf8-expressing* cells, further indicating their similarities to the *in vivo* AER (Figure 7.2. A).

This result is important as it was not previously clear how the AER extended posteriorly over the PR following Shh signalling inhibition. Early fate-mapping of the AER demonstrated that the AER shifts anteriorly during development (Vargesson et al., 1997), thus it was unlikely that the AER moved over the PR via the extension of cells. My results indicate that the AER is re-established over PR cells, likely due to the posterior expansion of *Grem1* expression domain which antagonises Bmps allowing for the expression of *Fgf8* in epithelial cells (Figure 7.2. B). Thus, during limb development, Shh signalling inhibits expression of *Grem1*, which effectively inhibits the formation of the AER over the PR.

7.2.3. Shh signalling intrinsically regulates proliferation in the chick wing PR to prevent it forming a digit

It has been proposed that Shh signalling in the chick wing is required to temporally regulate proliferation rates of PR cells to prevent the formation of an additional digit (Pickering et al., 2019). Shh signalling is initially required to promote proliferation through *Cyclin D2 but* is subsequently required to inhibit proliferation through a Bmp2- $p27^{kip1}$ pathway (Figure 7.3. A). Furthermore, as I have demonstrated, Shh signalling is required to inhibit the formation of the AER which *in vivo* supports the formation of an additional digit (Pickering and Towers, 2016, Pickering et al., 2019). The results I have presented in this thesis, which I will discuss below, support this model.

Firstly, I found that inhibiting Shh signalling results in a significant increase in proliferation in PR explants 48 hours after cyclopamine application, consistent with

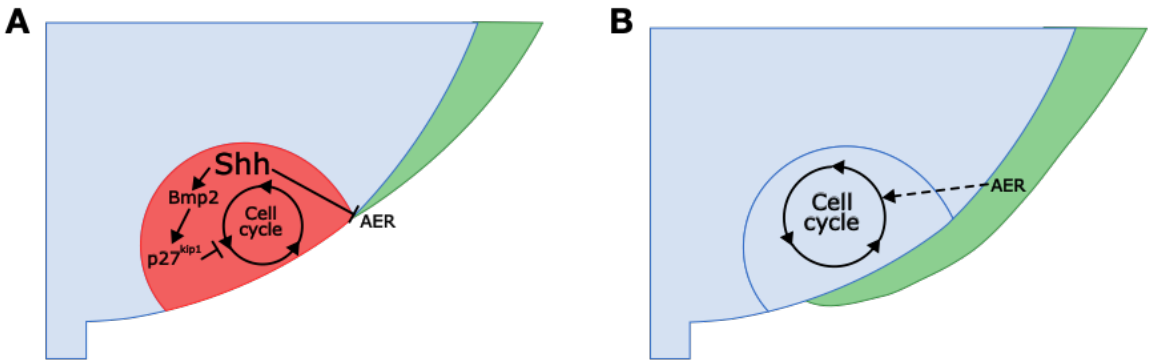

Figure 7.3. The current model detailing how Shh signalling regulates proliferation in the chick wing PR to prevent the formation of a PR-derived digit

A) Shh prevents the over-proliferation of cells by up-regulating a Bmp2-p27^{kip1} pathway in the PR which inhibits the cell cycle. Additionally, Shh signalling prevents the AER from forming over the PR. B) When Shh signalling is inhibited the Bmp2-p27^{kip1} pathway is lost leading to the over-proliferation of cells in the PR. The AER forms over the PR and supports increased proliferation rates throughout the AP axis.

experiments *in vivo* (Chinnaiya et al., 2014, Pickering and Towers, 2016, Pickering et al., 2019). This coincided with an increase in explant growth between 24 and 48 hours after treatment. Thus, these results indicate that reduction in proliferation rates of PR cells is intrinsically regulated by Shh signalling.

Secondly, I demonstrated inhibiting Shh signalling results in a complete loss of *p27^{kip1}* expression in PR explants. Furthermore, *Bmp2* expression was restricted to the proximal region of the explant likely due to Grem1 antagonism (see Section 7.2.2.). This is consistent with the loss of the Bmp2- p27^{kip1} pathway in the *in vivo* chick wing PR after the application of cyclopamine (Figure 7.4. A; Pickering et al., 2019). Thus, my results demonstrate that this pathway is intrinsically regulated by Shh signalling. Furthermore, it has been demonstrated *in vivo* that application of a

Bmp2-soaked bead after Shh signalling induces the expression of *p27^{kip1}* in the PR which reduces the proliferation rate of PR cells (Pickering et al., 2019). Thus, I can deduce that the increased proliferation rates in PR explants after Shh signalling inhibition are due to the loss of *p27^{kip1}* expression.

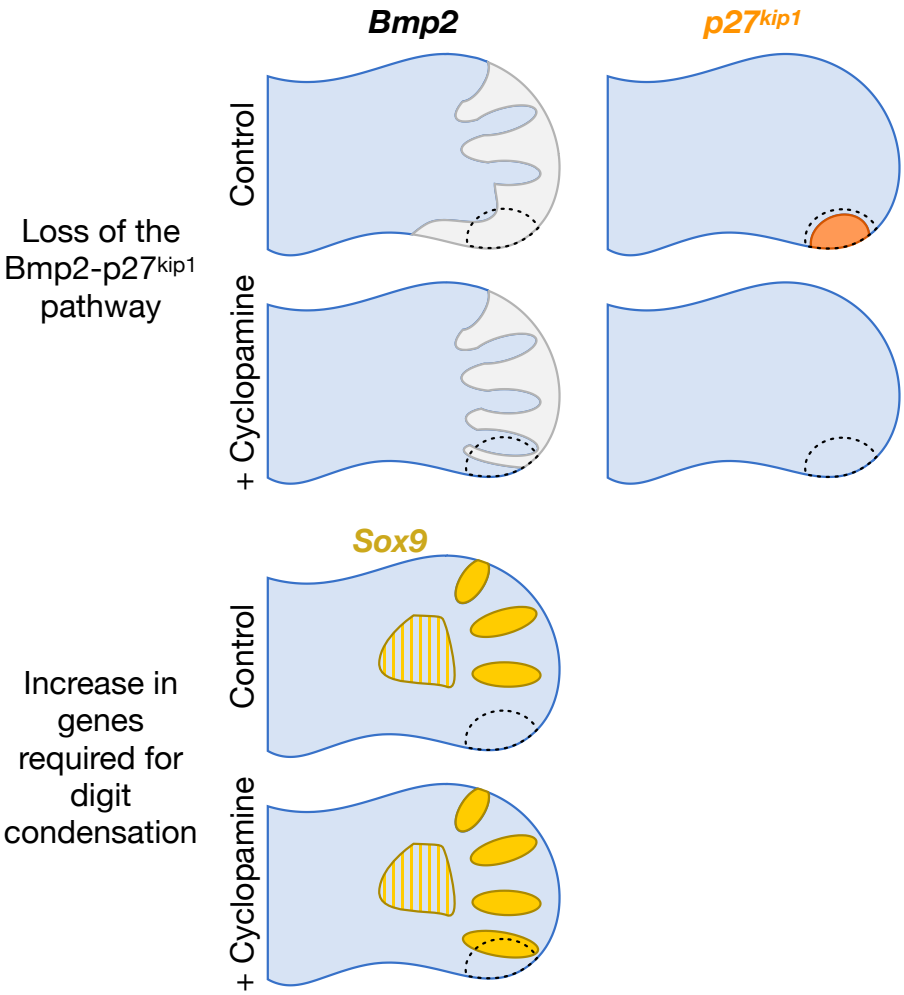

Figure 7.4. Predicted effects of inhibiting Shh signalling with cyclopamine in the chick wing at HH27 (48 hours after cyclopamine treatment).
A) When Shh signalling is inhibited *Grem1* and *Fgf8* expression extends posteriorly into the PR domain (PR indicated by black dashed line). *Mkp3* expression increases in the PR domain. B) When Shh signalling is inhibited there is an increase in *Sox9* expression in the PR domain.

Lastly, as already discussed, I demonstrated that AER-like cells form *de novo* in cyclopamine-treated PR explants, consistent with the formation of the AER over the PR *in vivo* following Shh inhibition (see Section 7.2.2.; Pickering and Towers, 2016). As my results indicate that proliferation is intrinsically regulated by Shh signalling in the PR, it is likely that the AER permissively supports an increase in proliferation within PR cells following Shh inhibition (Figure 7.3. B). This is consistent with experiments *in vivo* which concluded that the AER supports increased proliferation in PR cells following Shh inhibition (Figure 7.3. B; Pickering and Towers, 2016). In these experiments wings which were treated with cyclopamine and had the extended AER removed from the PR did not maintain the same rate of proliferation as contralateral limbs with an intact AER (Pickering and Towers, 2016). Therefore, my results support the model that Shh signalling intrinsically inhibits proliferation in PR cells via the Bmp2- $p27^{kip1}$ pathway. Simultaneously Shh signalling inhibits the formation of the AER over PR cells, thus preventing the AER from permissively supporting proliferation.

7.2.3.1. The developmental potential of PR explants

In the previous section, I demonstrated that Shh signalling inhibition causes the over-proliferation of PR explant cells, likely through a loss of $p27^{kip1}$ expression and the formation of AER-like cells. My data showed that PR explants express *Sox9* and *Bmp2* - both markers of digit formation (Figure 7.4. B; Bi et al., 1999, Healy et al., 1999) - in the proximal explant following inhibition of Shh signalling. By grafting cyclopamine-treated explants into host wings, I demonstrated that cyclopamine-treated PR explants produce phalanx-like cartilaginous condensations. Using *GFP*-expressing chicks, I was able to fate map a cartilaginous condensation which arose from a cyclopamine-treated PR explant. Therefore, my data is consistent with studies demonstrating that inhibition of Shh signalling at HH20/21 *in vivo r*esults in the formation of an PR-derived digit (Pickering and Towers, 2016, Pickering et al., 2019). Furthermore, the data in this thesis supports findings that the loss of the Bmp2-

$p27^{kip1}$ pathway and emergence of the AER over the PR are prerequisites for the formation of a digit from PR cells (Pickering and Towers, 2016, Pickering et al., 2019). It is likely that the emergence of AER-like cells both permissively supports increased PR proliferation rates and the formation of a phalanx-like structure. Prolonged exposure to Fgf8 *in vivo* can result in the formation of additional phalanges on the digits (Sanz-Ezquerro and Tickle, 2003) whilst implantation of an Fgf-soaked bead elongates a small cartilaginous condensation posterior to the digits into a rudimentary digit (Nikbakht and McLachlan, 1999).

It is important to note, however, that due to the poor survival rate of embryos post-grafting, I was not able to generate more than one *GFP*-expressing fate map within the timeline of my PhD. Nonetheless, my data suggests that inhibition of Shh signalling in PR explants leads to the over-proliferation of cells and the formation of phalanx-like cartilaginous condensations.

7.3. The avian wing has evolved a mechanism to prevent the formation of a PR digit

My results could indicate that the avian wing PR has evolved an intrinsic cell cycle inhibitory mechanism to prevent the formation of a PR digit. To examine this, I analysed the expression of G1-S phase regulators in the developing mouse forelimb. Mammals and birds diverged from a five-digit common ancestor approximately 300 million years ago (Figure 7.5 A; Carroll, 1969, Smithson et al., 1993). Therefore, the mouse forelimb, which retains the ancestral pentadactyly state - although not the ancestral phalangeal pattern as digits 2 to 5 all contain the same number of phalanges - presents an interesting model for examining how digit number evolved as it can be used as a good approximation for the ancestral limb of birds and mammals. It is important to note that the mouse PR - which is covered entirely by the AER (Pickering and Towers, 2016) - produces 2 digits (i.e. digit 4 and 5; Harfe et al., 2004). My results demonstrate that the expression of key G1-S phase regulators -

Cyclin D2, Bmp2 and *p27^{kip1}* - differs between mouse forelimbs and chick wings at equivalent stages of development.

I revealed that *Cyclin D2,* which promotes the G1-S phase transition is expressed throughout the distal part of the mouse forelimb, whilst in the chick wing it is restricted to the PR (Towers et al., 2008). Thus, this indicates that Cyclin D2 in the mouse limbs is not required for the specific promotion of proliferation of PR cells. It is of note that the shape of mouse and chick forelimbs are not similar, with mouse limbs being wider and more paddle-shaped across the AP axis than chick wings (see Fig 6.1. in Chapter 6.2.1.). Interestingly, the chicken *talpid 3* mutant - which expresses *Shh* more widely in the distal limb (Davey et al., 2006) - has a wider, more paddle-shaped wing with *Cyclin D2* expression throughout the distal portion (Towers et al., 2008). Furthermore, when Shh signalling is inhibited in the wing at HH20/21 the limb expands across the AP axis likely due to the over-proliferation of cells supported by an extended AER (Pickering and Towers, 2016). Thus, I can speculate that the wide paddle-shaped limb of the mouse is a result of increased proliferation across the AP-axis which is directed by increased Cyclin D2 activity in the distal limb and supported by the AER which overlies the PR. It is likely that this increased proliferation allows for 5-digit structures to self-organise in the limb field

Importantly, I demonstrated that neither *Bmp2* nor *p27^{kip1}* are expressed in the PR of the developing mouse limb. This can be compared with the chick wing where *Bmp2* is expressed in an area encompassing the PR whilst *p27^{kip1}* is expressed specifically in the PR (Pickering et al., 2019). The lack of *p27^{kip1}* expression in the developing mouse limb could indicate why mice with loss-of-function mutations do not appear to have any limb defects (Fero et al., 1996, Nakayama et al., 1996). This suggests that p27^{kip1} is not utilised in the mouse PR to inhibit proliferation, thus allowing it to form two digits.

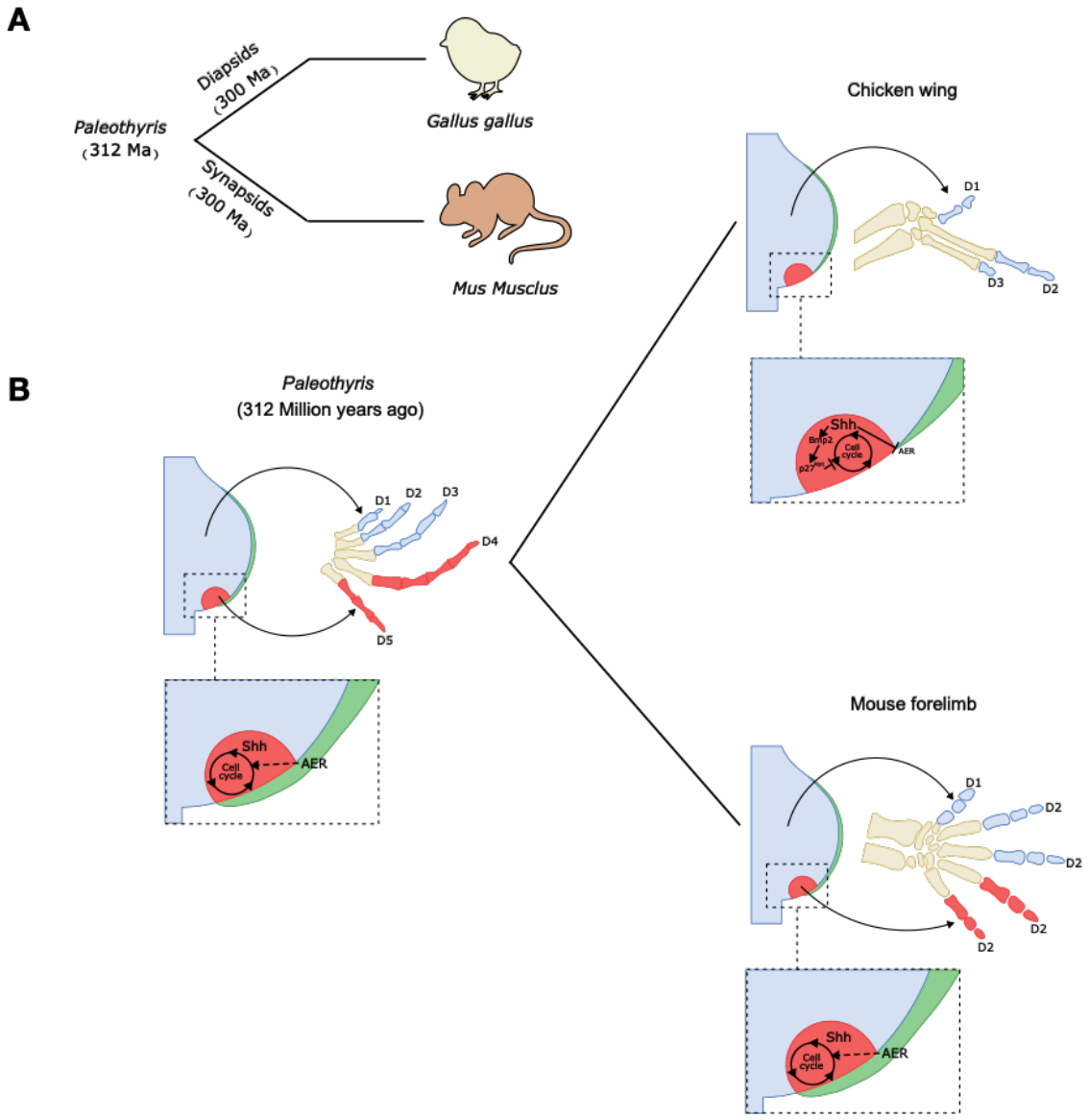

Figure 7.5. The avian PR has evolved a mechanism to prevent the formation of digits.

A) Approximately 300 million years ago, diapsids (which gave rise to dinosaurs, reptiles and birds) and synapsids (which gave rise to mammals) diverged from a common ancestor. B) The common ancestor of the birds and mammals (*Paleothyris)* had five digits. In this model, the common ancestor limb produces two digits - with proliferation being supported by the AER which likely covered the PR. This has been retained in the mouse limb, however, the number of phalanges in each digit has been reduced. In the chicken wing, the PR has evolved a mechanism in which Shh signalling simultaneously inhibits the AER from establishing over the PR, and decreases proliferation through a Bmp2-p27^{kip1} pathway. Thus, Shh signalling in the chick PR inhibits proliferation and prevents the formation of a digit resulting in the three-digit chick wing.

7.3.1. Implications for the evolution of digit number in birds and mammals

As discussed previously the mouse limb is a good approximation of the ancestral limb of birds and mammals as it has retained the ancestral pentadactyly state during its evolution, however it has decreased the number of phalanges in the digits. Therefore, I speculate that digits 1, 2 and 3 (i.e. the anterior digits) of the ancestral limb arose from non-PR mesenchyme, as is the case in the mouse forelimb and chick wing, and that the ancestral PR gave rise to digits 4 and 5, as is the case in the mouse (i.e. the posterior digits; Figure 7.5. B). In view of the data presented in Section 7.3., I speculate that, similarly to the mouse limb, Shh signalling did not control G1-S phase regulators to inhibit the proliferation of PR cells in the ancestral limb. Therefore, the data in my thesis indicates that the intrinsic control of proliferation through G1-S phase regulators has evolved in the avian PR to prevent the formation of digits (Figure 7.5 B).

Furthermore, as the AER extends over the PR of the mouse limb (Pickering and Towers, 2016), I speculate that this was also the case for the common ancestral limb. Therefore, the inhibition of the AER forming over the PR by Shh signalling in chick wings likely evolved to prevent the formation of additional digits. Thus, I present a model explaining how digit number has evolved in both mammals and birds from a five-digit ancestor (Figure 7.5 B).

7.4. Future directions

As mentioned, I began preliminary experiments to block Fgf signalling with SU5402 in the PR explants, however this resulted in the death of all explants (n = 4/4). However, I never got to repeat this experiment again during my PhD timeline. Thus, it would be interesting to try this experiment again to determine if this was a one-off effect of if the explants require some Fgf to survive. If the explants did survive, I would be very interested in going on to dual-inhibit Shh signalling and Fgf

signalling in the PR explants. As described above, the over-proliferation of PR explant cells may be supported by the *de novo* expression of *Fgf8*. Thus, inhibiting Fgfs would allow me to determine whether the AER plays a permissive role in supporting proliferation, as I have suggested in this thesis, or if it is required.

7.4.1. Understanding the role of G1-S phase regulators which promote proliferation in chick wing PR development

In this thesis, I have focused on the intrinsic mechanism causing the decrease in the proliferation in the chick wing PR. However, it has also been proposed that Shh signalling is required to promote proliferation in the PR initially through *N-myc, Cyclin D1* and *Cyclin D2* (Towers et al., 2008, Pickering et al., 2019). Therefore, it would be interesting to examine the expression patterns of these G1-S phase regulators in the PR explants under normal conditions and when Shh signalling is inhibited. I would expect that *N-myc*, Cyclin *D1* and *Cyclin D2* are all expressed in the PR explants under normal conditions. However, as Shh signalling is required for the maintenance of *Cyclin D2,* but not *N-myc* and Cyclin *D1* (Towers et al., 2008)*,* I would predict that *N-myc* and Cyclin *D1* expression would persist after Shh signalling is inhibited. By examining the expression patterns of these cell cycle regulators, we would be able to form a complete understanding regarding how Shh signalling promotes and inhibits proliferation in the PR of chick wings.

7.4.2. Understanding the mechanisms underpinning the formation of one digit from the chick leg PR

The ancestral limb contained five digits, with digits 4 and 5 likely forming from the PR which was covered by the AER. My data has suggested an evolutionary mechanism which has evolved in the chick wing PR to prevent the formation of any digits. In the chick wing, I have shown that Shh signalling intrinsically upregulates a cell-cycle inhibitory pathway and inhibits the establishment of the AER over the PR,

thus preventing any digits. However, I have not examined if this same evolutionary mechanism is present in the chick leg.

The development of the chick leg is interesting as it contains four digits. Furthermore, the most posterior digit arises from the PR (Towers et al., 2011) which is partially overlapped by the AER (Pickering and Towers, 2016). This raises questions such as, has the chick leg PR evolved the same inhibitory cell cycle mechanism present in the chick wing PR to prevent over-proliferation or does the overlying AER permissively support an increase in proliferation which leads to the formation of a chick leg PR digit? *In situ* hybridisations have revealed that the chick leg PR does express $p27^{kip1}$ (Pickering et al., 2019) thus suggesting that it has evolved a similar inhibitory cell cycle mechanism to the chick wing PR. Nonetheless, it would be fascinating to see if inhibition of Shh signalling at HH20/21 causes a subsequent over-proliferation of chick leg PR cells, similarly to the chick wing PR. I predict that the chick leg would form an additional digit, thus resulting in two PR-derived digits. However, further work is needed in this area to truly understand how the chick leg PR evolved to form a singular digit.

References

REFERENCES

AGARWAL, P., WYLIE, J. N., GALCERAN, J., ARKHITKO, O., LI, C., DENG, C., GROSSCHEDL, R. & BRUNEAU, B. G. (2003). Tbx5 is essential for forelimb bud initiation following patterning of the limb field in the mouse embryo. *Development,* 130, 623-33.

AKITA, K. (1996). The effect of the ectoderm on the dorsoventral pattern of epidermis, muscles and joints in the developing chick leg: a new model. *Anatomy and Embryology,* 193**,** 377-86.

AKIYAMA, R., KAWAKAMI, H., WONG, J., OISHI, I., NISHINAKAMURA, R. & KAWAKAMI, Y. (2015). Sall4-Gli3 system in early limb progenitors is essential for the development of limb skeletal elements. *Proceedings of the National Academy of Sciences,* 112**,** 5075-80.

ALTABEF, M., CLARKE, J. D. & TICKLE, C. (1997). Dorso-ventral ectodermal compartments and origin of apical ectodermal ridge in developing chick limb. *Development,* 124**,** 4547-56.

BI, W., DENG, J. M., ZHANG, Z., BEHRINGER, R. R. & DE CROMBRUGGHE, B. (1999). Sox9 is required for cartilage formation. *Nature Genetics,* 22**,** 85-9.

BOULDIN, C. M., GRITLI-LINDE, A., AHN, S. & HARFE, B. D. (2010). Shh pathway activation is present and required within the vertebrate limb bud apical ectodermal ridge for normal autopod patterning. *Proceedings of the National Academy of Sciences,* 107**,** 5489-94.

BURKE, A. C. & FEDUCCIA, A. (1997). Developmental patterns and the identification of homologies in the avian hand. *Science,* 278**,** 666-8.

BÜSCHER, D., BOSSE, B., HEYMER, J. & RÜTHER, U. (1997). Evidence for genetic control of Sonic hedgehog by Gli3 in mouse limb development. *Mechanisms of development,* 62**,** 175-82.

CAPDEVILA, J., TSUKUI, T., ESTEBAN, C. R., ZAPPAVIGNA, V. & BELMONTE, J. C. I. (1999). Control of vertebrate limb outgrowth by the proximal factor *Meis2* and distal antagonism of BMPs by Gremlin. *Molecular Cell,* 4**,** 839-49.

CARROLL, R. L. (1969). A Middle Pennsylvanian captorhinomorph, and the interrelationships of primitive reptiles. *Journal of Paleontology***,** 151-70.

CHATTERJEE, S. (1998). Counting the fingers of birds and dinosaurs. *Science,* 280**,** 355-.

CHAUBE, S. (1959). On axiation and symmetry in transplanted wing of the chick. *Journal of Experimental Zoology,* 140**,** 29-77.

CHEN, J. K., TAIPALE, J., COOPER, M. K. & BEACHY, P. A. (2002). Inhibition of Hedgehog signaling by direct binding of cyclopamine to Smoothened. *Genes & development,* 16**,** 2743-8.

CHIANG, C., LITINGTUNG, Y., LEE, E., YOUNG, K. E., CORDEN, J. L., WESTPHAL, H. & BEACHY, P. A. (1996). Cyclopia and defective axial patterning in mice lacking Sonic hedgehog gene function. *Nature,* 383**,** 407-13.

CHINNAIYA, K., TICKLE, C. & TOWERS, M. (2014). Sonic hedgehog-expressing cells in the developing limb measure time by an intrinsic cell cycle clock. *Nature Communications,* 5.

CHRIST, B., JACOB, H. & JACOB, M. (1977). Experimental analysis of the origin of the wing musculature in avian embryos. *Anatomy and embryology,* 150**,** 171-86.

COOKE, J. & SUMMERBELL, D. (1980). Cell cycle and experimental pattern duplication in the chick wing during embryonic development. *Nature,* 287**,** 697-701.

COOPER, K. L., HU, J. K.-H., TEN BERGE, D., FERNANDEZ-TERAN, M., ROS, M. A. & TABIN, C. J. (2011). Initiation of proximal-distal patterning in the vertebrate limb by signals and growth. *Science,* 332**,** 1083-6.

CROSSLEY, P. H., MINOWADA, G., MACARTHUR, C. A. & MARTIN, G. R. (1996). Roles for FGF8 in the induction, initiation, and maintenance of chick limb development. *Cell,* 84**,** 127-36.

CROWLEY, L. C., CHOJNOWSKI, G. & WATERHOUSE, N. J. (2016). Measuring the DNA content of cells in apoptosis and at different cell-cycle stages by propidium iodide staining and flow cytometry. *Cold Spring Harbor Protocols,* 2016**,** pdb. prot087247.

DAVEY, M. G., PATON, I. R., YIN, Y., SCHMIDT, M., BANGS, F. K., MORRICE, D. R., SMITH, T. G., BUXTON, P., STAMATAKI, D., TANAKA, M., MÜNSTERBERG, A. E., BRISCOE, J., TICKLE, C. & BURT, D. W. (2006). The chicken talpid3 gene encodes a novel protein essential for Hedgehog signaling. *Genes Dev,* 20**,** 1365-77.

DELGADO, I., LÓPEZ-DELGADO, A. C., ROSELLÓ-DÍEZ, A., GIOVINAZZO, G., CADENAS, V., FERNÁNDEZ-DE-MANUEL, L., SÁNCHEZ-CABO, F., ANDERSON, M. J., LEWANDOSKI, M. & TORRES, M. (2020). Proximo-distal positional information encoded by an Fgf-regulated gradient of homeodomain transcription factors in the vertebrate limb. *Science Advances,* 6**,** eaaz0742.

DROSSOPOULOU, G., LEWIS, K. E., SANZ-EZQUERRO, J. J., NIKBAKHT, N., MCMAHON, A. P., HOFMANN, C. & TICKLE, C. (2000). A model for anteroposterior patterning of the vertebrate limb based on sequential long- and short-range Shh signalling and Bmp signalling. *Development,* 127**,** 1337-48.

EBLAGHIE, M. C., LUNN, J. S., DICKINSON, R. J., MÜNSTERBERG, A. E., SANZ-EZQUERRO, J. J., FARRELL, E. R., MATHERS, J., KEYSE, S. M., STOREY, K. & TICKLE, C. (2003). Negative feedback regulation of FGF signaling levels by Pyst1/MKP3 in chick embryos. *Curr Biol,* 13**,** 1009-18.

ECHELARD, Y., EPSTEIN, D. J., ST-JACQUES, B., SHEN, L., MOHLER, J., MCMAHON, J. A. & MCMAHON, A. P. (1993). Sonic hedgehog, a member of a family of putative signaling molecules, is implicated in the regulation of CNS polarity. *Cell,* 75**,** 1417-30.

FERO, M. L., RIVKIN, M., TASCH, M., PORTER, P., CAROW, C. E., FIRPO, E., POLYAK, K., TSAI, L.-H., BROUDY, V., PERLMUTTER, R. M., KAUSHANSKY, K. & ROBERTS, J. M. (1996). A Syndrome of Multiorgan Hyperplasia with Features of Gigantism, Tumorigenesis, and Female Sterility in $p27^{kip1}$-Deficient Mice. *Cell,* 85**,** 733-44.

FLOMERFELT, F. & GRESS, R. (2016). Analysis of cell proliferation and homeostasis using EdU labeling. *Methods in molecular biology (Clifton, N.J.),* 1323**,** 211-20.

FRANCIS, P. H., RICHARDSON, M. K., BRICKELL, P. M. & TICKLE, C. (1994). Bone morphogenetic proteins and a signalling pathway that controls patterning in the developing chick limb. *Development,* 120**,** 209-18.

GODEFROIT, P., CAU, A., DONG-YU, H., ESCUILLIÉ, F., WENHAO, W. & DYKE, G. (2013). A Jurassic avialan dinosaur from China resolves the early phylogenetic history of birds. *Nature,* 498**,** 359-62.

GOODRICH, L. V., JOHNSON, R. L., MILENKOVIC, L., MCMAHON, J. A. & SCOTT, M. P. (1996). Conservation of the hedgehog/patched signaling pathway from flies to mice: induction of a mouse patched gene by Hedgehog. *Genes & development,* 10**,** 301-12.

GUI, H., LI, S. & MATISE, M. P. (2007). A cell-autonomous requirement for Cip/Kip cyclin-kinase inhibitors in regulating neuronal cell cycle exit but not differentiation in the developing spinal cord. *Developmental biology,* 301**,** 14-26.

HAMBURGER, V. (1938). Morphogenetic and axial self-differentiation of transplanted limb primordia of 2-day chick embryos. *Journal of Experimental Zoology,* 77**,** 379-99.

HAMBURGER, V. & HAMILTON, H. L. (1951). A series of normal stages in the development of the chick embryo. *Journal of Morphology,* 88**,** 49-92.

HARDY, A., RICHARDSON, M. K., FRANCIS-WEST, P. H., RODRIGUEZ, C., IZPISÚA-BELMONTE, J.-C., DUPREZ, D. & WOLPERT, L. (1995). Gene expression, polarising activity and skeletal patterning in reaggregated hind limb mesenchyme. *Development,* 121**,** 4329-37.

HARFE, B. D., SCHERZ, P. J., NISSIM, S., TIAN, H., MCMAHON, A. P. & TABIN, C. J. (2004). Evidence for an expansion-based temporal Shh gradient in specifying vertebrate digit identities. *Cell,* 118**,** 517-28.

HAYASHI, S., AKIYAMA, R., WONG, J., TAHARA, N., KAWAKAMI, H. & KAWAKAMI, Y. (2016). Gata6-dependent GLI3 repressor function is essential in anterior limb progenitor cells for proper limb development. *PLoS genetics,* 12**,** e1006138.

HEALY, C., UWANOGHO, D. & SHARPE, P. T. (1999). Regulation and role of Sox9 in cartilage formation. *Developmental Dynamics,* 215**,** 69-78.

HOPSON, J. A. (1995). Patterns of Evolution in the Manus and Pes of Non-Mammalian Therapsids. *Journal of Vertebrate Paleontology,* 15**,** 615-39.

HU, M. C., MO, R., BHELLA, S., WILSON, C. W., CHUANG, P.-T., HUI, C.-C. & ROSENBLUM, N. D. (2006). GLI3-dependent transcriptional repression of Gli1, Gli2 and kidney patterning genes disrupts renal morphogenesis. *Development,* 133**,** 569-78.

ITOU, J., KAWAKAMI, H., QUACH, T., OSTERWALDER, M., EVANS, S. M., ZELLER, R. & KAWAKAMI, Y. (2012). Islet1 regulates establishment of the posterior hindlimb field upstream of the Hand2-Shh morphoregulatory gene network in mouse embryos. *Development,* 139**,** 1620-9.

IULIANELLA, A. & STANTON-TURCOTTE, d. (2019). The Hedgehog receptor Patched1 regulates proliferation, neurogenesis, and axon guidance in the embryonic spinal cord. *Mechanisms of Development,* 160**,** 103577.

KINZLER, K. W., RUPPERT, J. M., BIGNER, S. H. & VOGELSTEIN, B. (1988). The GLI gene is a member of the Kruppel family of zinc finger proteins. *Nature,* 332**,** 371-4.

LAUFER, E., NELSON, C. E., JOHNSON, R. L., MORGAN, B. A. & TABIN, C. (1994). Sonic hedgehog and Fgf-4 act through a signaling cascade and feedback loop to integrate growth and patterning of the developing limb bud. *Cell,* 79**,** 993-1003.

LETTICE, L. A., DEVENNEY, P., DE ANGELIS, C. & HILL, R. E. (2017). The conserved Sonic Hedgehog limb enhancer consists of discrete functional elements that regulate precise spatial expression. *Cell Reports,* 20**,** 1396-408.

LETTICE, L. A., HORIKOSHI, T., HEANEY, S. J., VAN BAREN, M. J., VAN DER LINDE, H. C., BREEDVELD, G. J., JOOSSE, M., AKARSU, N., OOSTRA, B. A. & ENDO, N. (2002). Disruption of a long-range cis-acting regulator for Shh causes preaxial polydactyly. *Proceedings of the national academy of sciences,* 99**,** 7548-53.

LIPINSKI, R. J., GIPP, J. J., ZHANG, J., DOLES, J. D. & BUSHMAN, W. (2006). Unique and complimentary activities of the Gli transcription factors in Hedgehog signaling. *Experimental Cell Research,* 312**,** 1925-38.

LOOMIS, C. A., HARRIS, E., MICHAUD, J., WURST, W., HANKS, M. & JOYNER, A. L. (1996). The mouse Engrailed-1 gene and ventral limb patterning. *Nature,* 382**,** 360-3.

LYONS, K. M., PELTON, R. W. & HOGAN, B. L. M. (1990). Organogenesis and pattern formation in the mouse: RNA distribution patterns suggest a role for *Bone Morphogenetic Protein-2A (BMP-2A)*. *Development,* 109**,** 833-44.

MAAS, S. A., SUZUKI, T. & FALLON, J. F. (2011). Identification of spontaneous mutations within the long-range limb-specific Sonic hedgehog enhancer (ZRS) that alter Sonic hedgehog expression in the chicken limb mutants oligozeugodactyly and silkie breed. *Developmental Dynamics,* 240**,** 1212-22.

MADSEN, J. J. H. (1976) Allosaurus Fragilis: a Revised Osteology.

MARIANI, F. V., AHN, C. P. & MARTIN, G. R. (2008). Genetic evidence that FGFs have an instructive role in limb proximal–distal patterning. *Nature,* 453**,** 401-5.

MARIGO, V., JOHNSON, R. L., VORTKAMP, A. & TABIN, C. J. (1996). Sonic hedgehog differentially regulates expression of Gli and Gli3 during limb development. *Developmental Biology,* 180**,** 273-83.

MARSH, A. D. & ROWE, T. B. (2020). A comprehensive anatomical and phylogenetic evaluation of Dilophosaurus wetherilli (Dinosauria, Theropoda) with descriptions of new specimens from the Kayenta Formation of northern Arizona. *Journal of Paleontology,* 94**,** 1-103.

MARTIN, P. (1990). Tissue patterning in the developing mouse limb. *The International Journal of Developmental Biology,* 34**,** 323-36.

MCGREW, M. J., SHERMAN, A., LILLICO, S. G., ELLARD, F. M., RADCLIFFE, P. A., GILHOOLEY, H. J., MITROPHANOUS, K. A., CAMBRAY, N., WILSON, V. & SANG, H. (2008). Localised axial progenitor cell populations in the avian tail bud are not committed to a posterior Hox identity. *Development,* 135**,** 2289-99.

MERCADER, N., LEONARDO, E., AZPIAZU, N., SERRANO, A., MORATA, G., MARTÍNEZ-A, C. & TORRES, M. (1999). Conserved regulation of proximodistal limb axis development by Meis1/Hth. *Nature,* 402**,** 425-9.

MERCADER, N., LEONARDO, E., PIEDRA, M. E., MARTÍNEZ-A, C., ÁNGELES ROS, M. & TORRES, M. (2000). Opposing RA and FGF signals control proximodistal vertebrate limb development through regulation of Meis genes. *Development,* 127**,** 3961-70.

MERINO, R., RODRIGUEZ-LEON, J., MACIAS, D., GAÑAN, Y., ECONOMIDES, A. N. & HURLE, J. M. (1999). The BMP antagonist Gremlin regulates outgrowth, chondrogenesis and programmed cell death in the developing limb. *Development,* 126**,** 5515-22.

MICHAUD, J. L., LAPOINTE, F. & DOUARIN, N. M. L. (1997). The dorsoventral polarity of the presumptive limb is determined by signals produced by the somites and by the lateral somatopleure. *Development,* 124**,** 1453-63.

MICHOS, O., PANMAN, L., VINTERSTEN, K., BEIER, K., ZELLER, R. & ZUNIGA, A. E. (2004). Gremlin-mediated BMP antagonism induces the epithelial-mesenchymal feedback signaling controlling metanephric kidney and limb organogenesis. *Development,* 131**,** 3401-10.

MINGUILLON, C., NISHIMOTO, S., WOOD, S., VENDRELL, E., GIBSON-BROWN, J. J. & LOGAN, M. P. (2012). Hox genes regulate the onset of Tbx5 expression in the forelimb. *Development,* 139**,** 3180-8.

MININA, E., WENZEL, H. M., KRESCHEL, C., KARP, S., GAFFIELD, W., MCMAHON, A. P. & VORTKAMP, A. (2001). BMP and Ihh/PTHrP signaling interact to coordinate chondrocyte proliferation and differentiation. *Development,* 128**,** 4523-34.

NAKAMURA, Y., OZAKI, T., KOSEKI, H., NAKAGAWARA, A. & SAKIYAMA, S. (2003). Accumulation of p27KIP1 is associated with BMP2-induced growth arrest and neuronal differentiation of human neuroblastoma-derived cell lines. *Biochemical and Biophysical Research Communications,* 307**,** 206-13.

NAKAYAMA, K., ISHIDA, N., SHIRANE, M., INOMATA, A., INOUE, T., SHISHIDO, N., HORII, I., LOH, D. Y. & NAKAYAMA, K.-I. (1996). Mice Lacking $p27^{Kip1}$ display increased body size, multiple organ hyperplasia, retinal dysplasia, and pituitary tumors. *Cell,* 85**,** 707-20.

NIKBAKHT, N. & MCLACHLAN, J. C. (1999). Restoring avian wing digits. *Proceedings of the Royal Society of London. Series B: Biological Sciences,* 266**,** 1101-4.

NISHIMOTO, S., MINGUILLON, C., WOOD, S. & LOGAN, M. P. (2014). A combination of activation and repression by a colinear Hox code controls forelimb-restricted expression of Tbx5 and reveals Hox protein specificity. *PLoS genetics,* 10**,** e1004245.

NISHIMOTO, S., WILDE, S. M., WOOD, S. & LOGAN, M. P. (2015). RA acts in a coherent feed-forward mechanism with Tbx5 to control limb bud induction and initiation. *Cell reports,* 12**,** 879-91.

NISWANDER, L., JEFFREY, S., MARTIN, G. R. & TICKLE, C. (1994). A positive feedback loop coordinates growth and patterning in the vertebrate limb. *Nature,* 371**,** 609-12.

NISWANDER, L., TICKLE, C., VOGEL, A., BOOTH, I. & MARTIN, G. R. (1993). FGF-4 replaces the apical ectodermal ridge and directs outgrowth and patterning of the limb. *Cell,* 75**,** 579-87.

NORMAN, D. B., CROMPTON, A. W., BUTLER, R. J., PORRO, L. B. & CHARIG, A. J. (2011). The Lower Jurassic ornithischian dinosaur Heterodontosaurus tucki Crompton & Charig, 1962: cranial anatomy, functional morphology, taxonomy, and relationships. *Zoological Journal of the Linnean Society,* 163**,** 182-276.

NOVAS, F. E. (1994). New information on the systematics and postcranial skeleton of Herrerasaurus ischigualastensis (Theropoda: Herrerasauridae) from the Ischigualasto Formation (Upper Triassic) of Argentina. *Journal of Vertebrate Paleontology,* 13**,** 400-23.

OHUCHI, H., NAKAGAWA, T., YAMAMOTO, A., ARAGA, A., OHATA, T., ISHIMARU, Y., YOSHIOKA, H., KUWANA, T., NOHNO, T., YAMASAKI, M., ITOH, N. & NOJI, S. (1997). The mesenchymal factor, FGF10, initiates and maintains the outgrowth of the chick limb bud through interaction with FGF8, an apical ectodermal factor. *Development,* 124**,** 2235-44.

OSTROM, J. H. (1974). Archaeopteryx and the Origin of Flight. *The Quarterly Review of Biology,* 49**,** 27-47.

PADIAN, K. & CHIAPPE, L. M. (1998). The origin of birds and their flight. *Scientific American,* 278**,** 38-47.

PARR, B. A. & MCMAHON, A. P. (1995). Dorsalizing signal Wnt-7a required for normal polarity of D–V and A–P axes of mouse limb. *Nature,* 374**,** 350-3.

PICKERING, J., CHINNAIYA, K. & TOWERS, M. (2019). An autoregulatory cell cycle timer integrates growth and specification in chick wing digit development. *eLife,* 8.

PICKERING, J., RICH, C. A., STAINTON, H., ACEITUNO, C., CHINNAIYA, K., SAIZ-LOPEZ, P., ROS, M. A. & TOWERS, M. (2018). An intrinsic cell cycle timer terminates limb bud outgrowth. *eLife,* 7**,** e37429.

PICKERING, J. & TOWERS, M. (2016). Inhibition of Shh signalling in the chick wing gives insights into digit patterning and evolution. *Development,* 143**,** 3514-21.

PIEDRA, M. E., RIVERO, F. B., FERNANDEZ-TERAN, M. & ROS, M. A. (2000). Pattern formation and regulation of gene expressions in chick recombinant limbs. *Mechanisms of development,* 90**,** 167-79.

PIZETTE, S., ABATE-SHEN, C. & NISWANDER, L. (2001). BMP controls proximodistal outgrowth, via induction of the apical ectodermal ridge, and dorsoventral patterning in the vertebrate limb.

RASPOPOVIC, J., MARCON, L., RUSSO, L. & SHARPE, J. (2007). Digit patterning is controlled by a Bmp-Sox9-Wnt Turing network modulated by morphogen gradients. *Science,* 345**,** 566 - 70.

RIDDLE, R. D., ENSINI, M., NELSON, C., TSUCHIDA, T., JESSELL, T. M. & TABIN, C. (1995). Induction of the LIM homeobox gene Lmx1 by WNT6a establishes dorsoventral pattern in the vertebrate limb. *Cell,* 83**,** 631-40.

RIDDLE, R. D., JOHNSON, R. L., LAUFER, E. & TABIN, C. (1993). Sonic hedgehog mediates the polarizing activity of the ZPA. *Cell,* 75**,** 1401-16.

RODRIGUEZ-ESTEBAN, C., TSUKUI, T., YONEI, S., MAGALLON, J., TAMURA, K. & BELMONTE, J. C. I. (1999). The T-box genes Tbx4 and Tbx5 regulate limb outgrowth and identity. *Nature,* 398**,** 814-8.

ROS, M. A., DAHN, R. D., FERNANDEZ-TERAN, M., RASHKA, K., CARUCCIO, N. C., HASSO, S. M., BITGOOD, J. J., LANCMAN, J. J. & FALLON, J. F. (2003). The chick oligozeugodactyly (ozd) mutant lacks sonic hedgehog function in the limb. *Development,* 130**,** 527-37.

ROSELLÓ-DÍEZ, A., ROS, M. A. & TORRES, M. (2011). Diffusible signals, not autonomous mechanisms, determine the main proximodistal limb subdivision. *Science,* 332**,** 1086-8.

RUBIN, L. & SAUNDERS, J. W. (1972). Ectodermal-mesodermal interactions in the growth of limb buds in the chick embryo: Constancy and temporal limits of the ectodermal induction. *Developmental Biology,* 28**,** 94-112.

RUPPERT, J. M., VOGELSTEIN, B., ARHEDEN, K. & KINZLER, K. W. (1990). GLI3 encodes a 190-kilodalton protein with multiple regions of GLI similarity. *Molecular and cellular biology,* 10**,** 5408-15.

SAIZ-LOPEZ, P., CHINNAIYA, K., CAMPA, V. M., DELGADO, I., ROS, M. A. & TOWERS, M. (2015). An intrinsic timer specifies distal structures of the vertebrate limb. *Nature Communications,* 6**,** 8108.

SANZ-EZQUERRO, J. J. & TICKLE, C. (2003). Fgf signaling controls the number of phalanges and tip formation in developing digits. *Current biology,* 13**,** 1830-6.

SAUNDERS JR, J. & GASSELING, M. (1968). Ectoderm-mesenchymal interaction in the origins of wing symmetry. *Epithelial-Mesenchymal Interactions***,** 78-97.

SAUNDERS JR, J. W. (1948). The proximo-distal sequence of origin of the parts of the chick wing and the role of the ectoderm. *Journal of Experimental Zoology,* 108**,** 363-403.

SAUNDERS JR, J. W., GASSELING, M. T. & SAUNDERS, L. C. (1962). Cellular death in morphogenesis of the avian wing. *Developmental biology,* 5**,** 147-78.

SCHERZ, P. J., HARFE, B. D., MCMAHON, A. P. & TABIN, C. J. (2004). The limb bud Shh-Fgf feedback loop is terminated by expansion of former ZPA cells. *Science,* 305**,** 396-9.

SCHERZ, P. J., MCGLINN, E., NISSIM, S. & TABIN, C. J. (2007). Extended exposure to Sonic hedgehog is required for patterning the posterior digits of the vertebrate limb. *Developmental Biology,* 308**,** 343-54.

SEDAS PEREZ, S., MCQUEEN, C., STAINTON, H., PICKERING, J., CHINNAIYA, K., SAIZ-LOPEZ, P., PLACZEK, M., ROS, M. A. & TOWERS, M. (2023). Fgf signalling triggers an intrinsic mesodermal timer that determines the duration of limb patterning. *Nature Communications,* 14**,** 5841.

SHERR, C. J. & ROBERTS, J. M. (1999). CDK inhibitors: positive and negative regulators of G1-phase progression. *Genes Dev,* 13**,** 1501-12.

SHUBIN, N. H. & ALBERCH, P. (1986). A morphogenetic approach to the origin and basic organization of the tetrapod limb. *Evolutionary Biology: Volume 20.* Springer.

SMITH, J. C. (1980). The time required for positional signalling in the chick wing bud. *Development,* 60**,** 321-8.

SMITH, J. C. & WOLPERT, L. (1981). Pattern formation along the anteroposterior axis of the chick wing: the increase in width following a polarizing region graft and the effect of X-irradiation. *J Embryol Exp Morphol,* 63**,** 127-44.

SMITHSON, T., CARROLL, R., PANCHEN, A. & ANDREWS, S. (1993). Westlothiana lizziae from the Viséan of East Kirkton, West Lothian, Scotland, and the amniote stem. *Earth and Environmental Science Transactions of The Royal Society of Edinburgh,* 84**,** 383-412.

STAINTON, H. & TOWERS, M. (2018). Polarizing Region Tissue Grafting in the Chick Embryo Limb Bud. Springer New York.

STAINTON, H. & TOWERS, M. (2022). Retinoic acid influences the timing and scaling of avian wing development. *Cell Rep,* 38**,** 110288.

SUMMERBELL, D. (1981). The control of growth and the development of pattern across the anteroposterior axis of the chick limb bud. *J Embryol Exp Morphol,* 63**,** 161-80.

SUMMERBELL, D. & LEWIS, J. H. (1975). Time, place and positional value in the chick limb-bud. *Development,* 33**,** 621-43.

SUMMERBELL, D., LEWIS, J. H. & WOLPERT, L. (1973). Positional Information in Chick Limb Morphogenesis. *Nature,* 244**,** 492-6.

TAKAHASHI, M., TAMURA, K., BÜSCHER, D., MASUYA, H., YONEI-TAMURA, S., MATSUMOTO, K., NAITOH-MATSUO, M., TAKEUCHI, J., OGURA, K. & SHIROISHI, T. (1998). The role of Alx-4 in the establishment of anteroposterior polarity during vertebrate limb development. *Development,* 125**,** 4417-25.

TAKEUCHI, J. K., KOSHIBA-TAKEUCHI, K., MATSUMOTO, K., VOGEL-HÖPKER, A., NAITOH-MATSUO, M., OGURA, K., TAKAHASHI, N., YASUDA, K. & OGURA, T. (1999). Tbx5 and Tbx4 genes determine the wing/leg identity of limb buds. *Nature,* 398**,** 810-4.

TICKLE, C. (1981). The number of polarizing region cells required to specify additional digits in the developing chick wing. *Nature,* 289**,** 295-8.

TICKLE, C., SUMMERBELL, D. & WOLPERT, L. (1975). Positional signalling and specification of digits in chick limb morphogenesis. *Nature,* 254**,** 199-202.

TOWERS, M., MAHOOD, R., YIN, Y. & TICKLE, C. (2008). Integration of growth and specification in chick wing digit-patterning. *Nature,* 452**,** 882-6.

TOWERS, M., SIGNOLET, J., SHERMAN, A., SANG, H. & TICKLE, C. (2011). Insights into bird wing evolution and digit specification from polarizing region fate maps. *Nature communications,* 2**,** 426.

TURING, A. M. (1952). The chemical basis of morphogenesis. *Philosophical Transactions of the Royal Society of London. Series B, Biological Sciences,* 237**,** 37-72.

VARGESSON, N., CLARKE, J. D. W., VINCENT, K., COLES, C., WOLPERT, L. & TICKLE, C. (1997). Cell fate in the chick limb bud and relationship to gene expression. *Development,* 124**,** 1909-18.

VOGEL, A., RODRIGUEZ, C. & IZPISÚA-BELMONTE, J.-C. (1996). Involvement of FGF-8 in initiation, outgrowth and patterning of the vertebrate limb. *Development,* 122**,** 1737-50.

VOGEL, A., RODRIGUEZ, C., WARNKEN, W. & BELMONTE, J. C. I. (1995). Dorsal cell fate specified by chick Lmxl during vertebrate limb development. *Nature,* 378**,** 716-20.

WANEK, N., MUNEOKA, K., HOLLER-DINSMORE, G., BURTON, R. & BRYANT, S. (1989). A staging system for mouse limb development. *Journal of Experimental Zoology,* 249**,** 41-9.

WANG, B., FALLON, J. F. & BEACHY, P. A. (2000). Hedgehog-regulated processing of Gli3 produces an anterior/posterior repressor gradient in the developing vertebrate limb. *Cell,* 100**,** 423-34.

WEISHAMPEL, D. B., DODSON, P. & OSMÓLSKA, H. (2004). *The dinosauria [electronic resource],* Berkeley, Berkeley : University of California Press, c2004.

WELLES, S. P. (1984). Dilophosaurus wetherilli (Dinosauria, Theropoda). Osteology and comparisons. *Palaeontographica Abteilung A***,** 85-180.

WILLIAMSON, I., LETTICE, L. A., HILL, R. E. & BICKMORE, W. A. (2016). Shh and ZRS enhancer colocalisation is specific to the zone of polarising activity. *Development,* 143**,** 2994-3001.

XU, B., HRYCAJ, S. M., MCINTYRE, D. C., BAKER, N. C., TAKEUCHI, J. K., JEANNOTTE, L., GABER, Z. B., NOVITCH, B. G. & WELLIK, D. M. (2013). Hox5 interacts with Plzf to restrict Shh expression in the developing forelimb. *Proceedings of the National Academy of Sciences,* 110**,** 19438-43.

XU, B. & WELLIK, D. M. (2011). Axial *Hox9* activity establishes the posterior field in the developing forelimb. *Proceedings of the National Academy of Sciences,* 108**,** 4888-91.

YANG, Y., DROSSOPOULOU, G., CHUANG, P.-T., DUPREZ, D., MARTI, E., BUMCROT, D., VARGESSON, N., CLARKE, J., NISWANDER, L. & MCMAHON, A. (1997). Relationship between dose, distance and time in Sonic Hedgehog-mediated regulation of anteroposterior polarity in the chick limb. *Development,* 124**,** 4393-404.

YANG, Y. & NISWANDER, L. (1995). Interaction between the signaling molecules WNT7a and SHH during vertebrate limb development: dorsal signals regulate anteroposterior patterning. *Cell,* 80**,** 939-47.

YAO, H. H.-C. & CAPEL, B. (2002). Disruption of testis cords by cyclopamine or forskolin reveals independent cellular pathways in testis organogenesis. *Developmental biology,* 246**,** 356-65.

YASHIRO, K., ZHAO, X., UEHARA, M., YAMASHITA, K., NISHIJIMA, M., NISHINO, J., SAIJOH, Y., SAKAI, Y. & HAMADA, H. (2004). Regulation of retinoic acid distribution is required for proximodistal patterning and outgrowth of the developing mouse limb. *Developmental cell,* 6**,** 411-22.

ZAKANY, J. & DUBOULE, D. (2007). The role of Hox genes during vertebrate limb development. *Current Opinion in Genetics & Development,* 17**,** 359-66.

ZHU, J., NAKAMURA, E., NGUYEN, M.-T., BAO, X., AKIYAMA, H. & MACKEM, S. (2008). Uncoupling Sonic hedgehog control of pattern and expansion of the developing limb bud. *Developmental cell,* 14**,** 624-32.

ZHU, J., PATEL, R., TROFKA, A., HARFE, B. D. & MACKEM, S. (2022). Sonic hedgehog is not a limb morphogen but acts as a trigger to specify all digits in mice. *Developmental Cell,* 57**,** 2048-62.e4.

ZÚÑIGA, A., HARAMIS, A. P., MCMAHON, A. P. & ZELLER, R. (1999). Signal relay by BMP antagonism controls the SHH/FGF4 feedback loop in vertebrate limb buds. *Nature,* 401**,** 598-602.

ZWILLING, E. (1964). Development of fragmented and of dissociated limb bud mesoderm. *Developmental biology,* 9**,** 20-37.